THE UNIVERSITY
of EDINBURGH

Toward best practice in the design of tidal turbine arrays

Paul Andrew Jude Bonar

A thesis submitted for the degree of

Doctor of Philosophy

2017

You must know the sea, and know that you know it,
and not forget that it was made to be sailed over.

Captain Joshua Slocum

Abstract

In recent years, much research has focused on the possibility of using arrays of turbines to generate clean and predictable power from tidal currents. The first such array is now in development but a number of important questions remain unanswered. Among these, how should turbines be arranged within a tidal stream to maximise their collective performance? And what impacts will such devices have on the marine environment? In beginning to address these questions, this thesis takes two important steps toward establishing best practice in the design of tidal turbine arrays.

In the first part of the thesis, the social and ecological impacts of marine energy development are reviewed. This review highlights the importance of communication and public engagement in securing support for a marine energy project and identifies the effects of increasing noise and collision risk on marine life as the most pressing ecological issues to be addressed.

In the second part, theoretical models of tidal turbines are examined and a simple numerical model is used to extend existing theories on optimal turbine arrangement. The shallow water equations are used to simulate flow through an idealised channel and an actuator disc model is used to represent a single row of tidal turbines as a line sink of momentum. Optimal turbine arrangements are then sought for different and increasingly realistic flow conditions. Results provide new and important insights into the dynamics of flow through partial-width arrays and suggest that arranging turbines unevenly within the flow cross-section can increase considerably their collective power output.

Acknowledgements

Firstly, I would like to thank my supervisors, Prof Alistair Borthwick, Dr Vengatesan Venugopal, and Prof Thomas Adcock, for the tremendous amount of support and encouragement they have given me over the past few years. Their knowledge, patience, and generosity have far exceeded all expectations. I would also like to thank Prof Robin Wallace, Prof Ian Bryden, and Prof Gareth Harrison for their guidance at the beginning of my studies, and Prof Matthew Piggott and Prof Paolo Perona for their insightful examination at the end.

I am very grateful to the Energy Technology Partnership and the Saltire Prize Challenge competitors — Aquamarine Power, MeyGen, Pelamis Wave Power, ScottishPower Renewables, and West Islay Tidal Energy — for their financial support, and for the many opportunities I have been given to travel and take part in other projects during my studies. I would also like to thank our friends at Tsinghua University, Peking University, and the China University of Geosciences for making our time in Beijing so enjoyable.

I am deeply indebted to my friends in Edinburgh and to the many wonderful people that have contributed to this thesis, in particular: Dan Pearson, Marc Murray, Dr Ben Wilson, Dr Harry van der Weijde, Dr Sena Serhadlıoğlu, Dr Duncan Sutherland, Dr Grégory Payne, Prof Stephen Salter, Prof Scott Draper, Dr Jin Hwan Hwang, Dr Maggie Creed, Monika Kreitmair, and Lei Chen.

Finally, and most importantly, I would like to thank my parents, John Andy and Rita; my sisters, Sarah, Kate, Molly, and Jennifer; my nephew, Ray; my nieces, LilyKate and Angelina; and my girlfriend, Natalie, for their continued love and support. I could not have done this without you.

Declaration

I have composed this thesis myself and, except where otherwise noted, the work contained within it is entirely my own. Parts of this thesis have already been published, as noted in the text, but no part has been submitted previously for any other degree or professional qualification.

Paul A. J. Bonar

Contents

Nomenclature

Commonly used variables

B	Blockage ratio
C_d	Channel seabed drag coefficient
C_P	Power coefficient
C_T	Thrust coefficient
P_{av}	Power available to turbines
P_{diss}	Power dissipated in wake mixing
P_{ex}	Extractable power ($= P_{av} + P_{diss}$)
Q	Channel flow rate
T	Axial thrust
u	Streamwise component of flow velocity
α	Core velocity coefficient
β	Bypass velocity coefficient
ζ	Constant head difference across channel
Z	Constant head difference across entire domain
η	Extraction efficiency ($= P_{av}/P_{diss}$)
λ_0	Natural dynamic balance (ratio of inertial to drag forces) of channel
λ_1	Additional drag due to turbines
λ'	Modified dynamic balance ($= \lambda_0 + \lambda_1$)
ξ	Amplitude of oscillatory forcing across channel
Ξ	Amplitude of oscillatory forcing across entire domain

Commonly used subscripts

$_1$	At a position far upstream of the disc
$_2$	At a position immediately upstream of the disc
$_3$	At a position immediately downstream of the disc
$_4$	At the pressure equalisation point downstream of the disc
$_5$	At the velocity equalisation point far downstream of the disc
$_A$	Array-scale variable
$_G$	Global-scale variable
$_L$	Local-scale variable
$_{(max)}$	Maximum value
$_{(opt)}$	Optimal value

Chapter 1

Introduction

All who have watched the sea know of its immense power. Set against a backdrop of increasing energy demand and climate change, the extraction of clean and plentiful energy from restless waves and strong currents is an attractive prospect (MacKay, 2008a), particularly for the UK, which is located in shallow coastal waters at the end of a long Atlantic fetch.

1.1 Tides and tidal power

The tides observed at the coast are the response of Earth's oceans to the gravitational pull of the Moon, the Sun, and other astronomical bodies, further modified by Coriolis forcing and local bathymetry (Pugh, 1996). As tidal waves propagate around ocean basins, their energy is concentrated by certain coastal geometries. Amplitudes are enhanced where inlets narrow or produce constructive interference between incoming and outgoing waves, while currents accelerate where flows are constricted, such as in narrow channels or around headlands (Draper, 2011). The tides have been used to perform meaningful work for centuries (Cartwright, 1999). The most

practical means by which to harness their power is to place hydroelectric turbines in locations of strong and predictable current. Barriers may also be constructed to constrain the flow but the present thesis focuses on arrays of free-standing turbines, which offer the advantages of lower cost, incremental development, and reduced environmental impact (Draper, 2011).

Most tidal turbines are axial flow machines based on proven technology from the wind industry but there have also been proposals for cross-flow devices designed to maximise swept area while minimising support structure (e.g. McAdam et al., 2013; Salter, 2012). Regardless of design specifics, tidal turbines must be simple and inexpensive to deploy and maintain in large numbers, yet sufficiently sophisticated and robust to perform efficiently and consistently in hostile marine environments. Besides the obvious challenges involved in producing such devices, the design of a tidal turbine array is complicated by the need to understand its interactions with current resources and marine ecosystems.

1.2 Resource assessment

A key advantage of tidal power is that the resource, though localised and intermittent, is fundamentally predictable (Adcock et al., 2015). The task of accurately assessing the power available from strong currents, however, is complex. In recent years, century-old debates about seabed dissipation rates (e.g. Street, 1917; Taylor, 1920) have resurfaced as part of arguments over tidal current energy resources (e.g. Adcock et al., 2013; Salter, 2015). The order of magnitude difference between back-of-envelope estimates (e.g. Black and Veatch, 2005; MacKay, 2008b; Salter, 2005) has demonstrated the need for a systematic approach to resource assessment.

For initial evaluation and comparison of prospective sites, Draper et al. (2014a,b) present simple expressions to predict the maximum power that may be extracted from channels: (i) connecting two large basins (following Garrett and Cummins, 2005); (ii) connecting a large basin to an enclosed bay (following Blanchfield et al., 2008), and; (iii) within multiply-connected channel networks. These formulae require only basic information about a channel and its natural flow regime. For more complicated geometries and more refined resource estimates, detailed numerical models are required. Such models may be used to determine the maximum power available from a given site (e.g. Adcock et al., 2013) and to explore the effects of turbine arrangement on array performance (e.g. Funke et al., 2014).

1.3 Array design

Design of a tidal turbine array is complicated by the fact that current resources are not only complex and dynamic, but will be modified by turbines in ways that are difficult to predict *a priori*. Numerical models are thus essential to both accurate resource assessment and efficient array design but their use in array optimisation is limited by computational requirements.

The disparity in size between individual turbines and the regions over which large arrays may alter flow patterns requires that models be simplified to be computationally tractable (Adcock et al., 2015; Vennell et al., 2015). As such, two principal types exist: three-dimensional models, which simplify the large-scale flow to focus primarily on the performance of individual turbines; and two-dimensional (depth-averaged) models, which simplify the turbine representation to focus primarily on its interactions with the large-scale flow (Adcock et al., 2015; Vennell et al., 2015).

Array design is complicated because the performance of each turbine depends not only on its position and tuning, but also on the position and tuning of all the others and their collective interaction with the resource (Funke et al., 2016; Vennell et al., 2015). The computational effort required to optimise the position and tuning of each turbine in-concert with the others may be reduced by assuming that all turbines have equal drag coefficients (e.g. Divett et al., 2013) or by adopting gradient-based optimisation methods (e.g. Funke et al., 2014) (Vennell et al., 2015). The latter approaches are much more efficient than manual optimisation, may be used to incorporate design constraints, and set to achieve different goals, including power and profit maximisation (Funke et al., 2016). The disadvantages of these methods are that they are complex to implement and produce arrays that are optimised for a specific site and number of turbines, which cannot be used to inform more generally the arrangement of turbines at other sites. Interestingly, however, in many cases the adjoint-optimised arrays appear to agree with simple theoretical models in suggesting the optimal turbine arrangement to be a densely-filled single row (Vennell et al., 2015).

Array development is further complicated by the uncertainty surrounding impacts on marine ecosystems, which is exacerbated by a lack of baseline environmental data and the complexity of assessing impacts on a range of species (Bell and Side, 2011; Shields et al., 2009; Witt et al., 2012). The environmental impacts of tidal turbine arrays will not be fully understood until devices are installed and their effects monitored (Bell and Side, 2011; Cada et al., 2007). Even then, however, impacts will vary with location and season, with the design and scale of both devices and arrays, and may be cumulative, both in time and with an increasing number of devices (Shields et al., 2009; Witt et al., 2012).

1.4 Aim, objectives, and outline

In recent years, our understanding of tidal current resources and their response to energy extraction has advanced considerably. At the time of writing, however, the pace of development in industry is quicker still. MeyGen Ltd is presently installing four 1.5 MW turbines in the Inner Sound of Scotland's Pentland Firth. Quite how these turbines will interact with each other and the surrounding environment is not fully understood but it is hoped that this initial demonstration will provide useful insights to inform subsequent development, leading eventually to an array of 269 turbines capable of producing 398 MW of electricity — enough to power 175,000 homes (MeyGen Ltd, 2017). Promising though these plans are, the 'deploy and monitor' strategy is unlikely to produce an array that is optimised for either maximum power production or minimal environmental impact.

The optimal design of a tidal turbine array is a great challenge involving many competing economic, technical, and environmental constraints. Realistically, the MeyGen array need not be optimal but if it is potentially to set the standard for a new industry, it is vital that its design and operation be informed by the essential findings from each of the relevant fields of research.

Aim

The aim of this thesis is to take two important steps toward establishing best practice in the design of tidal turbine arrays, by identifying the key environmental issues to be addressed and extending existing theories on optimal turbine arrangement.

Objectives

- To review the scientific literature and identify the most significant social and ecological issues associated with marine energy development.
- To develop a verified numerical model to explore and extend existing theories on the optimal arrangement of tidal turbines.
- To interpret the findings of the review and the results of the model to make general recommendations to inform array design.

Outline

A list of the publications that have arisen from this thesis is presented on the following page. Chapter 2 presents a comprehensive review of the social and ecological impacts of marine energy development. Chapter 3 reviews theoretical models for tidal turbines and introduces the key concepts of blockage, resistance, and extraction efficiency. Chapter 4 describes the development of a depth-averaged numerical model to extend the two-scale actuator disc theory for partial-width turbine arrays. This model is used to explore the performance of partial-width arrays in flow with background roughness in chapter 5; the performance of nonuniform arrays in uniform flow in chapter 6; and the performance of partial-width arrays in oscillatory flow in chapter 7. The conclusions of the thesis are presented in chapter 8, along with recommendations for future work.

Publications arising from this thesis

- Bonar, P. A. J., Bryden, I. G., and Borthwick, A. G. L. (2015). Social and ecological impacts of marine energy development. *Renewable and Sustainable Energy Reviews*, 47:486–495.

- Bonar, P. A. J., Venugopal, V., Borthwick, A. G. L., and Adcock, T. A. A. (2016). Numerical modelling of two-scale flow dynamics. *Proceedings of the 5th Oxford Tidal Energy Workshop, Oxford, UK.*

- Bonar, P. A. J., Chen, L., Schnabl, A. M., Houlsby, G. T., Venugopal, V., Borthwick, A. G. L., and Adcock, T. A. A. Local blockage effects for turbines in tidal channels. *In preparation.*

- Bonar, P. A. J., Venugopal, V., Borthwick, A. G. L., and Adcock, T. A. A. Nonuniform turbine arrays in uniform tidal flow. *In preparation.*

Chapter 2

Social and ecological impacts of marine energy development*

Marine energy has the potential to play a significant role in the decarbonisation of the UK's electricity supply (Jeffrey et al., 2013) but no form of generation is without social or environmental impact (WaveNet, 2003). While much research effort has focused on the technological, economic, and institutional barriers to its deployment (Jeffrey et al., 2013), few definitive statements can be made as to the social and ecological impacts of marine energy development because the majority of devices are still undergoing commercial tests and vary considerably in terms of design and operation.

Although renewable energy is supported by the vast majority (Warren et al., 2005), reluctance to invest and public opposition to siting decisions remain significant obstacles to the expansion of renewable energy in the UK and Europe (West et al., 2010). The development of marine energy is further restricted by uncertainties regarding the cumulative impacts of energy extraction on marine ecosystems and a lack of baseline environmental data

* A slightly modified version of this chapter has been published as a review paper — see Bonar et al. (2015).

(Copping et al., 2013; Shields et al., 2009; Simas et al., 2009; Witt et al., 2012). For marine energy to be truly sustainable, its social and ecological impacts must be identified and measures by which to mitigate adverse effects established before devices are deployed in large arrays. To inform future research and encourage environmentally-sensitive developments, this chapter identifies the most significant social and ecological issues associated with wave and tidal current energy generation. Where appropriate, relevant knowledge is drawn from offshore oil, gas, and wind power developments. The chapter focuses primarily on the development of marine energy in the UK but its findings are relevant to marine energy developments worldwide.

2.1 Social impacts

Public opinions and social acceptance of renewable energy

In the early years of renewable energy development, social acceptance was assumed because public surveys revealed a high level of support for renewables (Walker, 1995; Wüstenhagen et al., 2007). Due to their lower energy density, however, renewable energy developments tend to be highly visible and spread across a number of sites, which means that siting decisions affect a great number of stakeholders (Wüstenhagen et al., 2007). Although an estimated 80% of the UK population support the use of renewable energy (Department of Energy & Climate Change, 2014), the success rate of planning applications is considerably lower. Between July 2012 and June 2013, for instance, 68% of onshore wind proposals submitted in the UK gained local approval, while in England and Wales the approval rates were just

59% and 46% respectively (RenewableUK, 2013). While opinion polls may simplify public responses to a certain extent (Walker, 1995), there is a clear mismatch between the UK's high level of support for renewable energy and the lower success rate of planning applications, known as 'the social gap' (Bell et al., 2005, 2013).

To explain this gap, Bell et al. (2005, 2013) propose that opponents include qualified supporters, who support renewable energy in principle but object to certain aspects of a given development, and perhaps self-interested NIMBYs (Not In My Back Yard), who oppose developments in their immediate vicinity. NIMBYism, however, has been widely criticised as a simplistic and pejorative term used to discredit the often well-founded objections of local residents (Devine-Wright, 2011a; Haggett, 2011; Wolsink, 1996). As a concept it lacks empirical support and is fundamentally inadequate as an explanation for the complex nature of public opinions and motives (Bell et al., 2005; Haggett, 2011; Krohn and Damborg, 1999; Michaud et al., 2008; Warren et al., 2005). The NIMBY label has also narrowed the focus of research to opposing attitudes, neglecting passive and supportive responses, and thereby limiting knowledge of public perceptions (Burningham et al., 2006; Devine-Wright, 2011a; Wolsink, 2006).

Support for renewable energy often stems from environmental concerns and ethical obligations to displace fossil fuel generation and reduce greenhouse gas emissions (Devine-Wright, 2011a; Ladenburg, 2010; Warren et al., 2005). Support may also be based on materialistic beliefs that renewable energy will create new employment opportunities for local workers (Dacre, 2007; Haggett, 2011; Ladenburg, 2010; Warren et al., 2005), provide cheap or free electricity (Devine-Wright, 2011a), and promote energy independence (Firestone and Kempton, 2007; Haggett, 2011; Jack Faucett Associates, Inc.,

1981; Ladenburg, 2010). The perceived benefits of the SeaGen tidal turbine installed in Northern Ireland were its familiar appearance (similar to that of a lighthouse) and visual 'fit' to the landscape (Devine-Wright, 2011a). Local residents felt a sense of pride and collective ownership of the groundbreaking scheme, which they believed truly put their area 'on the map' (Devine-Wright, 2011a). Similarly, Cornwall's Wave Hub development was supported for its potential economic benefits as well as its relatively low visual and environmental impacts (Bailey et al., 2011).

Ironically, the majority of public objections to renewable energy projects are also based on environmental and materialist grounds. Offshore renewable energy developments are often opposed due to concerns about the cumulative impacts of large developments on natural landscapes (Devine-Wright, 2011a; McLachlan, 2009; Walker, 1995; Warren et al., 2005; Wolsink, 1996, 2007) and marine life (Bailey et al., 2011; Devine-Wright, 2011a; Firestone and Kempton, 2007). Local stakeholders may also oppose developments fearing adverse impacts on local fisheries (Conway et al., 2010; Devine-Wright, 2011a; West et al., 2009), navigational safety (McLachlan, 2009), marine recreation (Firestone and Kempton, 2007), tourism (Haggett, 2008; McLachlan, 2009; Warren et al., 2005), property values (Warren et al., 2005), and even community harmony (Firestone and Kempton, 2007). Cornwall's Wave Hub development was opposed because some respondents feared a detrimental effect on local surfing conditions and a lack of compensation for displacement of the fishing industry from productive areas, while all respondents felt that the Wave Hub's job creation figures were exaggerated, possibly in an attempt to win the support of local communities* (West et al.,

* The South West Regional Development Agency estimated in 2009 that the Wave Hub would produce up to 100 direct and 1,000 indirect jobs (West et al., 2009). At the time of writing, Wave Hub employs 6 (RenewableUK, 2017; Wave Hub Ltd, 2017).

2009). Opposition may also be based on a desire to keep the ocean free of industrial development (Devine-Wright, 2011a; McLachlan, 2009; Warren et al., 2005) or perhaps a disbelief in, or simply apathy toward, global climate change (McLachlan, 2009; Warren et al., 2005).

Decision making, public engagement, and community ownership

Several authors have noted that support for renewable energy often follows a 'U'-shaped curve; with high support in principle, which declines when specific projects are proposed and increases again after their construction, perhaps even to higher than pre-development levels (Bailey et al., 2011; Wolsink, 2007). As such, it appears that besides any preconceived notions harboured by the public, opposition to renewable energy developments may be more related to the planning and decision making processes than to the projects themselves (Warren et al., 2005). Proposed solutions to this pattern of support and opposition include open communication between developers and local communities and greater public engagement in the planning stage (Krohn and Damborg, 1999; WaveNet, 2003). Public engagement through communication, consultation, or participation may speed up the decision making process and lead to greater level of support for the project (Devine-Wright, 2011b; Haggett, 2008; Yearley et al., 2003). Naturally, public engagement will not resolve all conflicts and the inclusion of local stakeholders may in fact result in a longer and more costly decision making process (Burningham et al., 2006; Echeverria, 2000; Irvin and Stansbury, 2004; Lawrence and Deagen, 2001; Rourke, 1984). However, this additional cost may prove a worthwhile investment if local knowledge allows developers

to identify concerns and potential conflicts early in the planning stage when it is easier to implement changes or consider alternatives (Haggett, 2008; Irvin and Stansbury, 2004; Jenkins and Garrison, 2013; Jones and Eiser, 2010; Portman, 2008; Walker, 1995; Yearley et al., 2003).

Experience from other forms of locally-unwanted land uses suggests that renewable energy developments may achieve greater public acceptance if they are implemented in such a way as to increase local community ownership and/or provide local benefits to compensate for their perceived negative impacts (Cass et al., 2010; Walker et al., 2010b). The offering of community funds as the gesture of a 'good neighbour' is fraught with difficulty, however, as such offers may be perceived as an attempt to influence the decision making process or silence opposition (Cass et al., 2010; Walker, 1995; Walker et al., 2010a). To assess the risks and benefits of novel technologies the public seeks advice from experts and authorities, but if these sources are viewed as untrustworthy the benefits of even familiar technologies may be ignored (Bronfman et al., 2012). In certain cases, renewable energy developers have shown a low level of community engagement in consultation and planning decisions, engendering cynicism amongst local stakeholders (Devine-Wright, 2011a). Moreover, when developers are community outsiders, trust becomes an issue because members of public may feel they are accepting a personal sacrifice for the benefit of developers (McLachlan, 2009; Wüstenhagen et al., 2007).

Despite evidence that suggests that the exclusion of stakeholders from decision making processes may dispel feelings of local ownership and lead to active opposition (Krohn and Damborg, 1999; McLachlan, 2009; Wolsink, 1996, 2007), the UK's marine renewables planning regime is strongly 'top-down' with little contribution from local authorities and communities (John-

son et al., 2012). A lack of public participation in planning does not automatically lead to protest because opponents may remain passive due to social pressures or a lack of confidence (Devine-Wright, 2011a; Waldo, 2012). Passive opposition undermines the certainty of the planning process, however, threatening conflicts, delays, and perhaps impasses (Waldo, 2012). It is thus unwise to assume the support of a passive population and instead a greater understanding of public opinions should be sought to improve renewable energy policies (Waldo, 2012; West et al., 2010).

External costs

Just as with any other energy facility, renewable energy developments may have external effects on natural land and seascapes, local economies, and tourism (Krueger et al., 2011; Ladenburg, 2010). In a Dutch study, Dröes and Koster (2014) found that the presence of an onshore wind turbine reduces the prices of the nearest houses by 2.6% and estimated the external costs of a single wind turbine to be at least 10% of its construction costs. In England and Wales, Gibbons (2014) found that the presence of a visible small to medium-sized onshore wind farm reduces the price of housing within 2 km by 5–6% on average. These results are consistent with studies that reveal the negative impacts of high voltage power lines and coal power plants on property values (Davis, 2011; Gibbons, 2014; Sims and Dent, 2005). Gibbons' (2014) findings suggest that households may be willing to pay £600–£1000 per year to avoid having a visible wind farm within 2 km of their property. Ladenburg and Dubgaard (2007) have shown that Danish households are willing to pay €33, €94, and €107 per year to increase the distance of an offshore wind farm from 8 km from the shore to 12, 18, or 50 km respectively. Similar results have been reported for offshore

wind farms in the USA by Krueger et al. (2011) and in both cases the most closely affected residents were willing to pay considerably more to reduce the visual impact. It is clear, therefore, that the external costs of renewable energy developments must be taken into consideration and balanced against the greater costs of deploying devices further offshore (Dröes and Koster, 2014; Krueger et al., 2011; Ladenburg and Dubgaard, 2007).

2.2 Ecological impacts

The ecological impacts of marine energy extraction remain unclear because interactions between devices and ecosystems are complex and dynamic — small changes may produce nonlinear responses and threshold effects in ecosystem structure and function (Scheffer et al., 2001) and although there exist theoretical frameworks to anticipate critical transitions (Scheffer et al., 2009, 2012), establishing cause and effect is extremely difficult (Lin and Yu, 2012; Wilson et al., 2007). Moreover, due to the emergent state of the industry and because research has thus far focused on the nature of marine resources and the technological aspects of exploiting them, there are few direct observations from which to draw conclusions (Bell and Side, 2011). Much less is known about marine ecosystems than terrestrial ecosystems due to limited access and the high cost of working in marine environments (Langhamer et al., 2010; Simas et al., 2009), and while it may be reasonable to suppose that the extraction of a small fraction of natural energy fluxes should result in minimal ecological implications, acceptable limits of extraction are not easily calculated (Shields et al., 2011). As such, the ecological impacts of marine energy will not be fully understood until prototype devices are installed and their effects monitored (Cada et al., 2007).

Research suggests that impacts are likely to vary with location and season, with the design and scale of both devices and arrays, and may be cumulative, both in time and with an increasing number of devices (Shields et al., 2009; Witt et al., 2012). Naturally, marine ecology must be considered during each stage of development and long-term studies must be undertaken to ensure adverse impacts are minimised or mitigated (Gill, 2005; Langhamer et al., 2010; Shields et al., 2009). The following subsections summarise present understanding of a number of potential ecological impacts.

Flow alteration

Marine energy devices may alter ambient flow patterns in different ways. Offshore wind turbines have fixed or floating support structures that may interact with local wave climates. Tidal turbines partially block current flows, accelerating flow around the device and creating highly-mixed flow in their wakes (El-Geziry et al., 2009; The Robert Gordon University, 2002). Wave energy extraction may alter nearshore currents, promote early wave breaking, and affect littoral drift and beach erosion. Research has shown that hydrodynamic processes play a key role in structuring soft-sediment communities but the ecological impacts of altering the hydrodynamics of energetic marine environments remain unclear (Langhamer, 2010; Shields et al., 2011). Waves and tides play a critical role in the regulation of marine ecosystems and modification of these natural energy fluxes may substantially alter the maintenance and functioning of these environments (Copping et al., 2013; Dacre, 2007; Shields et al., 2011).

Wave climates

Wave energy extraction may modify sediment suspension and transport (Shields et al., 2011; Simas et al., 2009), resulting in altered patterns and rates of shoreline erosion, deposition, and scour (Frid et al., 2012; Simas et al., 2009), reduced upper layer mixing, breaking waves and associated turbulence (Frid et al., 2012; Shields et al., 2011; Witt et al., 2012), and changes to beach morphology and coastal habitats (Boehlert and Gill, 2010; Shields et al., 2011). Since the majority of these processes already experience strong natural variation, however, the effects of energy extraction may be imperceptible (Shields et al., 2011). Millar et al.'s (2007) simulations of the 30 MW Wave Hub development off the coast of Cornwall, for instance, predict only a 1–2 cm reduction in wave height and negligible effects on wave periods. Similarly, Palha et al.'s (2010) modelling studies of a 202.5 MW array of Pelamis devices reveal changes in wave heights typically less than 5 cm and negligible effects on wave direction.

Current patterns

The extraction of energy from tidal currents alters the nature of the driving flow, so the potential impacts may range from the immediate vicinity of the device to several kilometres downstream (Ahmadian et al., 2012; Bryden and Couch, 2006; Couch and Bryden, 2004; Neill et al., 2009). Far-field impacts may be negligible at pilot-scale, so site-specific numerical modelling will be required to assess both the hydrokinetic resource and the far-field extraction effects (Polagye and Malte, 2011). Research suggests that the impacts of tidal current energy extraction may include modifications to current velocities and dynamics (Dacre, 2007), sediment transport pathways (Neill et al.,

2012; The Robert Gordon University, 2002), patterns and rates of erosion, deposition, and scour (Boehlert and Gill, 2010; Cada et al., 2007; Dacre, 2007; The Robert Gordon University, 2002), turbidity (Dacre, 2007; The Robert Gordon University, 2002), water quality (Ahmadian et al., 2012; Dacre, 2007; The Robert Gordon University, 2002), and even wave climates (Dacre, 2007; Frid et al., 2012). Through increased mixing, tidal energy devices may alter the amount and location of primary production and hence the suitability of foraging habitats (Frid et al., 2012; Scott, 2007). This is a source of major concern because recent studies of North Sea waters have shown 50% of a range of marine predators to forage in less than 5% of the 1000 km of transects surveyed, and only at certain times related to tidal mixing (Scott, 2007; Scott et al., 2010). Modelling studies have ruled out significant effects on water levels, however, because even full-scale arrays are likely to have a minimal impact on tidal elevations (Ahmadian et al., 2012; Neill et al., 2012). Results from the European Marine Energy Centre (EMEC) tidal turbine test site in the Orkney Islands highlight the production of complex turbulent flow, particularly near the seabed (Osalusi et al., 2009a,b; Shields et al., 2011). GIven that energetic channels are naturally turbulent, however, the extent to which this turbulent flow is enhanced by energy extraction remains unclear (Shields et al., 2011). Research from the SeaGen tidal turbine site reveals no significant changes to benthic habitats as a result of modified flow dynamics, turbulence, and scour patterns (Copping et al., 2013).

Sediment and nutrient transport

Marine energy developments may modify sedimentation patterns and in turn affect benthic communities (Shields et al., 2009). Erosion may be

expected alongside tidal turbines where currents are accelerated, while deposition may be expected upstream and downstream where currents are decelerated (Ahmadian et al., 2012; Ahmadian and Falconer, 2012; Shields et al., 2011). Scour pits, which form as flow accelerates around monopile substructures and erodes the seabed, represent a threat to both the stability of the support structure and the surrounding environment (Dacre, 2007). These pits are often colonised by mobile, fast-growing plant and animal species, and may affect local ecosystems by attracting non-native species (Zucco et al., 2006b). Scour protection may have a similar impact by introducing new materials to the seabed (Dacre, 2007; Whitehouse et al., 2011; Wilson and Elliott, 2009) and while it has been suggested that the protective layer results in a net habitat gain, the habitat gained may be notably different to the habitat lost (Whitehouse et al., 2011). Since the effects of scour are localised to an area roughly 6–10 times the support structure diameter, however, the ecological impact of scour is considered to be low (Dacre, 2007; Zucco et al., 2006b).

Modified sedimentation patterns and suspended sediment levels may adversely affect marine ecology by increasing local turbidity and decreasing light availability (Gill, 2005; Kadiri et al., 2012; Simas et al., 2009), altering nutrient levels, total metal and bacteria concentrations (Ahmadian et al., 2012; Kadiri et al., 2012; Shields et al., 2009), mobilising buried contaminants (Dacre, 2007; Gill, 2005), and scouring or smothering benthic habitats (Gill, 2005; Simas et al., 2009; Whitehouse et al., 2011). In addition, marine energy devices may alter circulation patterns and hence the transport of nutrients and larvae (Bell and Side, 2011), thereby influencing food availability and patterns of recruitment, reproduction, and predation (Copping et al., 2013; Shields et al., 2009; Simas et al., 2009). Variations in nutrient

levels may result in decreased primary productivity of algae (Witt et al., 2012) or even toxic algal blooms and deoxygenation (Gill, 2005). Depending on currents, however, dispersion should be rapid and thus any such impacts minimal and temporary (Dacre, 2007; Langhamer et al., 2010).

Disturbance to benthic habitats

During the installation and decommissioning phases of marine energy developments, benthic habitats may be disrupted and sessile organisms destroyed by the temporary anchoring of construction vessels, the digging and refilling of trenches for power cables, and the permanent anchoring of piles or mooring systems (Gill, 2005; Simas et al., 2009). Sediment transport pathways may be modified, benthic habitats disturbed, and the seabed eroded by construction activities and the thrashing of mooring lines during storms (Dacre, 2007; Kellermann et al., 2006; Krivtsov and Linfoot, 2012). Since this disturbance is localised and often temporary, however, the principal risk is to sensitive habitats (Dacre, 2007; OSPAR Commission, 2009; The Robert Gordon University, 2002). Preliminary research suggests that thermal radiation from cables may affect microbial activity in soft sediment habitats (OSPAR Commission, 2009), but the ecological impacts of device foundations and cable routes will require long-term study because changes in benthic habitats may occur with time delays of years (Langhamer, 2010).

Artificial reefs

The introduction of a hard substrate to a soft sediment environment may significantly impact marine ecology by creating an 'artificial reef' (Langhamer et al., 2010). Artificial reefs may alter local hydrodynamics and

sediment transport patterns, and enhance biomass and biodiversity by providing a rich food source and refuge from predators (Langhamer, 2010; Page et al., 1999; Wilhelmsson and Malm, 2008). Studies of offshore oil and gas platforms reveal higher levels of species richness and abundance than nearby areas (Consoli et al., 2012) and suggest that such structures provide valuable habitats for the recruitment and reproduction of a number of species (Helvey, 2002; Page et al., 1999; Schroeder and Love, 2004). However, the favourable conditions and greater prey densities of artificial reefs may also attract predators and non-native species (Davis et al., 1982; Grecian et al., 2010; Langlois et al., 2005; Sundberg and Langhamer, 2005), which may alter the composition and structure of the local ecosystem (Langlois et al., 2005; Lin and Yu, 2012; Page et al., 2006). Research from Sweden's Lysekil wave energy research site reports high concentrations of predators and suspension feeders around foundations (Langhamer, 2010; Lin and Yu, 2012), and studies of offshore wind turbine monopiles reveal an abundance of filter feeders, possibly as a result of active adult migration (Wilhelmsson and Malm, 2008). Due to the species-specific response observed, however, it is unclear whether artificial reefs are truly beneficial to benthic habitats (Gill, 2005; Langhamer et al., 2010; Langhamer and Wilhelmsson, 2009), and whether marine energy foundations should therefore be designed to enhance biodiversity and abundance or to minimize the impact on existing flora and fauna (Freeman et al., 2013; Gill, 2005; Langhamer et al., 2010; Langhamer and Wilhelmsson, 2009; The Robert Gordon University, 2002).

Marine protected areas

The potential for conflict exists where marine energy developments impact protected species and areas of conservation. The UK is internationally im-

portant for marine life, with Scotland's 24 cetacean species strictly protected by the EU Habitats Directive, and Special Areas of Conservation established for bottlenose dolphins, harbour porpoises, Atlantic grey seals, and harbour seals (Dolman and Simmonds, 2010; Skeate et al., 2012). In the Pentland Firth and Orkney Islands, for which large developments are planned, there are several Special Areas of Conservation and Special Protection Areas, mainly supporting sea birds and seals (Johnson et al., 2012). The development of marine energy may also benefit marine life, however, through the formation and active management of *de facto* marine reserves where fish stocks and benthic habitats are allowed to regenerate (Alexander et al., 2013; Sundberg and Langhamer, 2005; Witt et al., 2012).

Biofouling and pollution risk

Marine renewables must be designed to survive harsh marine environments and withstand high winds, strong currents, corrosion, fouling by debris, and encrustation by sea creatures (Dacre, 2007; WaveNet, 2003). Similar to artificial reefs, biofouling may benefit local ecosystems by enhancing biodiversity and species abundance, and providing refuge from predation (Frid et al., 2012; Langhamer et al., 2010; Lin and Yu, 2012). However, biofouling may also yield high sedimentation rates, resulting in eutrophication of the benthic ecosystem and lower biodiversity (Cada et al., 2007; Langhamer et al., 2010). Routine operation and maintenance activities carry risks of pollution, including chemical spills and the leaching of chemicals from anti-fouling paints (Boehlert and Gill, 2010; Lin and Yu, 2012; Witt et al., 2012) which may reduce the health and fitness of a range of marine species (Simmonds and Brown, 2010; Witt et al., 2012). Research suggests that biofouling may also reduce the efficiency of marine renewables by in-

creasing the mass and surface roughness of devices and mooring lines, and increase both the difficulty and costs of maintenance (Cada et al., 2007; Langhamer et al., 2010; Simas et al., 2009). However, studies from Sweden's Lysekil wave energy research site report no significant changes to the efficiency of point absorbers as a result of biofouling, and although increased surface roughness and turbulence may increase energy dissipation through viscous losses, this issue will be less significant for heavily damped systems (Langhamer et al., 2009).

Electromagnetic fields

Several studies have suggested that the electromagnetic fields (EMFs) emitted by submarine power cables may interfere with marine species' orientation and navigation, abilities to detect predators or prey, or result in adverse effects on growth, reproduction, or survival rates (Gill, 2005; Gill and Bartlett, 2010; Lin and Yu, 2012; Öhman et al., 2007; OSPAR Commission, 2009). However, laboratory-based studies have demonstrated that magnetic fields do not have significant impacts on the movements of migratory fish or on the survival or reproduction of several benthic animals (Bochert and Zettler, 2004; Zucco et al., 2006a). Some elasmobranch fish species have been shown to respond to EMFs, though these responses appear to be species-specific and perhaps even individual-specific (Gill et al., 2009); and while the swimming speed of eels does appear to be influenced by EMFs, it is unclear if this represents a biologically significant effect (Gill and Bartlett, 2010; Westerberg and Lagenfelt, 2008). In general, the risks of EMF emissions from marine energy developments are considered to be quite low but more research is required to validate this assumption (Freeman et al., 2013; Gill et al., 2012; Leeney et al., 2014).

Collision risk

With the deployment of marine renewables, a number of species are placed at risk of collision or entanglement with moving machinery or mooring lines, which may result in recoverable injury, permanent debilitation, or delayed or instant mortality (Benjamins et al., 2014; Wilson et al., 2007). The presence of devices may also modify habitat use and migration patterns, and alter survival or reproductive rates, which may drastically affect species population size and viability (Boehlert and Gill, 2010; Freeman et al., 2013; Kirby et al., 2013; Wilson et al., 2007). Marine renewables will be deployed in energetic marine environments, and such areas, particularly those with high tidal activity, are key foraging sites for marine birds and mammals (Freeman et al., 2013; Sparling et al., 2013; Wilson et al., 2007). Visibility is likely to be reduced in areas of strong tidal mixing due to increased turbidity and entrained air bubbles in the water column, and increasingly efficient energy converters will be more difficult for marine life to detect (Wilson et al., 2007). Small animals prefer regions of high turbidity as a refuge from predators, so the presence of devices may result in either avoidance of key foraging grounds or increased collision risks for fish and their predators (Wilson et al., 2007).

Tidal turbines (5–30 rpm) rotate slower than conventional hydropower turbines (80–600 rpm) or vessel propellers (70–140 rpm) (Copping et al., 2013), so objects are expected to be pushed safely between the blades rather than collide with them (Dacre, 2007; Wilson et al., 2007). Tidal turbine pilot sites in Northern Ireland, Scotland, and the USA have reported some degree of avoidance during operation but no incidences of strike-related injury or significant habitat exclusion (Copping et al., 2013). Normandeau Associates, Inc. (2009) have shown that even when fed directly into a 3.6 m

hydrokinetic turbine the survival rate for test fish was greater than 99%, with only two fatalities, one related to experimental malfunction and the other exhibiting no obvious external injuries (Copping et al., 2013).

Collision rates may be affected by a range of environmental and design parameters including flow rate, topography, visibility, and background noise, as well as the visual appearance of devices, their position in the water column, and relative orientation to other devices (Wilson et al., 2007). The placement of several devices in arrays may represent a complicated obstacle for approaching animals or create traps from which escape options are limited (Sparling et al., 2013; Wilson et al., 2007). Research suggests that the collision risk of an array may be greater than the sum of its parts, and that careful consideration should be given to the spacing between devices in arrays; as greater spacing may increase overall visibility and options for avoidance and safe passage between devices but may also increase the foraging area avoided by diving birds and marine mammals (Hammar et al., 2013; Wilson et al., 2007). The ability of marine animals to detect an obstacle and avoid a collision depends on body size, habitat use, foraging tactics, curiosity, underwater agility, and sensory capabilities (Wilson et al., 2007). Research suggests that when locked onto prey, echolocating animals may become blind to objects at greater distances, and that distraction by social interaction or concentrated food sources may also reduce marine mammals' perception of a collision threat (Wilson et al., 2007). Nevertheless, the risk of collision is considered to be quite low, particularly for agile species, and collisions are likely to be limited to young, old, transient, diseased, or disorientated individuals due to a lack of experience or reduced capabilities (Frid et al., 2012; Wilson et al., 2007).

Underwater noise

Underwater noise is a source of concern because sound is used by a wide range of species for communication, navigation, foraging, avoiding predators, and finding potential mates (Dacre, 2007; Gill, 2005). Unfortunately, however, impact assessments are limited by a lack of information regarding device performance data and species' behavioural responses (Robinson and Lepper, 2013). Little is known about background noise levels, the sound levels produced during each stage of development, or how these sounds may affect the ability of marine mammals to detect them (Nedwell et al., 2003; Patrício et al., 2009; Robinson and Lepper, 2013; Shields et al., 2009). Assessment of the impact of underwater noise is complex, partly because sound levels vary with device design, array layout, and oceanographic conditions (Dacre, 2007; Patrício et al., 2009) and partly because of the nature of sound transmission underwater, as it is possible that received sound levels could be higher at certain distant locations than at locations nearer to the source (Popper and Hastings, 2009). While a considerable amount of further research is required to assess definitively the ecological impact of anthropogenic sound on marine life (Boehlert and Gill, 2010; Popper and Hastings, 2009; Wilson et al., 2007), a range of potential impacts have been suggested. Underwater noise may result in physical harm, temporary or permanent hearing loss (Popper and Hastings, 2009), altered behaviours or patterns of movement (Boehlert and Gill, 2010; Frid et al., 2012), loss of habitat (Carstensen et al., 2006; Madsen et al., 2006; Tougaard et al., 2003), masking of important biological sounds (Weilgart, 2007; Wright et al., 2007), and increased vulnerability to predation and other hazards (Dacre, 2007; Simmonds and Brown, 2010). Moreover, noise-induced stress may result in hypertension, hormonal imbalance, and reduced resistance to disease among

marine mammals, although these effects may be practically impossible to measure (Simmonds and Brown, 2010; Weilgart, 2007; Wright et al., 2007).

The sounds produced by installation activities are a source of considerable concern, and several authors have highlighted pile-driving activities as particularly harmful (Madsen et al., 2006; Nedwell et al., 2003; Richardson et al., 1995). While detection distances depend on a variety of factors including species' hearing abilities and background noise levels (Wahlberg and Westerberg, 2005), research suggests that pile-driving activities may produce sound levels upwards of 185 dB re 1 μPa at 1 m (rms) (Bell and Side, 2011; Caltrans, 2001), which may be heard hundreds of kilometers away, mask biological sounds up to 80 km away, induce behavioural responses up to 20 km away, and inflict severe injuries on animals nearer to the sound source (Nedwell et al., 2003; Thompsen et al., 2006). During the construction of both the Horns Rev and Nysted offshore wind farms in Denmark, porpoises were driven from the construction area, returning only after pile-driving had ceased (Carstensen et al., 2006; Madsen et al., 2006; Tougaard et al., 2003). Similarly, the notable decline in haul-outs of harbour seals at the Scroby Sands wind farm corresponded exactly with pile-driving activities, although this may also be related to increased vessel activity in the area (Skeate et al., 2012). Thus far pile-driving has been limited to offshore wind farms, because the first wave and tidal energy devices have been installed using anchors or pile-drilling techniques (Bell and Side, 2011). Tidal turbine pilot sites in Northern Ireland and the USA have reported temporary displacement of marine life during installation activities and some degree of avoidance during operation but no incidences of significant habitat exclusion (Copping et al., 2013). In fact, studies of the SeaGen tidal turbine pilot site have shown harbour porpoises and seals to

swim freely within areas in which acoustic deterrence might be expected (Copping et al., 2013).

Performance data from marine energy devices are not yet available, but Bell and Side (2011) estimate that the sound levels produced during normal operation will not exceed 160 dB re 1 μPa at 1 m (rms). This is consistent with Robinson and Lepper's (2013) estimate that the sound produced by operating devices will be no greater than a modest-sized vessel travelling at a moderate speed. Studies of juvenile Chinook salmon have shown that tidal turbine noise may result in non-lethal levels of tissue damage, but that even after 24 hours of constant exposure to 155–163 dB re 1 μPa (rms), there was no damage to the auditory systems of the fish (Halvorsen et al., 2011). Robinson and Lepper (2013) conclude that the sound produced during the construction or operation of marine renewables is unlikely to cause damage or injury to marine species at relatively close range, or significant behavioural effects at long range. However, underwater noise and vibrations affect different species in different ways and with larger arrays and extended installation periods, noise exposure and habitat exclusion may become significant ecological concerns (Boehlert and Gill, 2010; Dacre, 2007; Frid et al., 2012).

Behavioural responses

Knowledge of marine species' perceptions of devices remains limited because behavioural responses are likely to be unpredictable, as animals may respond irrationally to novel situations (Simas et al., 2009; Wilson et al., 2007). Marine renewables may attract a variety of fish, predators, and curious species (Langton et al., 2011; Wilson et al., 2007) and the impacts of operational noise, vibrations, and EMFs will depend on their frequency, in-

tensity, and duration, as well as the abilities of marine species to habituate to them (Gill, 2005). Floating devices may attract sea birds and semi-aquatic species as perching posts or potential haul-out sites (Grecian et al., 2010; Wilson et al., 2007). Moving machinery poses a risk of injury, however, so manufacturers may design buoys to deter marine life and prevent damage to devices (Grecian et al., 2010; Wilson et al., 2007).

Alternatively, the looming appearance, movement, and low frequency noise of marine renewables may trigger avoidance responses, which may drive animals from key foraging, breeding, and resting grounds as well as alter migration routes and species' fitness levels (Wilson et al., 2007). Habitat alteration and changes to energy budgets may dramatically influence survival rates and population size, particularly during breeding seasons (Langton et al., 2011; Wilson et al., 2007). While studies have shown marine mammals to exhibit avoidance behaviour at first, experience suggests that over time they will learn to coexist with operating devices (Dacre, 2007).

2.3 Discussion

Social impacts

The most likely explanation for the complex nature of public responses is that renewable energy is interpreted by individuals in a way that reflects their personal beliefs about the environment and society as a whole (Krohn and Damborg, 1999). Individuals may support or oppose renewable energy based solely on these beliefs, and for some or all of the reasons outlined previously, without any understanding of the technological aspects of electricity generation (Conway et al., 2010). Renewable energy developments

may be seen as a source of clean, renewable power or as industrial installations, and their perceived 'fit' to the landscape may simply be a matter of taste (Krohn and Damborg, 1999; McLachlan, 2009; Wolf et al., 2009). Similarly, their experimental status may be interpreted positively, as part of a potential solution to climate change, or negatively, as suggesting that the impacts are unknown or unknowable (McLachlan, 2009; West et al., 2009). Experience of offshore wind developments suggests that aesthetic perceptions strongly influence individual responses (Warren et al., 2005) and while wave and tidal energy devices have a lower profile above the water level, flashing lights and exclusion zone markers will increase their visual impact (Bailey et al., 2011; Dacre, 2007; Haggett, 2008; WaveNet, 2003). Although renewable energy developments are generally deemed more acceptable when placed out of sight from coastlines (Jones and Eiser, 2010), placement further offshore does not guarantee public support because developments may still be seen as a threat to seascapes and marine life (Bailey et al., 2011; Haggett, 2008; Waldo, 2012). Interestingly, even individuals with the same core values may have opposing views of a proposed development, leading to a unique type of debate with environmentalists on both sides of the argument (Warren et al., 2005). 'Green-on-green' conflicts arise when one type of ethical or aesthetic value (e.g. to reduce greenhouse gas emissions) directly opposes another (e.g. to preserve a natural landscape) (Waldo, 2012; Warren et al., 2005).

Studies of public perceptions of wind power reveal a strong connection between the feeling and cognitive components of attitudes, meaning that negative opinions regarding the visual impact of wind turbines are often closely linked with beliefs that they are inefficient and unprofitable (Waldo, 2012). Moreover, surveys have shown that individuals who oppose wind

farms perceive wind turbines to be noisier and more visually intrusive than wind power supporters, regardless of actual noise levels or number of turbines (Gipe, 1995; Krohn and Damborg, 1999; Warren et al., 2005; Wolsink and Sprengers, 1993). These findings suggest a bias and prejudice inherent in public opinions of renewable energy; that regardless of the facts, responses are determined by individuals' own values and beliefs (Warren et al., 2005).

Research suggests that the threat of public hostility plays a key role in shaping the way decision-makers think about and undertake public engagement (Devine-Wright, 2011b; Walker et al., 2010a). Devine-Wright (2011b) argues that local opposition is a logical outcome of the flawed conceptions and practices of public engagement, and describes a vicious cycle in which poor public engagement practices (offering few opportunities for public involvement) lead to increased local opposition and hence to poorer public engagement practices (offering fewer opportunities for public involvement), which in turn lead to greater local opposition and so on. Breaking this cycle will require a rethinking of current public engagement practices, with a focus on nurturing social consent (Devine-Wright, 2011b; Devine-Wright et al., 2013). As each case is different, there is no simple formula to enhance public support (Devine-Wright et al., 2013; Haggett, 2011; Walker, 1995) but Devine-Wright et al. (2013) highlight the importance of local benefit provision, timely and meaningful engagement, trust, and fair and inclusive planning procedures.

Experience of wind energy has shown community ownership, in which community members invest to become part owners of the project, to be an effective means of encouraging not only support for renewable energy, but also community empowerment and self-sufficiency (Haggett, 2011; Walker, 2008). Micro-generation projects often face significant challenges, however,

and with marine energy developments there may be limited requirement to engage with local planning processes and hence less incentive to consider community ownership (Johnson et al., 2013; Walker, 2008). Small-scale installations may not make the best use of marine energy resources, but direct ownership is only one way by which local communities may benefit from renewable energy projects. In 1972, following an appeal to the Westminster parliament, the Shetland Islands Council was granted a share in the development of its emerging oil industry and authority over certain aspects of its operation (Johnson et al., 2013). As a result, the Shetland Islands benefitted greatly from the new developments as community shares in oil revenue were recycled into the local economy (Johnson et al., 2013). Though the nature of the marine energy industry is notably different, it has been suggested that this model could be repeated quite well with marine renewables (Johnson et al., 2012, 2013).

Ecological impacts

Perhaps the greatest barrier to the deployment of marine energy is the overwhelming lack of certainty surrounding the environmental impacts, exacerbated by considerable variation in device design, a lack of baseline environmental data, and the complexity of assessing the ecological impacts on a range of species (Copping et al., 2013; Shields et al., 2009; Witt et al., 2012). The marine energy industry has progressed faster than proper monitoring procedures, resulting in inadequate environmental assessments and little calibration between them (Boehlert and Gill, 2010; Evans, 2007; Inger et al., 2009). To satisfy the EU Habitats Directive requirements, the Scottish Government has adopted a policy of 'survey, deploy, and moni-

tor' to identify and mitigate adverse environmental impacts (Johnson et al., 2012). Besides the obvious difficulties of monitoring even immediate ecosystem responses, this initiative requires that established courses of action be reversed if necessary, which may not always be possible (Copping et al., 2013; Johnson et al., 2012).

While the ecological impacts of marine energy extraction remain largely unclear, several authors have suggested means by which to minimise potential impacts. For example, the harmful effects of underwater noise may be reduced through the use of acoustic deterrents, soft-start mechanisms, or sound-dampening techniques and materials such as vibropiling and bubble curtain systems (Nedwell et al., 2003; Würsig et al., 2000; Zucco et al., 2006b). Similarly, EMF emissions and the risks of contamination and pollution may be greatly reduced through the use of adequate cable shielding, non-toxic chemicals, and by ensuring that hydraulic fluids are well sealed within machines (Cada et al., 2007). Moreover, installation activities should be timed to protect sensitive species and habitats (Boehlert and Gill, 2010; Nedwell et al., 2003), and where possible feeding grounds and migratory routes should be avoided (Langhamer et al., 2010; Snyder and Kaiser, 2009; Sundberg and Langhamer, 2005). To minimise their environmental impact, proposals should be assessed on a case-by-case basis, and marine ecology should be considered at each phase of development; by selecting sites appropriately, conducting baseline environmental studies and risk assessments, identifying and mitigating adverse effects as early as possible, and continuously monitoring for long-term or cumulative impacts (Bell and Side, 2011; Gill, 2005; Shields et al., 2009; Witt et al., 2012).

2.4 Conclusions

This chapter summarises present understanding of both the social (e.g. Bell et al., 2013; Devine-Wright et al., 2013; West et al., 2010) and ecological (e.g. Copping et al., 2013; Shields et al., 2011; Simas et al., 2009) issues associated with marine energy development. For marine energy to be truly sustainable, a greater understanding of both the associated social and ecological impacts is essential. Modifications to wave climates, flow patterns and marine habitats, particularly through increased underwater noise and collision risk, are identified as key ecological issues in need of further research. Each development is unique but it is clear that renewable energy policies will benefit greatly from a deeper understanding of public opinions; how they are formed and how they evolve in response to a given development strategy (Devine-Wright et al., 2013; Waldo, 2012; Walker, 1995; West et al., 2009, 2010; Wolsink, 1996).

Public responses to proposed renewable energy developments are technology and location specific, and influenced by a wide range of factors (Bailey et al., 2011; Haggett, 2011; Warren et al., 2005; Wolsink, 1996). Individuals and groups may not be opposed to renewable energy *per se* but rather to certain characteristics of a particular development (Walker, 1995). Certain locations may be closely linked with a sense of identity and belonging that industrial installations may appear to threaten, despite their environmental benefits (Devine-Wright, 2011a,b; Devine-Wright and Howes, 2010; McLachlan, 2009). Research suggests that open communication, education, information sharing, and improved public engagement practices can lead to greater public acceptance of renewable energy developments (Inger et al., 2009; Krohn and Damborg, 1999; Waldo, 2012; WaveNet, 2003). By avoid-

ing recurrent delays and exaggerated economic projections, and ensuring that procedures remain fair and inclusive, developers can gain the trust and confidence of local communities (Bailey et al., 2011; Bronfman et al., 2012; Gross, 2007; Irvin and Stansbury, 2004; Portman, 2008; Walker et al., 2010b; West et al., 2009; Wolsink, 1996, 2000). However, there are still several unresolved issues in UK marine legislation regarding the rights of developers, and stakeholders' rights to marine resources and to participate in decision making processes (Haggett, 2011; Johnson et al., 2012; Portman, 2008; Todd, 2012). The resolution of these issues may greatly influence public opinions of marine energy and responses to future developments.

While the environmental impacts of marine renewables must be viewed within the wider context of continued reliance on fossil fuels and climate change (Frid et al., 2012; Grecian et al., 2010; Shields et al., 2011), it is vital that the haste to exploit wave and tidal current resources does not inadvertently create new environmental threats or exacerbate existing ones (Dolman and Simmonds, 2010; Portman, 2008). Though research suggests that animals are unlikely to be killed or seriously injured as a result of collision with devices or exposure to operational or pile-drilling noise, current information is limited to a small number of deployments and few observational studies (Copping et al., 2013; Freeman et al., 2013; Kirby et al., 2013; Sparling et al., 2013). Due to the emergent state of the industry, and because research is primarily focused on resource assessments and the technological aspects of generation, the ecological impacts of marine renewables will not be fully understood until devices are installed and their effects monitored (Bell and Side, 2011; Cada et al., 2007). Even then, impacts will vary with location and season, with the design and scale of both devices and arrays, and may be cumulative, both in time and with an increasing number of de-

vices (Frid et al., 2012; Leeney et al., 2014; Shields et al., 2009; Witt et al., 2012). Accordingly, it is vital that developers establish an iterative design process whereby results from environmental monitoring studies, as well as performance and cost data, are fed back to encourage more efficient, more cost-effective, and more environmentally-sensitive designs. A number of authors have called for the integration of multi-disciplinary scientific research to investigate the environmental effects of marine energy and to mitigate any adverse ecological impacts (Boehlert and Gill, 2010; Cada et al., 2007; Copping et al., 2013; Freeman et al., 2013; Gill, 2005; Kirby et al., 2013; Leeney et al., 2014; Witt et al., 2012). A more strategic and collaborative research effort between developers, academia, and the public sector will lead to improvements in environmental monitoring standards and in best practices for device and array design (Boehlert and Gill, 2010; Freeman et al., 2013; Kirby et al., 2013; Leeney et al., 2014).

Chapter 3

Theoretical models of tidal turbines

Ocean tides are a promising source of clean and predictable energy but the design of a tidal turbine array is complicated by the complex and dynamic nature of the tidal current resource and the various ways in which turbines interact with the flow field. The fundamental problem is that the power available to a tidal turbine depends on the throughflow velocity, which in turn depends on the balance of forces driving and resisting the flow (Garrett and Cummins, 2008). Part of the resistance to flow will be natural, due to background roughness and other dynamic effects, but part will be due to the turbine itself, which slows the flow passing through and accelerates the flow passing around it (Garrett and Cummins, 2005, 2007; Vennell, 2010). One of the key challenges in modelling tidal turbine arrays is to capture accurately the interactions between the turbines and the resource at each of the relevant length scales (Adcock et al., 2015; Vennell et al., 2015). More difficult still is the task of finding the optimal position and tuning for each turbine within a large array (Funke et al., 2014; Vennell et al., 2015).

Detailed numerical models may provide accurate solutions to specific problems but it is often the case that simple theoretical models provide the most useful insights. In recent years, such models have improved greatly our understanding of both turbine performance and the response of current resources to energy extraction. In this chapter, theoretical models of tidal turbines are reviewed under three broad headings: (i) those that use actuator disc theory to model flow through a single turbine; (ii) those that use the shallow water equations or an electrical analogy to model flow through a channel, or network of channels, containing a large number of turbines, and; (iii) those that combine a number of such models to explore the optimal arrangement of tidal turbines in arrays.

3.1 Turbine models

Actuator disc theory was developed by Rankine (1865) and Froude (1889) to model ship propellers and later adapted by Betz (1920) and Joukowsky (1920) to explore the performance of wind turbines. This model simplifies complex fluid problems by replacing the turbine rotor with a simple porous disc that presents a uniform resistance to the incoming flow. Analysis of the resulting simplified flow field allows important observations to be made about the physics of energy extraction from fluid flow.

Unbounded actuator disc model

Betz (1920) and Joukowsky (1920) used actuator disc theory to explore the performance of an idealised wind turbine. In this classic analysis, the turbine is represented by a disc of cross-sectional area A, corresponding to the swept area of the turbine rotor, and an axial thrust T, representing the

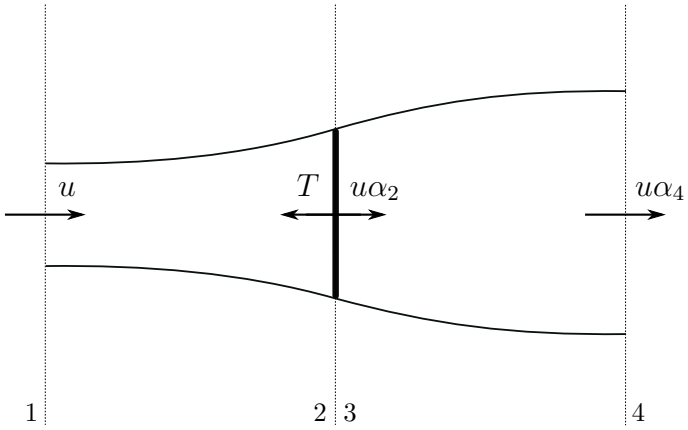

Figure 3.1: Classic actuator disc model of a turbine in unbounded flow. Side/plan view, adapted from Houlsby et al. (2008).

resistance to flow through it. The thrust exerted by the disc causes the streamtube of flow passing through it to slow and expand. The equal and opposite thrust exerted on the disc by the flow is used to extract power. The basic physics of the problem is intuitive. If the resistance of the disc is too small, flow will pass through it largely unaffected and little power will be extracted. If its resistance is too great, flow through the disc will be severely reduced and its power similarly limited. Between these extremes, there must exist an optimal resistance to maximise the power output.

To investigate this further, control volume techniques are applied to the streamtube of core flow passing through the disc (figure 3.1). The flow is assumed to be uniform, steady, incompressible, and unidirectional, with viscous forces and rotation confined to the surface of the streamtube (Draper, 2011). As flow passes through the streamtube, its velocity reduces from the upstream velocity u to $u\alpha_2$ at the disc and a minimum of $u\alpha_4$ further downstream, in which α_2 and α_4 are the turbine plane and wake velocity coefficients, respectively. The fluid static pressure, meanwhile, increases from the upstream pressure p to p_2 in front of the disc, reduces instantaneously to p_3 behind it, and recovers to once again equal the upstream static pressure further downstream. Following Houlsby et al. (2008), the condition of the

flow is considered at four stations: 1, located far upstream of the disc; 2 and 3, located immediately upstream and downstream of the disc, respectively; and 4, located sufficiently far downstream of the disc that the static pressure is again uniform across the cross-section, although the velocity is not.

Applying conservation of energy to the core flow between stations 1 and 2 and between stations 3 and 4 gives:

$$p + \frac{1}{2}\rho u^2 = p_2 + \frac{1}{2}\rho(u\alpha_2)^2, \tag{3.1}$$

$$p_3 + \frac{1}{2}\rho(u\alpha_2)^2 = p + \frac{1}{2}\rho(u\alpha_4)^2, \tag{3.2}$$

in which ρ is the fluid density. Combining these equations gives an expression for the static pressure difference across the disc:

$$p_2 - p_3 = \frac{1}{2}\rho u^2(1 - \alpha_4^2), \tag{3.3}$$

from which an expression for the applied thrust follows:

$$T = \frac{1}{2}\rho A u^2(1 - \alpha_4^2). \tag{3.4}$$

An alternative expression for the thrust is obtained by applying conservation of momentum to the flow between stations 1 and 4:

$$T = \rho A u^2 \alpha_2(1 - \alpha_4). \tag{3.5}$$

Combining equations 3.4 and 3.5 gives:

$$\alpha_2 = \frac{1 + \alpha_4}{2}, \tag{3.6}$$

which shows that the velocity at the disc is simply the average of the upstream and downstream values. The applied thrust and extracted power

may then be expressed in terms of a single parameter, α_4:

$$T = \frac{1}{2}\rho A u^2(1-\alpha_4^2) = \frac{1}{2}\rho A u^2 C_T, \tag{3.7}$$

$$P = Tu\alpha_2 = \frac{1}{2}\rho A u^3(1-\alpha_4^2)\left(\frac{1+\alpha_4}{2}\right) = \frac{1}{2}\rho A u^3 C_P, \tag{3.8}$$

in which C_T is a dimensionless thrust coefficient that defines the ratio of applied thrust to the integral of the upstream dynamic pressure, and C_P is a dimensionless power coefficient that defines the ratio of extracted power to upstream kinetic flux. Maximising equation 3.8 with respect to α_4 gives a maximum C_P of 16/27, which is obtained when $\alpha_4 = 1/3$ and $\alpha_2 = 2/3$. This result — that a wind turbine may extract no more than 59.3% of the wind's kinetic energy — was derived independently by Betz and Joukowsky, but is commonly known as the Betz limit. Okulov and van Kuik (2012) note that this limit was probably also deduced by other authors but not by Lanchester (1915), as is commonly reported.

The analysis used to derive this limit assumes a highly simplified fluid flow. It does not consider, for instance, either wake rotation or frictional drag between the fluid and the rotating blades, both of which will reduce the available power (Glauert, 1947; Wilson and Lissaman, 1974). Moreover, Houlsby et al. (2008) note that the ambiguity of the static pressure difference across the disc means that an expression for the resulting pressure thrust cannot be developed and, as a result, its effects are simply neglected. Houlsby et al. have since shown, however, that in the limit of unbounded flow this pressure thrust is negligible. It is also clear that further downstream of the disc, an additional amount of energy will be removed from the fluid as the slower core flow mixes with the faster bypass flow (Corten, 2000; Garrett and Cummins, 2007).

Bounded disc models

Despite the simplifications involved in its development, the Betz limit has proven a useful benchmark by which to assess wind turbine performance. In recent years, actuator disc theory has been extended to explore the performance of tidal turbines. The first notable extension is the volume-flux constrained (i.e. 'rigid lid') model due to Garrett and Cummins (2007), which accounts for the fact that, unlike wind turbines, tidal turbines operate in flows that are bounded by the proximity of the seabed and free surface and perhaps by the presence of neighbouring turbines. The second is the open channel model due to Houlsby et al. (2008) (and later Houlsby and Vogel (2016)) which accounts for the fact that, in open channel flow, the free surface deforms in response to energy extraction.

Both of these models assume that the flow boundaries are flat, smooth, and parallel; that, for the purposes of control volume analysis, the flow may be separated into core and bypass streamtubes containing the flow passing through and around the disc, respectively, and; that the flow conditions at the model inlet are unaffected by the performance of the disc (Vogel, 2014). The models differ, however, in their treatment of static head variation along the channel (Vogel, 2014). Open channel theory shows that the removal of energy from a subcritical flow causes a reduction in fluid depth and an associated increase in velocity downstream (Draper, 2011; White, 2009). While this is modelled explicitly in the model of Houlsby et al. (2008), Garrett and Cummins (2007) simplify the problem by assuming a small change in depth and treating the static head variations as pressure variations along a channel of constant cross-section. The rigid lid model is therefore an approximation to the open channel model, which becomes exact as the Froude number of the flow tends to zero (Vogel, 2014).

Rigid lid actuator disc model

Garrett and Cummins (2007) extended the classic unbounded actuator disc model to explore the performance of an idealised tidal turbine in bounded flow. In this analysis, a disc of cross-sectional area A is placed into a flow of constant cross-sectional area AR, in which the turbine blockage ratio $B = 1/R$, and control volume techniques are used to analyse separately the core and bypass flow streamtubes (figure 3.2). The key difference between this bounded flow analysis and the previous unbounded analysis is that the bypass flow must now accelerate around the disc (Draper, 2011). As the core streamtube expands, the confining effect of the flow boundaries causes the bypass streamtube to contract. This constriction causes the bypass velocity to increase, in accordance with mass flux conservation, and the bypass static pressure to reduce, in accordance with energy conservation (Draper, 2011). Continuity gives the peak velocity coefficient for the bypass flow as:

$$\beta_4 = \frac{1 - B\alpha_2}{1 - B(\alpha_2/\alpha_4)}. \tag{3.9}$$

Applying conservation of energy to the core flow upstream and downstream

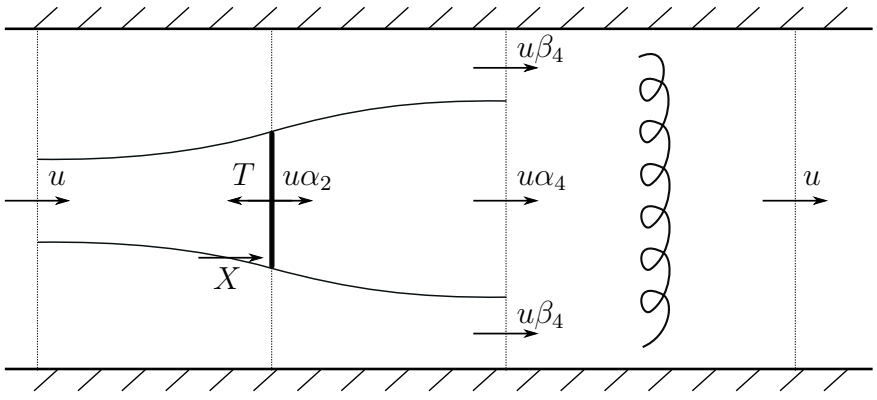

Figure 3.2: Actuator disc model of a turbine in volume-flux constrained flow. Side/plan view, adapted from Houlsby et al. (2008).

of the disc, and to the bypass flow between stations 1 and 4:

$$p_2 - p_3 = p - p_4 + \frac{1}{2}\rho u^2(1 - \alpha_4^2), \tag{3.10}$$

$$p - p_4 = \frac{1}{2}\rho u^2(\beta_4^2 - 1), \tag{3.11}$$

and combining equations 3.10 and 3.11 gives an expression for the static pressure difference across the disc:

$$p_2 - p_3 = \frac{1}{2}\rho u^2(\beta_4^2 - \alpha_4^2), \tag{3.12}$$

from which an expression for the applied thrust follows:

$$T = (p_2 - p_3)A = \frac{1}{2}\rho A u^2(\beta_4^2 - \alpha_4^2) = \frac{1}{2}\rho A u^2 C_T. \tag{3.13}$$

Applying conservation of momentum to both the core and bypass flows between stations 1 and 4:

$$\frac{pA}{B} - \frac{p_4 A}{B} - T = \rho A u^2 \alpha_2(\alpha_4 - 1) + \frac{\rho A u^2}{B}(1 - B\alpha_2)(\beta_4 - 1), \tag{3.14}$$

$$\therefore p - p_4 = \frac{TB}{A} + \rho u^2 \left(\frac{\alpha_2}{\alpha_4}\right) \frac{B(1 - \alpha_4^2)}{(1 - B(\alpha_2/\alpha_4))}, \tag{3.15}$$

and combining equations 3.11, 3.13, and 3.15 gives:

$$\alpha_2^2(B - 3B\alpha_4) + \alpha_2(2\alpha_4^2 + 2B\alpha_4^2) + (-\alpha_4^2 - \alpha_4^3) = 0. \tag{3.16}$$

For bounded flow, the model solution is a function of both turbine blockage B and tuning α_4. The most convenient solution of equation 3.16 is:

$$\alpha_2 = \frac{1 + \alpha_4}{(1 + B) + \sqrt{(1 - B)^2 + B(1 - (1/\alpha_4)^2)}}. \tag{3.17}$$

In the limit of unbounded flow (i.e. as $B \to 0$), $\alpha_2 \to (1+\alpha_4)/2$ and $\beta_4 \to 1$, which are consistent with the classic analysis. In the limit of fully blocked

flow (i.e. as $B \to 1$), $\alpha_2 \to \alpha_4$ and β_4 becomes undefined. This result is intuitive because when the cross-section is fully blocked, there is no space for either bypass flow or further expansion of the core flow downstream of the disc. The available power is given by:

$$P = Tu\alpha_2 = \frac{1}{2}\rho A u^3 \alpha_2(\beta_4^2 - \alpha_4^2) = \frac{1}{2}\rho A u^3 C_P. \tag{3.18}$$

For all B, equation 3.18 is maximised by $\alpha_4 = 1/3$, for which equation 3.17 gives $\alpha_2 = 2/(3(1+B))$. Substituting these into equation 3.18 gives:

$$P_{(max)} = \frac{1}{2}\rho A u^3 \left(\frac{16}{27}\right)\frac{1}{(1-B)^2}, \tag{3.19}$$

$$\therefore C_{P(max)} = \left(\frac{16}{27}\right)\frac{1}{(1-B)^2}, \tag{3.20}$$

from which it is clear that much more power may be extracted from bounded flow than from unbounded flow. In the limit of unbounded flow, $C_{P(max)} \to 16/27$, which is consistent with the classic analysis, whereas for bounded flow, $C_{P(max)}$ increases monotonically above this limit with blockage (Draper, 2011). This is explained as follows. In unbounded flow, the static pressure in the near wake of the disc is assumed to be atmospheric ($p_4 = p$), which implies that the disc only extracts energy from the kinetic energy flux of the moving fluid (Nishino and Draper, 2015). It is for this reason that the power coefficient C_P is traditionally defined in terms of the fluid kinetic flux. The thrust exerted by the disc slows the incoming flow, converting a fraction of its kinetic energy into a static pressure difference across the disc. The extracted power is the product of the equal and opposite thrust exerted on the disc and the throughflow velocity. In bounded flow, however, the expansion of the core streamtube causes a constriction of the bypass streamtube, which causes the bypass velocity to increase ($\beta_4 > 1$, in ac-

cordance with mass flux conservation) and the bypass static pressure to decrease ($p_4 < p$, in accordance with energy conservation). In this way, the confining effect of the flow boundary induces a streamwise pressure gradient in the bypass streamtube, which must be balanced (by definition, since the core and bypass pressures are equal at station 4) by an equal pressure gradient in the core streamtube. This streamwise pressure gradient increases the static pressure difference across the disc (as is seen by comparing equations 3.12 and 3.3), thereby increasing the available power.

The physical effect underlying this performance enhancement is pressure gradient drag, a well-known phenomenon in aerodynamics and wind tunnel testing (e.g. Glauert, 1928b; Taylor, 1928). As noted by Glauert (1928a), the streamwise pressure gradient induced in bounded flow produces a greater drag force than a body would experience in unbounded flow. The additional drag experienced by the body is a result of the additional work done in deflecting and accelerating flow around it (Glauert, 1933). As compared to a disc in unbounded flow, a disc in bounded flow must therefore experience an additional pressure thrust X. Following Houlsby et al. (2008), an expression for X may be developed by applying conservation of momentum to the bypass flow between stations 1 and 4:

$$pA\left(\frac{1}{B} - \alpha_2\right) - p_4 A\left(\frac{1}{B} - \frac{\alpha_2}{\alpha_4}\right) + X = \rho A u^2 \left(\frac{1}{B} - \alpha_2\right)(\beta_4 - 1). \quad (3.21)$$

Substituting the expression for p_4 given by equation 3.11 and setting $p = 0$, to consider only changes from atmospheric pressure, gives:

$$X = \frac{1}{2}\rho A u^2 \left(\frac{\alpha_2}{\alpha_4}\right)(\beta_4 - 1)(1 - \alpha_4), \quad (3.22)$$

and since $\alpha_4 \leq 1 \leq \beta_4$ for bounded flow, X must be finite and positive for all B. In unbounded flow, there are no boundaries to cause bypass

acceleration ($\beta_4 = 1$) and thus no induced pressure gradient ($p_4 = p$) to produce the additional pressure thrust X, so the Betz limit applies. In bounded flow, however, X accelerates flow both around and through the disc, allowing C_P to exceed the Betz limit.

The fact that more power may be extracted from a bounded flow implies that the disc extracts power not only from the fluid kinetic flux, but also from the induced pressure head (Nishino and Draper, 2015). It is for this reason that, in bounded flow, C_P may easily exceed the Betz limit and even unity. In fact, for this volume-flux constrained flow, because the disc is assumed to extract power only from the pressure head and not from the kinetic flux, in the limit of fully blocked flow, C_P may approach infinity. This is because, as the blockage approaches unity, the cross-sectional area of the bypass streamtube must approach zero and, to conserve mass flux, the bypass velocity must therefore tend to infinity (Draper, 2015). This causes the static pressure difference across the turbine to become infinitely large and, because C_P is defined only in terms of the kinetic flux, the available power to appear infinite. It is clear then that, for bounded flow, the Betz limit is not applicable and C_P is an imperfect metric for turbine performance. However, despite efforts by Houlsby et al. (2008) to introduce a new power coefficient to account for the contributions of both the kinetic flux and the pressure head to the extracted power, the traditional C_P is still widely used.

In addition to the four stations defined previously, the condition of the flow may now be considered at a fifth station, located sufficiently far downstream of the disc that the core and bypass flows have completely mixed and the flow is once again of uniform velocity and static pressure (figure 3.2). Stations 4 and 5 may now be referred to as the near and far wakes

respectively. The near wake is the location at which the streamtube of core flow stops expanding. It is at this point that the core velocity is lowest ($u\alpha_4$), the bypass velocity is highest ($u\beta_4$), and the core and bypass pressures have equalised (p_4). Downstream of this point the core and bypass flows mix together to produce a flow of uniform velocity and pressure. In the far wake the velocity is once again equal to the upstream velocity u but the static pressure p_5 is now lower than the upstream static pressure p.

Between the near and far wakes some additional energy is dissipated as mixing of the core and bypass streamtubes restores the flow to a uniform state. Recognising that the power extracted by the disc therefore constitutes only a fraction of the total power removed from the flow, Garrett and Cummins introduced a measure of extraction efficiency η, defined as the ratio of power extracted by the disc (available power) to total power removed from the flow (extractable power), which includes wake mixing losses. (η is often termed the 'basin' or 'farm efficiency' to distinguish it from the traditional measure of efficiency, C_P.) The extractable power may be expressed in terms of the difference in energy flux between the model inlet and outlet, while the available power (given by equation 3.18) is the product of the thrust exerted on the disc and the throughflow velocity. In volume-flux constrained flow, the extraction efficiency is:

$$\eta = \frac{P_{av}}{P_{ex}} = \frac{Tu\alpha_2}{(p - p_5)Au} = \alpha_2. \tag{3.23}$$

For all B, maximum efficiency ($\eta = 1$) coincides with zero power extraction (as is seen by substituting $\alpha_4 = 1$ into equations 3.17, 3.9, and 3.18), while for maximum power extraction ($\alpha_4 = 1/3$), $\eta = 2/3(1 + B)$. This suggests that, for an optimally tuned turbine, the efficiency ranges from $2/3$ for $B = 0$ to $1/3$ for $B = 1$. Thus, although a turbine in bounded flow may extract

more power than one in unbounded flow, it does so less efficiently (Draper, 2011). This is because the greater thrust that may be applied in highly blocked flow increases the difference between the core and bypass velocities and thus produces greater mixing losses. As noted by Draper and Nishino (2014a,b), the most important conclusion is that, although both metrics are important, high extraction efficiency does not coincide with maximum power extraction.

A key assumption of the volume-flux constrained model is that the change in depth associated with energy extraction is small compared with the total depth of fluid. Noting that maximum efficiency means zero power extraction, Garrett and Cummins revisit this assumption for a disc tuned to maximise available power ($\alpha_4 = 1/3$). The deformation of the free surface will be greatest in the near wake, where the static pressure is lowest. For an optimally-tuned disc, equation 3.11 gives:

$$p - p_4 = \frac{4B(3-B)}{9(1-B)^2}\rho u^2. \tag{3.24}$$

The change in depth will be small as long as this change in pressure ($p - p_4$) is small compared to the static pressure $\rho g h$, or mathematically, as long as:

$$\frac{u^2}{gh} << \frac{9(1-B)^2}{4B(3-B)}. \tag{3.25}$$

The requirement that the Froude number ($u/\sqrt{gh}$) of the flow is small is therefore generally sufficient to ensure that the change in depth is small. This requirement becomes more strict as the blockage increases, however, because increasing bypass velocities are associated with greater changes in depth (Garrett and Cummins, 2007).

Open channel actuator disc model

Houlsby et al. (2008) extended the works of both Garrett and Cummins (2007), which incorporates the effects of blockage, and Whelan et al. (2009), which explores the effects of free surface deformation, to explore the performance of an idealised tidal turbine placed into an open channel flow. This open channel model accounts for the fact that removal of energy from a subcritical flow causes a reduction in fluid depth and an associated increase in velocity downstream of the turbine (White, 2009). Though somewhat counterintuitive, the increase in fluid kinetic flux downstream of a tidal turbine is consistent with open channel theory (Draper, 2011; White, 2009).

The analysis proceeds much as before but the energy of the flow is now expressed in terms of its total head and the pressures at stations 1, 4, and 5 are assumed to be hydrostatic (figure 3.3). The thrust exerted on the flow now produces a discontinuous change in fluid depth across the disc, which begins to recover immediately. As the bypass flow accelerates around the disc, the bypass depth reduces in accordance with energy conservation. The rising core and falling bypass depths equalise in the near wake of the

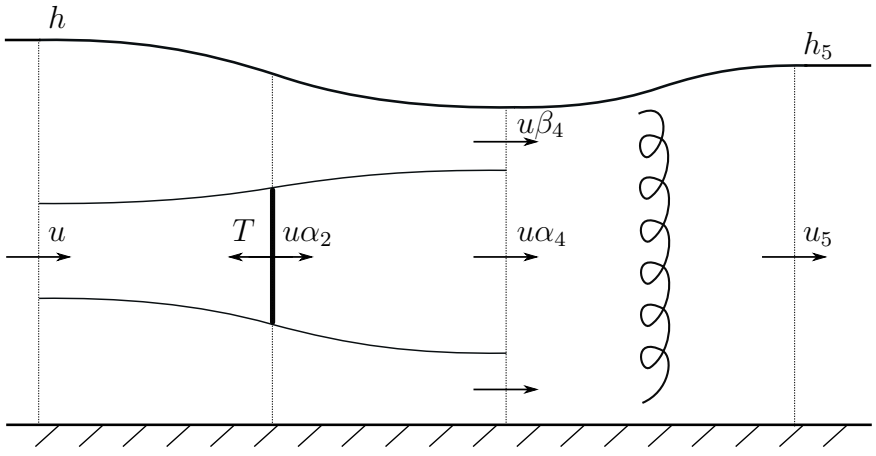

Figure 3.3: Actuator disc model of a turbine in open channel flow. Side view, adapted from Houlsby et al. (2008).

disc. Downstream of this point, the core and bypass flows mix together to produce a flow of uniform velocity and depth in the far wake. In the far wake, the depth h_5 is lower than the upstream depth h and, because mass flux is conserved, the velocity u_5 is greater than the upstream value u. Applying conservation of energy to the core flow upstream and downstream of the disc, and to the bypass flow between stations 1 and 4:

$$h + \frac{u^2}{2g} = h_2 + \frac{(u\alpha_2)^2}{2g}, \tag{3.26}$$

$$h_3 + \frac{(u\alpha_2)^2}{2g} = h_4 + \frac{(u\alpha_4)^2}{2g}, \tag{3.27}$$

$$h + \frac{u^2}{2g} = h_4 + \frac{(u\beta_4)^2}{2g}, \tag{3.28}$$

in which g is gravitational acceleration. Combining equations 3.26, 3.27, and 3.28 gives an expression for the change in depth across the disc:

$$h_2 - h_3 = \frac{u^2}{2g}(\beta_4^2 - \alpha_4^2), \tag{3.29}$$

from which an expression for the applied thrust follows:

$$T = \frac{1}{2}\rho g A(h_2 - h_3) = \frac{1}{2}\rho u^2 Bbh(\beta_4^2 - \alpha_4^2), \tag{3.30}$$

in which b is the channel width. Applying conservation of momentum to both the core and bypass flows between stations 1 and 4:

$$\frac{1}{2}\rho g b(h^2 - h_4^2) - T = \rho u^2 Bbh\alpha_2(\alpha_4 - 1) + \rho u^2 bh(1 - B\alpha_2)(\beta_4 - 1), \tag{3.31}$$

and substituting the expression for T given by equation 3.30 gives:

$$\begin{aligned} &\frac{1}{2}\rho g b(h^2 - h_4^2) - \frac{1}{2}\rho u^2 Bbh(\beta_4^2 - \alpha_4^2) \\ &\quad = \rho u^2 Bbh\alpha_2(\alpha_4 - 1) + \rho u^2 bh(1 - B\alpha_2)(\beta_4 - 1). \end{aligned} \tag{3.32}$$

In addition, conservation of mass flux in the bypass flow requires that:

$$h_4 = \frac{h(1 - B\alpha_2)}{\beta_4} + hB\frac{\alpha_2}{\alpha_4}. \tag{3.33}$$

Combining equations 3.28, 3.32, and 3.33 gives:

$$\alpha_2 = \frac{2(\beta_4 + \alpha_4) - \dfrac{(\beta_4 - 1)^3}{B\beta_4(\beta_4 - \alpha_4)}}{4 + \dfrac{(\beta_4^2 - 1)}{\alpha_4\beta_4}}. \tag{3.34}$$

Solution of the open channel model is more complex, requiring specification of turbine blockage B, tuning α_4, and bypass velocity coefficient β_4. An expression for β_4 may be developed by substituting the expression for h_4 given by equation 3.33 into equation 3.28:

$$\frac{B\alpha_2(\beta_4 - \alpha_4)}{\alpha_4\beta_4} = \frac{(\beta_4 - 1)}{\beta_4} - \frac{Fr^2}{2}(\beta_4^2 - 1), \tag{3.35}$$

in which Fr is the Froude number $(u/\sqrt{gh})$ of the flow. Substituting the expression for α_2 given by equation 3.34 into equation 3.35 gives:

$$\begin{aligned}&\beta_4^4\left(\frac{Fr^2}{2}\right) + \beta_4^3(2Fr^2\alpha_4) - \beta_4^2(Fr^2 - 2B + 2)\\ &-\beta_4(2Fr^2\alpha_4 + 4\alpha_4 - 4) + \left(\frac{Fr^2}{2} - 2B\alpha_4^2 + 4\alpha_4 - 2\right) = 0.\end{aligned} \tag{3.36}$$

Equation 3.36 is quartic equation that may be solved for β_4 once the blockage B, tuning α_4, and upstream Froude number Fr have been specified. Exact solution of the model requires that $0 \leq \alpha_4 \leq \alpha_2 \leq 1 \leq \beta_4$ and that the upstream flow is subcritical (i.e. $Fr < 1$). Expressions for the applied thrust and available power follow:

$$T = \frac{1}{2}\rho Bbhu^2(\beta_4^2 - \alpha_4^2) = \frac{1}{2}\rho Bbhu^2C_T, \tag{3.37}$$

$$P_{av} = Tu\alpha_2 = \frac{1}{2}\rho Bbhu^3\alpha_2(\beta_4^2 - \alpha_4^2) = \frac{1}{2}\rho Bbhu^3C_P. \tag{3.38}$$

As in the volume-flux constrained analysis, the available power increases monotonically with blockage. In open channel flow, however, the available power also increases, albeit to a lesser extent, with the Froude number. This is because larger Froude numbers are associated with greater deformation of the free surface, which acts increasingly to constrain and thereby accelerate flow in both the core and bypass streamtubes (Vogel, 2014). Interestingly, for all B, the maximum power again occurs close to $\alpha_4 = 1/3$, the optimal tuning in both of the previous analyses (Draper, 2011).

It is also worth noting that, under the appropriate asymptotic limits, the open channel model is entirely consistent with both the unbounded and volume-flux constrained models (Draper, 2011). Firstly, as $Fr \to 0$, the change in depth $\triangle h$ approaches zero (i.e. $h_4 \to h$) and, in the limit, equation 3.33 gives:

$$\beta_4 = \frac{1 - B\alpha_2}{1 - B(\alpha_2/\alpha_4)}, \tag{3.39}$$

and the quartic given by equation 3.36 reduces to a quadratic:

$$\beta_4^2(B-1) - \beta_4(2\alpha_4 - 2) + (-B\alpha_4^2 + 2\alpha_4 - 1) = 0. \tag{3.40}$$

Combining equations 3.39 and 3.40 gives an expression identical to that given by equation 3.16 for volume-flux constrained flow. Secondly, as $B \to 0$, the change in depth $\triangle h$ again approaches zero (i.e. $h_4 \to h$) so that, in the limit, equation 3.33 gives $\beta_4 = 1$ and, given that $(\beta_4 - 1)^3$ approaches zero faster than B does, equation 3.34 reduces to $\alpha_2 = (1+\alpha_4)/2$. These expressions are consistent with the classic unbounded analysis. The open channel model is therefore consistent with the volume-flux constrained model in the limit of small Froude number and with the unbounded model in the limit of small blockage (Draper, 2011).

Applying conservation of momentum to both the core and bypass flows between stations 1 and 5:

$$\frac{1}{2}\rho g b\big[h^2-(h-\triangle h)^2\big]-T=\rho u b h\bigg(\frac{uh}{h-\triangle h}-u\bigg), \tag{3.41}$$

and substituting the expression for T given by equation 3.37 gives:

$$\begin{aligned}\frac{1}{2}\bigg(\frac{\triangle h}{h}\bigg)^3-\frac{3}{2}\bigg(\frac{\triangle h}{h}\bigg)^2\\ +\big[1-Fr^2+\frac{C_T B Fr^2}{2}\big]\bigg(\frac{\triangle h}{h}\bigg)-\frac{C_T B Fr^2}{2}=0.\end{aligned} \tag{3.42}$$

Equation 3.42 is a cubic equation that may be solved for the relative change in depth $\triangle h/h$ once B, Fr, and C_T have been specified. Note also that as $Fr \rightarrow 0$, the only physically admissible solution is $\triangle h/h \rightarrow 0$. An expression for the power dissipated in wake mixing follows:

$$\begin{aligned}P_{diss}=\frac{1}{2}\rho u^3 b h B\bigg[\alpha_2\alpha_4^2+\frac{(1-B\alpha_2)}{B}\beta_4^2\\ -\frac{1}{B}\bigg(\frac{h}{h-\triangle h}\bigg)^2+\frac{2g(h_4-h_5)}{u^2 B}\bigg],\end{aligned} \tag{3.43}$$

and combining equations 3.38 and 3.43 gives:

$$P_{ex}=\rho g u b h \triangle h\bigg[1-Fr^2\frac{(1-(\triangle h/2h))}{(1-(\triangle h/h))^2}\bigg]. \tag{3.44}$$

This expression is simply the rate at which the flow loses potential energy ($\rho g u b h \triangle h$) multiplied by an additional term to account for the increase in kinetic flux downstream of the disc. This shows that, in open channel flow, tidal turbines extract potential, rather than kinetic, energy (Draper, 2011). In fact, by extracting potential energy ($h_5 < h$) from the flow, the turbines increase the kinetic energy of the flow downstream ($u_5 > u$), in accordance with open channel flow theory (Draper, 2011; White, 2009).

In open channel flow, the extraction efficiency is:

$$\eta = \frac{P_{av}}{P_{ex}} = \frac{Tu\alpha_2}{\rho g u b h \triangle h}\left[1 - Fr^2\frac{(1-(\triangle h/2h))}{(1-(\triangle h/h))^2}\right]^{-1}. \tag{3.45}$$

Substituting the expression for T given by equation 3.41 into the numerator of equation 3.45 and neglecting terms proportional to Fr^2 and $\triangle h/h$, it may be shown that as $Fr \to 0$, $\eta \to \alpha_2$, which is consistent with the volume-flux constrained analysis. Alternatively, equation 3.41 may be rearranged and combined with equation 3.45 to give:

$$\eta = \alpha_2\left[\frac{1-(\triangle h/2h) - Fr^2(1-(\triangle h/h))^{-1}}{1 - Fr^2(1-(\triangle h/2h))(1-(\triangle h/h))^{-2}}\right]. \tag{3.46}$$

For the majority of tidal flows, which are characterised by small but finite Froude numbers and changes in depth, efficiency may be approximated as:

$$\eta \approx \alpha_2\left[1 - \frac{1}{2}\frac{\triangle h}{h}\right]. \tag{3.47}$$

This result shows that free surface deformation reduces the efficiency of the extraction. This is because, while the deformation acts to constrain and thereby accelerate both the core and bypass flows, it constrains and accelerates the bypass flow relatively more and thus introduces greater mixing losses (Draper, 2011).

Interestingly, physically admissible solutions to equation 3.36 do not always exist. The loss of a valid solution in an open channel flow problem typically implies the onset of critical flow at some point in the flow field (Draper, 2011; Houlsby et al., 2008). Noting this, Houlsby et al. reconsider each expression to determine the limits of the model. Equations 3.28 and 3.32 express quantities (the specific energy of the bypass flow and the momentum of the entire flow, respectively) that have a minimum value when

plotted against fluid depth. This means that it is possible for some or all of the flow to become critical. Were this to occur, critical flow would first develop in the bypass flow in the near wake of the disc, where the velocity is greatest and the depth of flow is lowest (Houlsby et al., 2008).

As the bypass flow accelerates around the disc, the local depth decreases in accordance with energy conservation. Tuning the turbine to extract more power further increases the velocity and reduces the depth of the bypass flow. However, if the bypass depth reduces below the critical depth, the bypass flow will back up and a hydraulic jump will form downstream of the disc. Since this scenario is too complicated to describe with a simple actuator disc model, the onset of critical bypass flow is the point at which real solutions cease to exist (Draper, 2011).

For a given flow field, defined by its spatial dimensions and upstream Froude number, the open channel model may be used to explore the effects of blockage and tuning on turbine performance. Figures 3.4–3.9 highlight the variation of power coefficient C_P, thrust coefficient C_T (plotted on a base–10 logarithmic scale), and extraction efficiency η, with blockage B and tuning α_4 for flows of upstream Froude number 0.1 and 0.2. The most notable effect of increasing Fr is to reduce the number of admissible combinations of B and α_4 since, the higher the initial Froude number, the easier it is for the bypass flow to become critical. For a given B and α_4, increasing Fr is shown to increase both the thrust exerted on the turbine and the available power. However, since increasing Fr also increases the equal and opposite thrust exerted on the flow, the amount of power dissipated in wake mixing increases such that the extraction efficiency is lower. Thus, although a turbine in open channel flow may extract more power than one in flow with a rigid lid, it does so less efficiently.

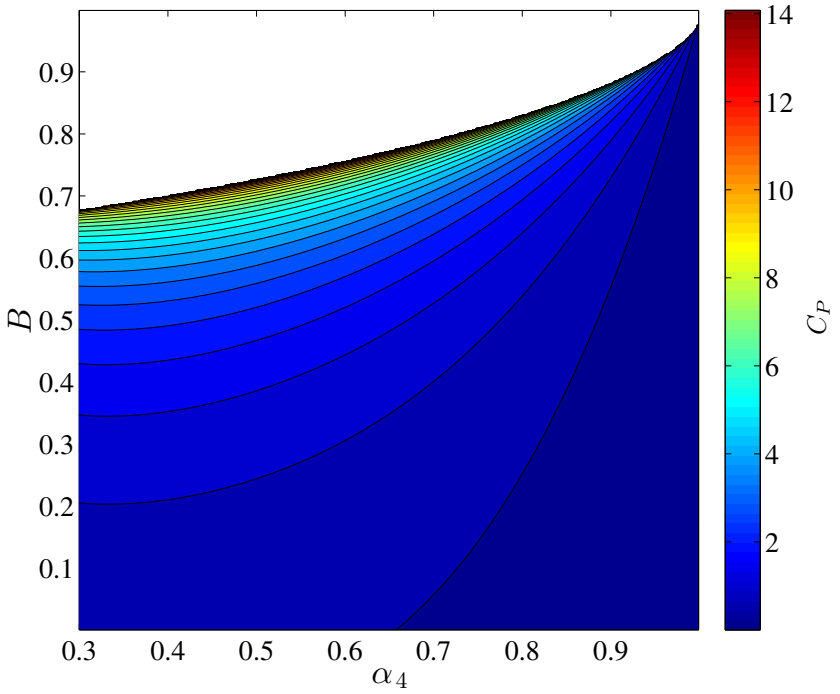

Figure 3.4: Variation of power coefficient C_P with blockage B and tuning α_4 for a flow with Froude number $Fr = 0.1$.

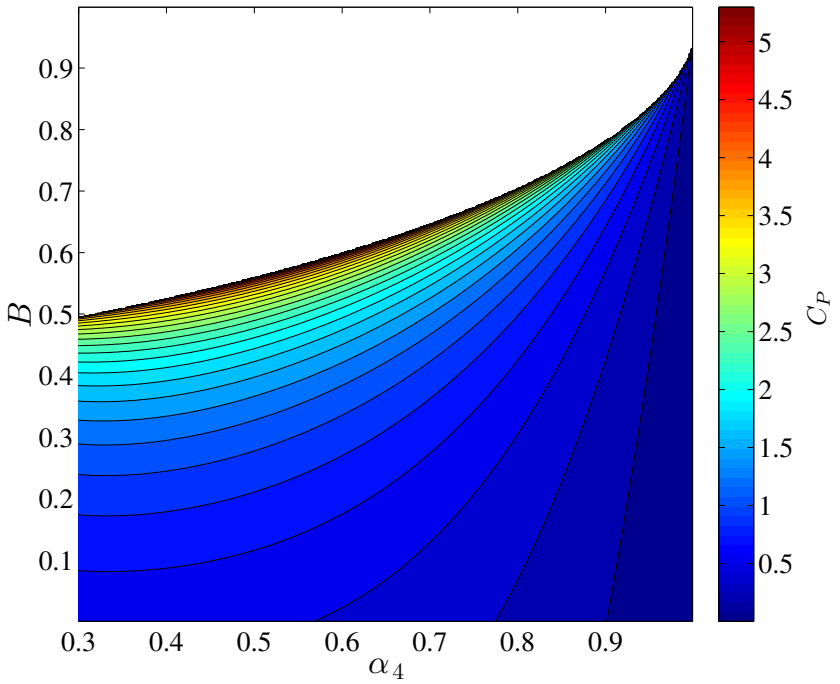

Figure 3.5: Variation of power coefficient C_P with blockage B and tuning α_4 for a flow with Froude number $Fr = 0.2$.

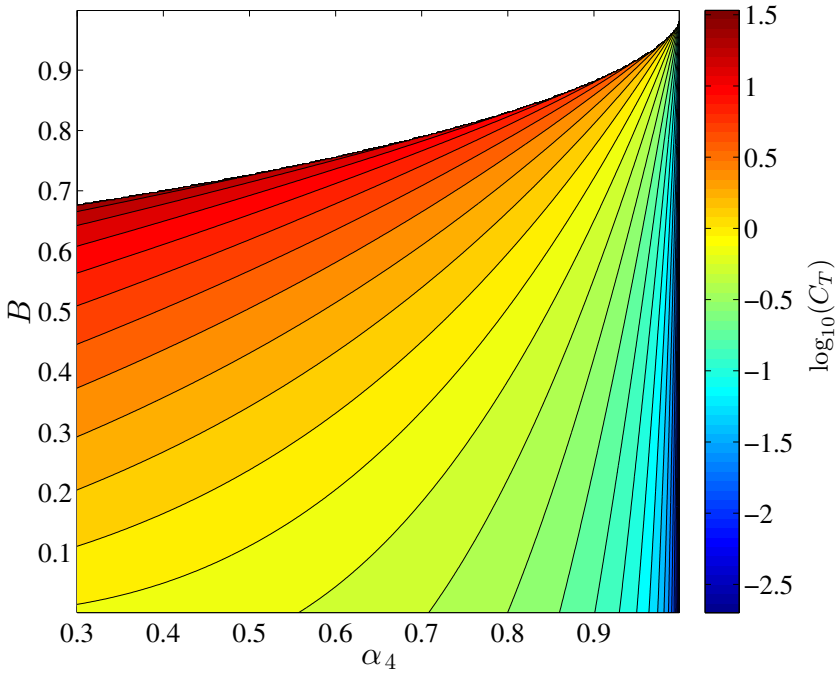

Figure 3.6: Variation of the common logarithm of thrust coefficient (C_T) with blockage B and tuning α_4 for a flow with Froude number $Fr = 0.1$.

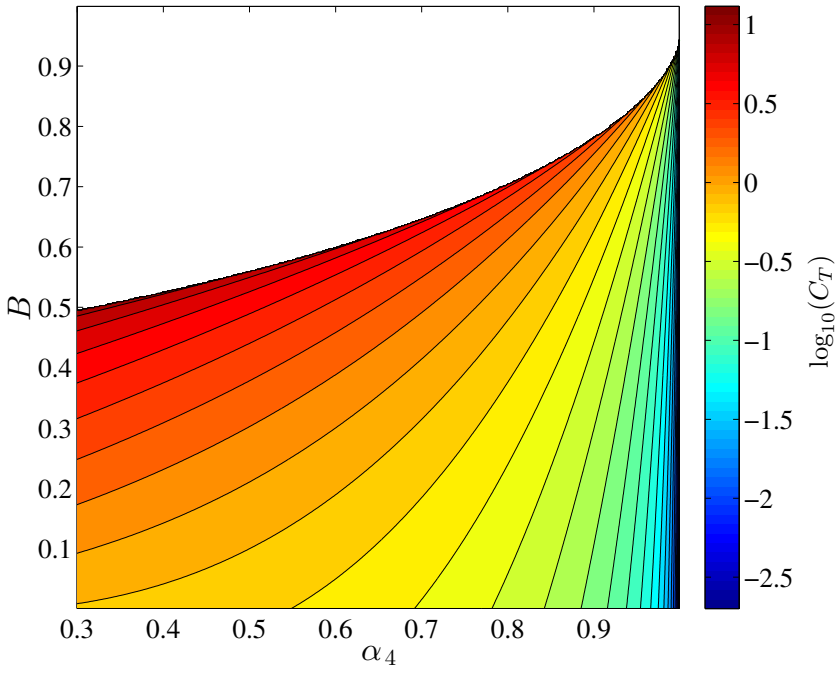

Figure 3.7: Variation of the common logarithm of thrust coefficient (C_T) with blockage B and tuning α_4 for a flow with Froude number $Fr = 0.2$.

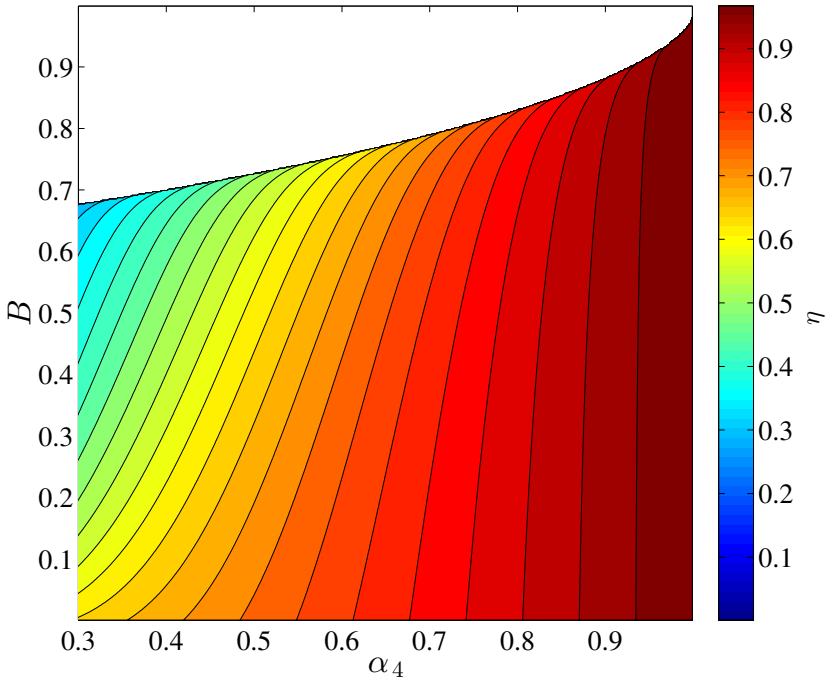

Figure 3.8: Variation of extraction efficiency η with blockage B and tuning α_4 for a flow with Froude number $Fr = 0.1$.

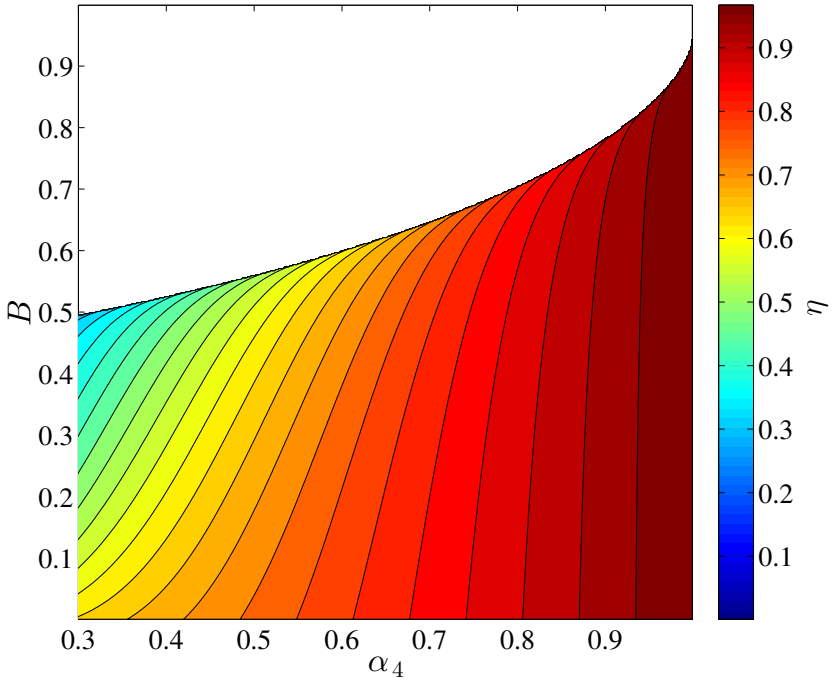

Figure 3.9: Variation of extraction efficiency η with blockage B and tuning α_4 for a flow with Froude number $Fr = 0.2$.

As in the volume-flux constrained analysis, high extraction efficiency does not coincide with maximum power extraction. For a given change in depth, equation 3.47 shows that the more the core flow is slowed, the less efficient the energy extraction. This implies that, for a given power output, extraction efficiency increases with blockage. Simply put, this is because less power is dissipated in wake mixing when a large amount of water is slowed a little than when a small amount of water is slowed a lot (Draper, 2011). The maximum power coefficient occurs close to $\alpha_4 = 1/3$ for all blockage ratios but maintaining this tuning as the blockage increases results in excessively high thrusts and mixing losses. For instance, given a Froude number of 0.2 and a blockage of 0.4, $C_{P(max)}$ is 1.91, which means that the maximum available power is almost twice the upstream kinetic flux through the same cross-sectional area. To achieve this, however, a thrust equivalent to 4.43 times the integral of the upstream dynamic pressure (corresponding C_T), or 24 times the integral of the dynamic pressure at the turbine (corresponding local thrust coefficient, C_{TL}), must be exerted on the flow. At this level of thrust, the power available to the turbine constitutes only 42% of the power extracted from the flow. Unlike for wind turbines, therefore, it is not practical to design tidal turbines for maximum power coefficient. Instead, designers ought to be mindful of the tradeoff between maximising power output and minimising both turbine loading and wake mixing losses.

Limitations

Actuator disc models require a number of simplifying assumptions related to both the turbine, which is represented as a thin, uniformly porous disc with no support structure, and the flow, which is assumed to be uniform, steady, and unidirectional. These simplifications mean that disc models are unable

to incorporate a number of important characteristics of real current flows, including rapid changes in cross-section and flow velocity (Draper, 2011). For simplicity, the models also assume that the flow conditions at the inlet are unaffected by the resistance of the disc. This limits the applicability of actuator disc models to situations in which the effects of energy extraction on the flow are negligible, whereas, in reality, the increasing resistance will reduce the inflow velocity and ultimately limit the available power (Draper, 2011; Vogel, 2014).

3.2 Channel models

Assessing the potential of a tidal channel to deliver useful power is complicated by the fact that turbines present additional resistance to flow (Garrett and Cummins, 2005; Vennell, 2010). Little power will be extracted if only a few turbines are placed in the channel but if too many are added, the flow through the channel will be severely reduced and its potential to produce power similarly limited (Garrett and Cummins, 2005). As with a single turbine, the power output of a tidal channel is maximised by finding the optimal resistance to flow. At channel-scale, however, the extractable power depends on the balance of forces driving and resisting flow through the channel.

Simple tidal channel

Garrett and Cummins (2005) developed a simple analytical model to explore the potential of a tidal channel to deliver useful power. In this classic analysis, the idealised channel is one of slowly varying cross-section, con-

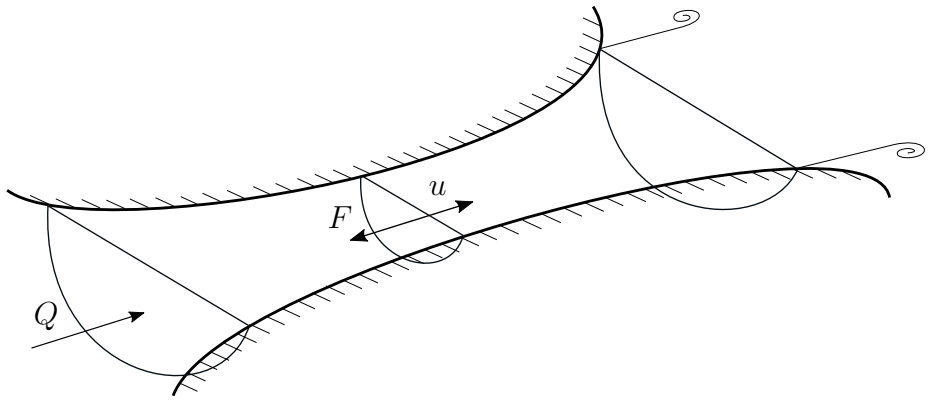

Figure 3.10: Idealised channel connecting two large tidal basins. Oblique view, adapted from Garrett and Cummins (2005).

necting two large bodies of water with different tidal elevations (figure 3.10). The velocity of the current passing through the channel is assumed to be a function of both time and streamwise position but independent of spanwise position. This allows the flow to be modelled using the one-dimensional shallow water approximation to the momentum equation:

$$\frac{\partial u}{\partial t} + u\frac{\partial u}{\partial x} + g\frac{\partial \xi}{\partial x} = -F, \tag{3.48}$$

in which u is the current velocity, x is the streamwise distance along the channel, g is acceleration due to gravity, ξ is the free surface elevation, and F is an opposing force per unit mass, associated with both natural and additional drag. The additional drag due to the turbines is assumed to be an arbitrary function of streamwise position but independent of spanwise position. This means that although the number of turbine rows may vary, the turbines within each row are assumed to block the cross-section completely.

For simplicity, Garrett and Cummins assume: (i) that the channel length and cross-section are approximately constant in time; (ii) that the Froude number and tidal range are sufficiently small that depth and velocity may be considered functions of position only; (iii) that the channel is sufficiently

short compared to the tidal wavelength that the flow rate is approximately constant along its length, and; (iv) that the elevations in the adjoining basins are unaffected by changes in channel flow rate (Draper, 2011). Equation 3.48 is then integrated along the length of the channel to give:

$$c\frac{dQ}{dt} - g\xi_0 = -\int_0^L F dx - \frac{1}{2}|u_e|u_e, \tag{3.49}$$

in which $c = \int_0^L A^{-1}\, dx$ (with $A(x)$ the local cross-sectional area), Q is the channel flow rate, ξ_0 is the difference in elevation between the channel ends (assumed to be $\xi_0(t) = a\cos(\omega t)$, with a the amplitude and ω the frequency of the tidal forcing), and u_e is the current velocity at the channel exit. The final term in equation 3.49 comes from integration of the nonlinear advection term in equation 3.48 and the assumption that, although no energy is lost as the flow enters the channel, some energy is lost as it exits as a jet into relatively still water (Draper, 2011).

Flow through the channel is resisted by the combination of natural energy losses associated with background roughness and exit separation, and additional energy losses associated with tidal turbines. In the general case, the resistance due to background roughness is assumed to be quadratic in velocity, and natural and additional losses are given as separate terms:

$$c\frac{dQ}{dt} - g\xi_0 = -\int_0^L F_t dx - \alpha|Q|Q, \tag{3.50}$$

in which:

$$\alpha = \int_0^L C_d(hA^2)^{-1} dx + \frac{1}{2}(A_e)^{-2}, \tag{3.51}$$

where $\int_0^L F_t\, dx$ represents the drag associated with the turbines, C_d is the natural drag coefficient of the channel, and A_e is the cross-sectional

area of the flow at the channel exit. Assuming that the turbine drag is also quadratic in velocity, Garrett and Cummins introduce variables $Q' = (ga)^{-1}c\omega Q$, $t' = \omega t$, and $\lambda_0 = ga\alpha(c\omega)^{-2}$ to express equation 3.50 in non-dimensional form as:

$$\frac{dQ'}{dt'} - \cos(t') = -(\lambda_0 + \lambda_1)|Q'|Q', \tag{3.52}$$

in which λ_0 represents losses associated with background roughness and exit separation, and λ_1 represents turbine drag. There are clearly a range of problems to consider depending on how the tidal forcing is balanced, in the unexploited case, by acceleration and natural losses. The natural dynamic balance of a channel falls between the inertial limit (i.e. $\lambda_0 = 0$), in which forcing is balanced entirely by acceleration, and the quasi-steady limit (i.e. $\lambda_0 \to \infty$), in which forcing is balanced entirely by natural losses.

For all λ_0, equation 3.52 is solved numerically to find the turbine drag λ_1 that maximises non-dimensional power output. Returning to dimensional variables, Garrett and Cummins show that the maximum extractable power, averaged over the tidal cycle, is:

$$P_{ex(max)} = \gamma\rho g a Q_{(max)}, \tag{3.53}$$

in which γ is a term that depends on the natural dynamic balance λ_0, a is the unexploited peak head difference, and $Q_{(max)}$ is the unexploited peak flow rate. Interestingly, the range of γ is small, varying only from 0.24 in the inertial limit to 0.21 in the quasi-steady limit. This means that given the maximum forcing and peak unexploited flow rate, the maximum extractable power from any tidal channel may be estimated to within $\sim$10% as $0.22\rho g a Q_{(max)}$. This result is independent of both the type and arrangement of turbines. More precise estimates of γ and thus power potential may

be obtained if the phase lag between the maximum forcing and peak flow rate is also known.

Although accurate resource assessments require detailed numerical models, this simple analytical model has been shown to provide useful estimates of the maximum average power that may be extracted from a tidal channel (Sutherland et al., 2007). Importantly, the model also shows that this power is not related in any simple way to the unexploited kinetic flux but rather to the work done by the tidal forcing (Draper, 2011).

Multiply-connected channels

For more complicated coastal geometries, accurate assessment of the extractable power is more complex. If turbines are to be deployed in multiply-connected channels, the additional resistance will cause not only reduction of flow through the subchannel containing the turbines but diversion of flow into less obstructed subchannels (Polagye and Malte, 2011; Sutherland et al., 2007). In such a case, the extractable power therefore depends on the relative resistances of each subchannel (Atwater and Lawrence, 2010; Cummins, 2013). This problem may be greatly simplified by considering a useful analogy — that of an equivalent electrical circuit.

Equivalent circuit analysis was introduced by Miles (1971) to analyse surface wave resonance in harbours and later adopted by Lighthill (1978) to describe flow through connected channels (Draper, 2011). More recently, electrical analogies have been used by Rainey (2009, 2010) to determine the optimal position for a tidal barrage in the Severn Estuary, by Cummins (2013) to analyse the power potential of a split tidal channel, and by Draper et al. (2014b) to explore the performance of turbine arrays in multiply-connected channel networks. As noted by Draper et al. (2014b),

the electrical analogy simplifies complex flow problems by replacing the channel network with an equivalent electrical circuit, within which the driving head is represented as an alternating voltage V; the flow rate as a time-varying electrical current I; the mass of water as an inductance L; and the natural and additional drag forces as resistances R_n and R_t. With the circuit analogue complete, the maximum extractable power is determined by maximising the power dissipated in the resistor representing the turbines.

Draper et al. first use an equivalent circuit to reinterpret the results of Garrett and Cummins (2005), rewriting the governing equation as:

$$V = L\frac{dI}{dt} + (R_n + R_t)I. \tag{3.54}$$

Viewing the turbines as resistors, it is obvious that energy extraction reduces the channel flow rate and that there must therefore exist a maximum amount of power to be extracted. Moreover, the maximum power transfer theorem states that maximum power is drawn by a load when its impedance is set to match the source impedance. This explains why Garrett and Cummins (2005) found the maximum extractable power to be a simple function of the unexploited peak head difference and flow rate (Draper et al., 2014b).

Draper et al. extend their analysis to consider the performance of turbines in a split tidal channel (figure 3.11). In this case, equation 3.54 is used to model flow through two parallel subchannels within a larger tidal channel. Measurements of the channel dimensions and natural flow characteristics are used to calculate an equivalent voltage V, electrical current I, inductance L, and natural resistance R for the main channel and each of the subchannels within it. The turbines are then included as an additional resistance R_t in subchannel 2, while subchannel 3 is left unexploited. Solving the resulting system of equations gives an expression for the maximum

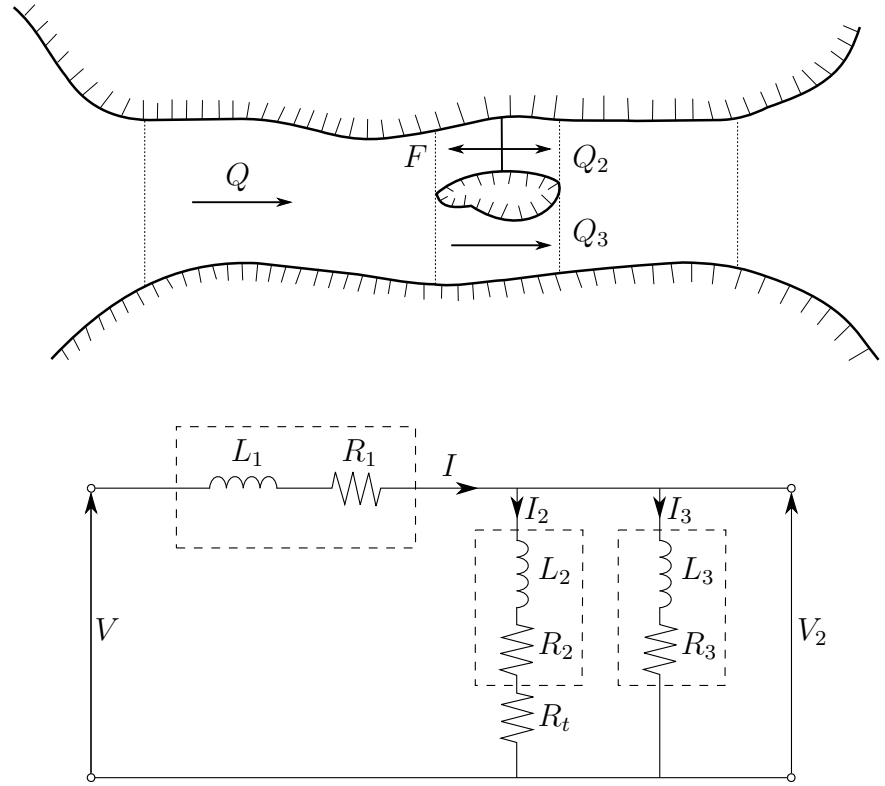

Figure 3.11: Split tidal channel and equivalent electrical circuit. Plan views, adapted from Draper et al. (2014b).

extractable power, averaged over a tidal cycle:

$$P_{ex(max)} = \gamma \rho g a_2 Q_2 \left[\frac{Q}{Q_3(1 + (a_2/a)(Q_2/Q_3))} \right], \tag{3.55}$$

in which a and a_2 are the unexploited peak head differences, and Q, Q_2, and Q_3 the unexploited peak flow rates, in the main channel and subchannels, respectively. The form of equation 3.55 is notably similar to that of equation 3.53 but includes an additional term to account for the presence of connecting and parallel channels (Draper et al., 2014b). Assessment of the power potential of the parallel subchannel is further complicated by the fact that γ now depends on six dimensionless parameters related to the natural dynamic balance of the channel, the relative inductance and drag in the circuit, and the turbine drag. Interestingly, however, the range of γ

is again small and a value of 0.22 is found to give a good approximation for a range of split channel geometries. Setting $\gamma = 0.22$, equation 3.55 may therefore be used to predict the power potential of one of two parallel subchannels, solely using estimates of the unexploited peak amplitudes and flow rates. Draper et al. also recognised that equation 3.55 may also be applied to any number of parallel subchannels, by grouping adjacent exploited and unexploited subchannels to represent a two-subchannel system.

Finally, Draper et al. explore the applicability of the electrical analogy to more complex channel networks. A circuit representation of the Pentland Firth is developed and used to determine the maximum amount of power that may be extracted from different subchannels. Estimates of flow rates and maximum power from the circuit model are found to agree reasonably well (typically to within 20%) with those obtained from the depth-averaged numerical model of Draper et al. (2014c). This demonstrates that, although equivalent circuits require some simplification, they may be used to provide initial estimates of the power potential of multiply-connected channels and to help guide and interpret results from more computationally-intensive numerical models (Cummins, 2013; Draper et al., 2014b).

Limitations

Analytical channel models may be used to provide useful estimates of the power potential of a given tidal site but because they represent turbines as a simple resistive force, they are unable to distinguish between the total amount of power that may be extracted from the flow and the smaller amount available to the turbines after mixing losses are subtracted (Draper et al., 2014b). This force representation also requires that turbines be arranged to block completely the flow cross-section, which would be highly im-

practical in reality. Real arrays will inevitably have gaps between turbines, which will present paths of lower resistance to flow and thereby reduce the extractable power (Vogel, 2014). To assess accurately the maximum power available to different arrangements of turbines within a channel, a more detailed turbine representation is required (Draper et al., 2014b).

3.3 Combined models

Actuator disc models provide a useful description of turbine performance but are unable to account for the balance of forces that drive currents through channels. Analytical channel models use this balance to calculate the maximum extractable power but lack a detailed turbine representation. More recent works have focused on combining these different types of model to explore the optimal arrangement of tidal turbines in arrays. In this section, three such combined models are discussed.

Array spanning a channel

Vennell (2010) combined the channel model of Garrett and Cummins (2005) and the actuator disc model of Garrett and Cummins (2007) to explore the performance of an array of turbines completely spanning a tidal channel (figure 3.12). By combining these models, Vennell was able to explore the interactions between the turbine array and the large-scale flow through the channel that determine the maximum available power.

As discussed previously, actuator disc and channel models make different assumptions about the dynamics of tidal flows (Garrett and Cummins, 2008). To combine the different types of model, Vennell assumes that the turbine array occupies only a short section of the channel within which the

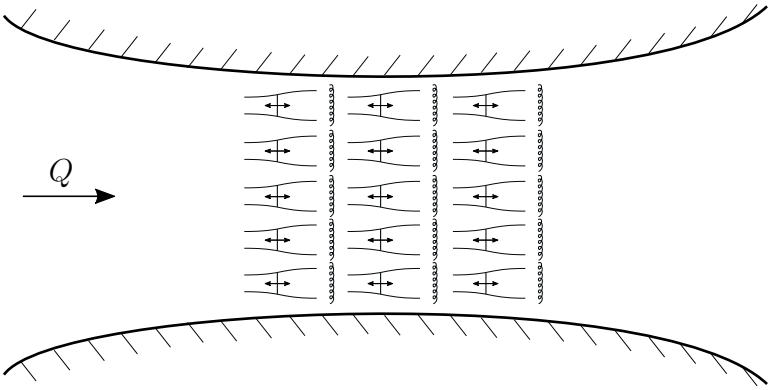

Figure 3.12: Combined array and channel model. Plan view, adapted from Vennell (2010).

flow is quasi-steady and turbine drag dominates natural losses. The models are coupled by equating the channel model's non-dimensional turbine drag coefficient λ_1 and the actuator disc model's thrust coefficient C_T as follows:

$$\lambda_1 = n^* C_T, \tag{3.56}$$

in which C_T is the thrust coefficient for a uniform row of turbines and n^* is the non-dimensional number of identical turbine rows. It is also assumed that although the array only occupies a short section of the channel, the streamwise spacing is sufficient to allow complete mixing of flow between successive turbine rows. Coupling the models with equation 3.56 generates a set of equations that may then be solved numerically.

Vennell uses the combined model to show that the potential of a tidal channel is simply a function of its natural dynamic balance λ_0. Increasing the amount of natural losses in the channel is shown to reduce its potential because background roughness dissipates energy that would otherwise be available for extraction. Vennell shows that the turbine drag λ_1 required to extract this potential depends solely on the channel's natural dynamic balance. This optimal λ_1, which may be achieved using different turbine arrangements, is found to increase with λ_0, implying that more turbines are

required to extract less power as the natural losses increase.

In this combined model, the performance of the array depends on the channel flow rate but, importantly, the channel flow rate also depends on the performance of the array. As such, the turbine tuning that maximises available power is no longer simply given by $\alpha_4 = 1/3$, but instead depends on the arrangement of turbines, i.e. the number of full-width rows and their blockage ratios. The optimal tuning increases from $\alpha_4 = 1/3$ in the limit of unbounded flow to approach unity as the flow becomes fully blocked. This shows that the performance of a small array (with resistance much less than the natural impedance of a channel) depends solely on its power coefficient, while the performance of a large array (which may alter the channel flow rate) also depends on its extraction efficiency (Draper and Nishino, 2014a,b). By continuously adjusting tunings, it is possible to maintain optimal performance as more turbines are added to the array. Interestingly, although adding turbines always increases the maximum available power, there is a diminishing return because the additional power provided by each new row decreases as the optimally-tuned array increases in size (Vennell, 2010). As noted by Vogel (2014), the trade-off between maximising the overall power output of the array and maximising the power available to each turbine is an important consideration in array design.

In a later work, Vennell (2011) extends this combined model to allow for changes in channel cross-section and to better account for the interactions between successive turbine rows by allowing each row to be tuned separately. Surprisingly, in many circumstances the optimal 'in-concert' tunings are found to be either equal or quite close to the optimal uniform tunings predicted by the original model. Vennell explains that this is because optimal tunings are essentially the same for rows with the same blockage, even

in constricted or quasi-steady channels.

The foregoing models provide many useful insights into the performance of turbine arrays in tidal channels. Optimal turbine tuning is shown to depend on both the type of channel and the arrangement of turbines within it. It is also shown that large arrays of optimally-tuned turbines may extract most of a channel's potential, although it is unlikely that such deployments will be economically viable. Finally, it is shown that to maximise available power output, turbines should be arranged to fill each row as densely as possible before starting a new row downstream (Vennell, 2010). It is important to note, however, that because these combined models incorporate the model of Garrett and Cummins (2007), they also assume that the Froude number of the flow is small and that the turbine drag is strictly quadratic in flow rate (Draper, 2011). Further, because the models also incorporate the model of Garrett and Cummins (2005), they also assume that turbines may be arranged to span the entire width of a channel whereas, in reality, only part of the cross-section may be available.

Partial-width arrays

The actuator disc models discussed previously assume that the turbines present a uniform resistance to flow and, as such, are only applicable to scenarios in which an array spans the entire cross-section (Vogel, 2014). In reality, however, practical constraints may require part of the cross-section to remain unexploited to allow safe passage of vessels and marine life. If an array spans only part of a cross-section, an additional, large-scale flow develops. Just as with flow through a single turbine, the flow through the array is slowed by the aggregate thrust from the turbines and the flow around the array accelerates to ensure conservation of mass flux through

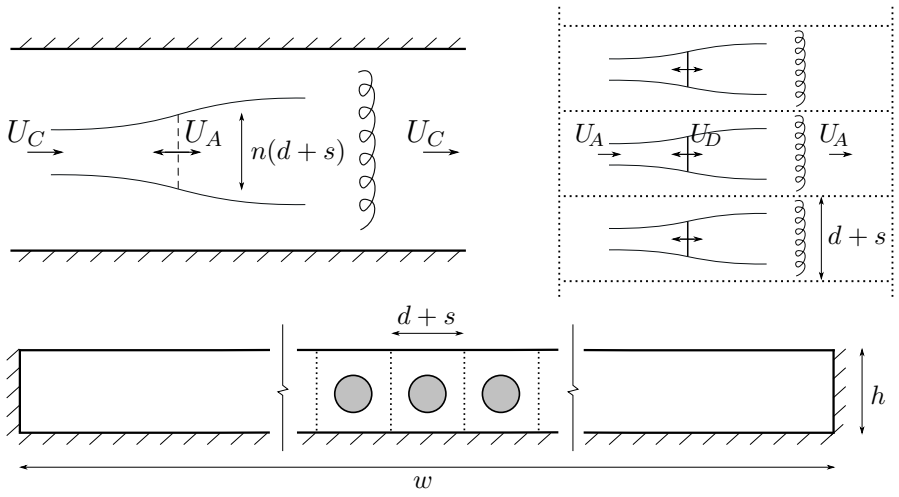

Figure 3.13: Two-scale actuator disc model. Plan views (above) and streamwise cross-sectional view (below), adapted from Nishino and Willden (2012).

the channel (Nishino and Willden, 2012; Vogel et al., 2016). In this case, because flow is not only able to pass around the turbines within the array but also bypass the array entirely, a more sophisticated model is required.

The two-scale actuator disc model proposed by Nishino and Willden (2012) extends the model of Garrett and Cummins (2007) to explore the performance of an array partially spanning a wide cross-section. By assuming that array-scale flow events take place over much greater spatial and temporal scales than those on the scale of the turbines, Nishino and Willden introduce a scale separation hypothesis that allows flow through a partial-width array to be modelled as the combination of two loosely-coupled disc models of different scales: a local-scale model, which describes the flow through the turbines within the array; and an array-scale model, which describes the flow through the array within the channel.

The two-scale model considers an array of n identical turbines of diameter d, arranged in a single row with uniform lateral spacing s (figure 3.13). In addition to the local and array-scales, a global scale is defined to relate directly the flow through the turbines to the flow through the channel. Nishino and Willden define a blockage B, tuning α, thrust coefficient C_T,

and power coefficient C_P for each scale, and use the subscripts L, A, and G to denote local-, array-, and global-scale respectively. The global blockage B_G is now defined as the product of the array blockage B_A, which represents the ratio of array width to channel width, and the local blockage B_L, which represents the ratio of turbine cross-sectional area to that of its individual flow passage (figure 3.13). The local and array-scale models are coupled by equating their respective expressions for the array-scale thrust coefficient:

$$C_{TA} = \alpha_{2A} B_L C_{TL}, \tag{3.57}$$

$$C_{TA} = (1 - \alpha_{4A}) \Big[\frac{1 + \alpha_{4A} - 2B_A \alpha_{2A}}{(1 - B_A(\alpha_{2A}/\alpha_{4A}))^2} \Big]. \tag{3.58}$$

As the array-scale tuning α_{2A} is reduced, the value of C_{TA} given by equation 3.58 (developed using array-scale parameters) increases while the value given by equation 3.57 (developed using local-scale parameters) decreases. As such, there exists a unique value of α_{2A} to solve the model, which may be determined numerically for a given turbine arrangement (i.e. specific values of B_G, B_A, and B_L) and local-scale tuning α_{2L}.

The disc models discussed previously implicitly assume an array completely spanning the flow cross-section and thus a single scale of wake mixing behind the turbines (Vogel, 2014). For a given blockage, these models predict that as the resistance of the turbines increases, the available power first increases before decreasing as the turbines cause the flow to divert progressively around them. General results from the two-scale model are best described by the following example. Figure 3.14 illustrates the effects of turbine tuning on the local and global power coefficients for the combination of a high local blockage ($B_L = 0.436$) and moderate array blockage ($B_A = 0.3$). As α_{2L} decreases from unity the turbines begin to apply thrust to, and extract power from, the flow. Due to the high B_L, the local-scale

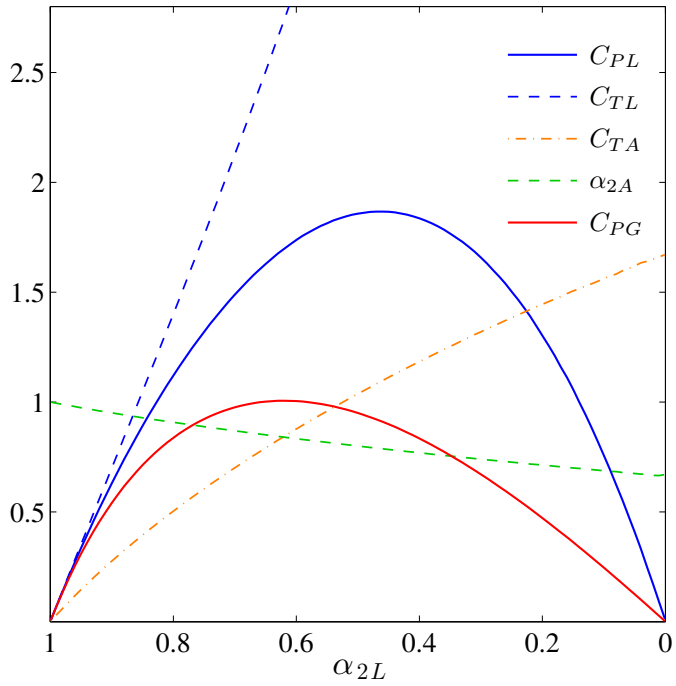

Figure 3.14: Effect of local tuning α_{2L} on the performance of an array with high local blockage ($B_L = 0.436$) and moderate array blockage ($B_A = 0.3$). Adapted from Nishino and Willden (2012).

power coefficient C_{PL} peaks at a high value corresponding to a high induction factor (low α_{2L}). It is important to recognise, however, that C_{PL} represents the ratio of available power to array-scale kinetic flux, which is reducing as the applied thrust increases. A more appropriate performance metric is the global-scale power coefficient C_{PG}, which represents the ratio of available power to channel-scale kinetic flux and which, relative to C_{PL}, peaks at a lower value corresponding to a lower induction factor (higher α_{2L}). This example shows that for partial-width arrays, performance depends not only on the turbine tuning α_{2L}, but rather on the balance between this local-scale slowing effect and the array-scale choking effect represented by α_{2A} (Nishino and Willden, 2012). Array performance is maximised by tuning the turbines to slow the flow as much as possible without producing either excessive diversion of flow around the turbines within the array or

excessive reduction of flow through the array.

For a given B_A and B_L, there is an optimal turbine tuning (i.e. an optimal thrust coefficient) that produces the maximum global power coefficient, $C_{PG(max)}$. Interestingly, the two-scale model also enables comparison between different arrangements of the same global blockage B_G in terms of the width of the array B_A and the size of the turbines within it B_L. For a given B_G, it is found that there is an optimal B_L to maximise $C_{PG(max)}$. This optimal B_L is not simply the maximum possible value (i.e. the optimal spacing between turbines is not zero) but rather determined by the balance between a beneficial local blockage effect and a detrimental array-scale choking effect. As the lateral spacing between turbines is reduced (i.e. as B_L increases and B_A decreases), $C_{PG(max)}$ initially increases as the decreasing potential for flow to divert between the turbines within the array allows for higher optimal thrusts. As B_L is further increased, however, $C_{PG(max)}$ starts to reduce as the increasing potential for flow to divert around the entire array necessitates lower optimal thrusts. Peak power and thrust coefficients are not exactly coincident due to their differing dependence on velocity but arranging and tuning turbines to produce the peak global power coefficient is shown to require a near-peak global thrust coefficient (figure 3.19).

The effects of turbine arrangement on array performance are best illustrated by figure 3.15, which plots the maximum global power coefficient for a range of local and global blockages. The diagonal line on this plot represents arrangements in which turbines are evenly spaced across the cross-section (i.e. $B_L = B_G$), for which the two-scale model reduces to the disc model of Garrett and Cummins (2007) and the maximum power coefficient is again given by $C_{PG(max)} = 16/27\,(1 - B_G)^{-2}$. The white line represents arrangements in which the lateral spacing is optimised to maximise $C_{PG(max)}$. The

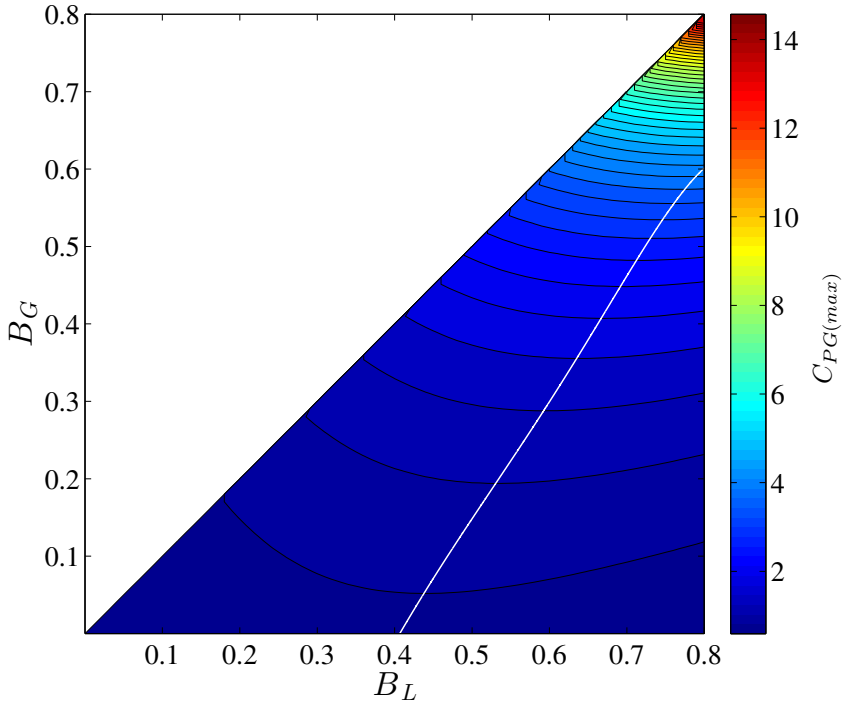

Figure 3.15: Variation of maximum global power coefficient $C_{PG(max)}$ with local blockage B_L and global blockage B_G. Adapted from Nishino and Willden (2012).

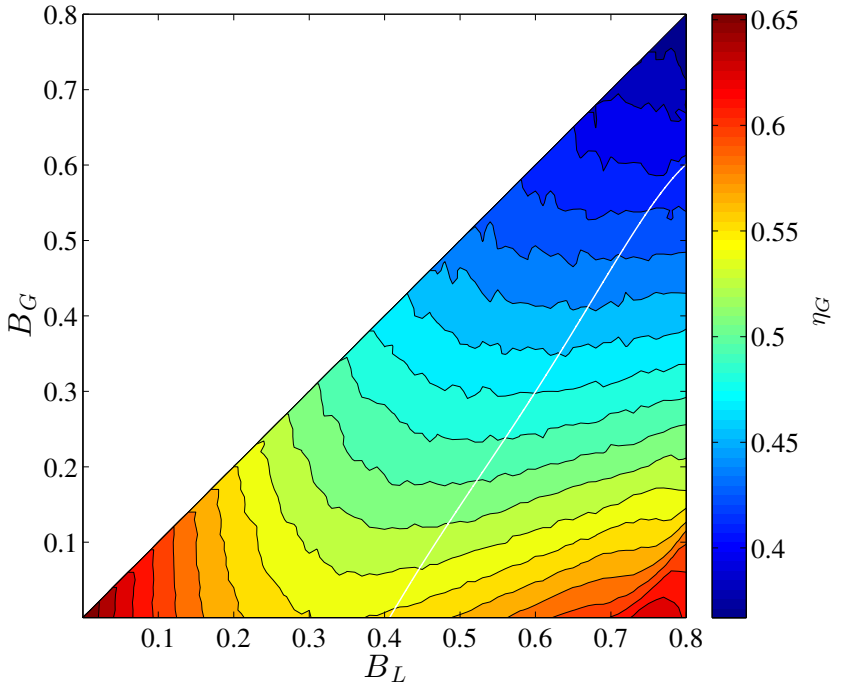

Figure 3.16: Global extraction efficiency η_G corresponding to maximum global power coefficient $C_{PG(max)}$.

fact that these lines do not coincide shows that evenly spacing turbines across a cross-section is suboptimal because a higher power coefficient can always be achieved by spacing the turbines to exploit local blockage effects (Nishino and Willden, 2012). As previously discussed, however, designing turbines for maximum power coefficient results in extreme turbine loading and excessive mixing losses (figure 3.16). Moreover, for turbines in channels, the maximum power coefficient does not necessarily coincide with maximum available power (Draper, 2011; Vennell, 2010).

Further insights may be gained by considering the case of an infinitely wide channel, in which the local blockage B_L is finite but the global blockage is negligible ($B_G = 0$). Figure 3.17 illustrates that as B_L is increased from zero, $C_{PG(max)}$ increases from the Betz limit of ~ 0.593 to another limiting value of ~ 0.798 at $B_L \approx 0.4$, before returning to the Betz limit as B_L approaches unity. This is explained as follows. For the limiting values of $B_L = 0$ and $B_L = 1$, the array cannot exploit local blockage effects to increase $C_{PG(max)}$ above, in this case, the Betz limit. For $B_L = 0$, each turbine is situated within its own infinite medium and the optimal strategy is to tune each turbine in accordance with the classic Betz analysis. For $B_L = 1$, each turbine is completely blocking its individual flow passage, so the entire array acts as a single isolated turbine. As such, the optimal strategy is to tune the array as a whole to the Betz tunings. As B_L increases from 0 to 1, the array effectively changes shape from a number of isolated turbines to a single isolated turbine and the optimal tunings reflect this transition (figure 3.18). For $B_G = 0$, $B_L \approx 0.4$ is the local blockage for which $C_{PG(max)}$ is maximised. However, maximising $C_{PG(max)}$ also essentially maximises $C_{TG(opt)}$, thereby minimising the global extraction efficiency — a trend that also appears to hold for finite global blockages (figure 3.19).

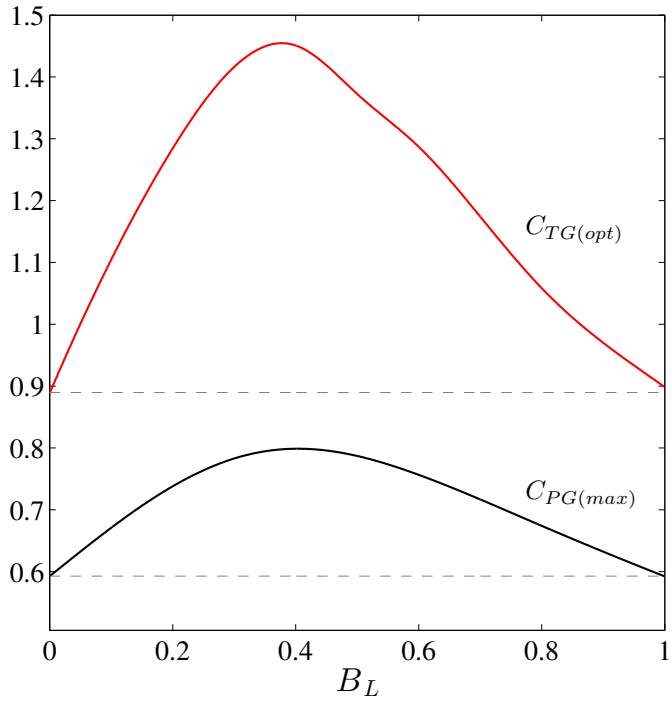

Figure 3.17: Variations of maximum global power coefficient $C_{PG(max)}$ and optimal global thrust coefficient $C_{TG(opt)}$ with local blockage B_L for an array in an infinitely wide channel ($B_G = 0$). Results from the classic Betz analysis shown as dashed lines. Adapted from Nishino and Willden (2012).

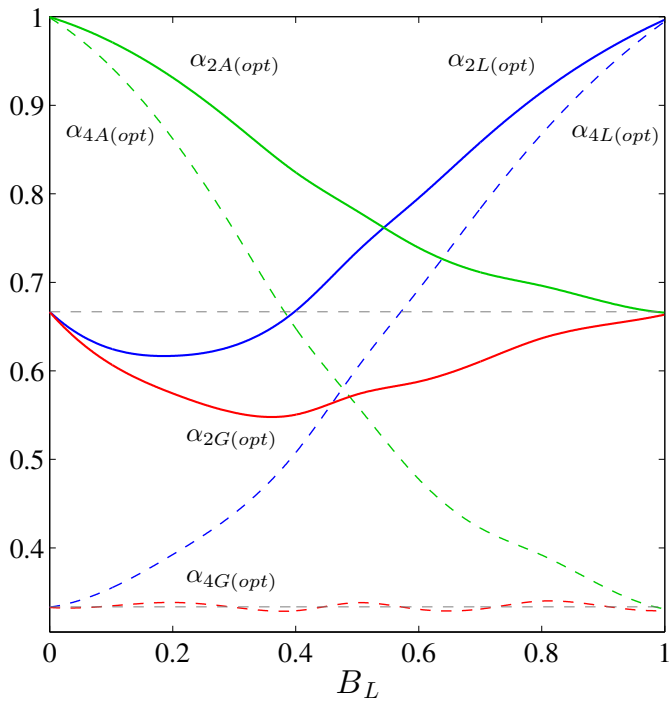

Figure 3.18: Optimal tunings for an array in an infinitely wide channel ($B_G = 0$). Results from the classic Betz analysis shown as grey dashed lines. Adapted from Nishino and Willden (2012).

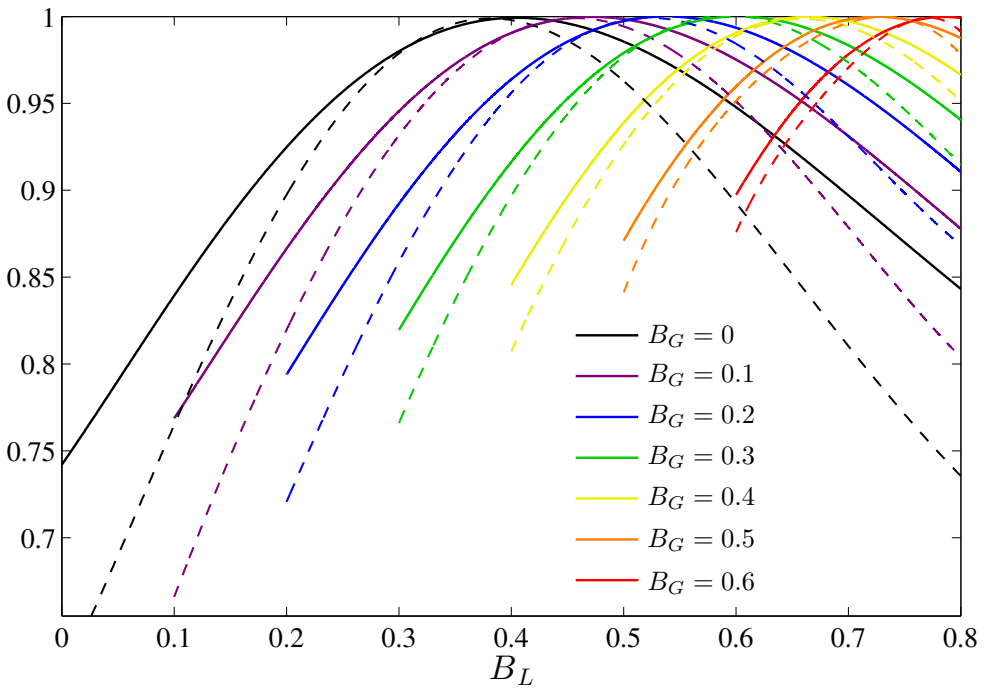

Figure 3.19: Variations of normalised maximum global power coefficient $C_{PG(max)}$ (solid lines) and optimal global thrust coefficient $C_{TG(opt)}$ (dashed lines) with local blockage B_L for a range of global blockages B_G.

In a later work, Nishino and Willden (2013) extend the two-scale theory to better account for the effects of array-scale flow expansion, so that the model is equally applicable to short rows in which the separation of local and array-scale flows is less well-defined (Nishino and Draper, 2015). Predictions from the extended model have been shown to agree well with three-dimensional Reynolds-averaged Navier-Stokes simulations of porous discs, which suggests that array performance is predominantly determined by local and array-scale flow dynamics (Nishino and Willden, 2013). More recently, the two-scale model has been extended to investigate the effects of free surface deformation by Vogel et al. (2016), the performance of cross-stream aligned sub-arrays by Cooke et al. (2016), and the potential for local blockage effects to enhance the performance of wind turbines by Nishino (2016) and Zapata et al. (2017). Further works by Willden et al. (2014),

Divett (2014), and Divett et al. (2014) have sought to extend the two-scale model to incorporate channel-scale dynamics but, as of yet, no model has captured fully the dynamics of flow through a partial-width array within a channel.

Centred and staggered arrangements

The combined models discussed previously provide many useful insights into the performance of turbines in arrays but incorporate either explicitly or implicitly the assumption that turbines will be spaced sufficiently far apart to avoid wake interactions. In reality, however, practical constraints may require that turbines be placed close enough to experience wake interactions on the scale of either individual turbines or entire rows. With this in mind, Draper and Nishino (2014a,b) proposed extended actuator disc models to describe the idealised flow field around a disc placed in either the decelerated wake or accelerated bypass of another disc placed further upstream (figure 3.20). By assuming a streamwise spacing that is sufficient for pressure equalisation but insufficient for significant wake mixing, Draper and Nishino extended the model of Garrett and Cummins (2007) to explore

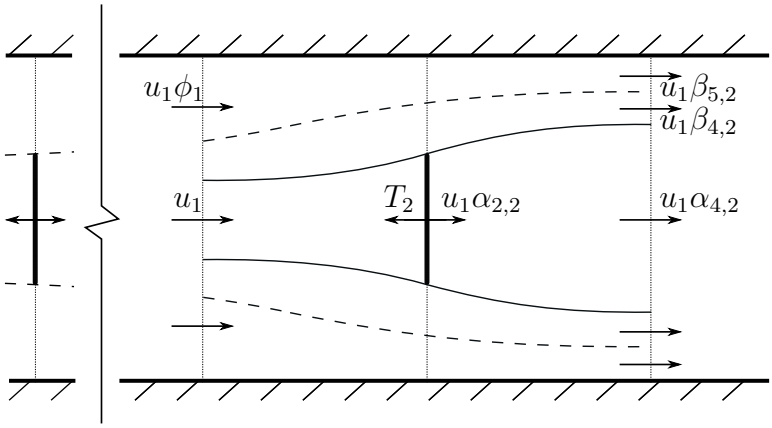

Figure 3.20: Actuator disc model of a centred turbine arrangement. Side/plan view, adapted from Draper and Nishino (2014a,b).

the performance of turbines in centred and staggered arrangements. The extended models are then used to investigate the effects of wake interaction on the performance of closely spaced rows or turbines within arrays.

The effect of the first (upstream) disc is to create a non-uniform inflow for the second (downstream) disc, which Draper and Nishino define in terms of a wake region with cross-sectional area $r_1 A$ and velocity $u\alpha_{4,1}$ and a bypass region with area $(1 - r_1)A$ and velocity $u\beta_{4,1}$. The second disc may be placed either into the wake to be centred, or into the bypass to be staggered, behind the first disc. In this model, velocity coefficients are represented by subscripts containing two numbers: the former, as previously, representing streamwise location and the latter representing the disc to which it refers. The first disc defines the flow field for the second but due to the assumption of pressure equalisation between the discs, the second disc has no effect on the performance of the first. The flow field around the second disc is clearly more complicated than that around the first but by applying arguments of continuity, momentum, and energy, Draper and Nishino develop expressions to describe the performance of both discs. Being unaffected by the presence of the second disc, the power coefficient of the first disc is given by an expression indentical to that developed by Garrett and Cummins (2007):

$$C_{P1} = \alpha_{2,1}(\beta_{4,1}^2 - \alpha_{4,1}^2), \tag{3.59}$$

while the power coefficient of the second disc, being dependent on both the performance of the first disc and their relative positions, is given by one of two expressions:

$$C_{P2\,(centred)} = (\alpha_{4,1}^3)\,\alpha_{2,2}(\beta_{4,2}^2 - \alpha_{4,2}^2), \tag{3.60}$$

$$C_{P2\,(staggered)} = (\beta_{4,1}^3)\,\alpha_{2,2}(\beta_{4,2}^2 - \alpha_{4,2}^2). \tag{3.61}$$

The extended models allow Draper and Nishino to compare different configurations of the two turbines in terms of both individual and average power coefficients C_{P1}, C_{P2}, and C_P, and average extraction efficiency η. To simplify the analysis, it is assumed that the disc blockage ratios are always equal so that the performance of the two disc configuration is a function of only their relative positions and individual resistances.

For centred discs, the maximum average power coefficient $C_{P(max)}$ is achieved by applying a larger resistance with the second disc than with the first because, in this arrangement, the performance of the second disc is enhanced by maintaining a high flow rate through the first. For staggered discs, however, $C_{P(max)}$ is achieved by applying a larger resistance with the first disc than with the second because, in this arrangement, the performance of the second disc is enhanced by using the first disc to accelerate flow into the path of the second. The enhancements that may be achieved by allowing the discs to present different resistances to the incoming flow are relatively insignificant for centred arrangements and although considerable for staggered arrangements, require markedly uneven distributions of thrust and power between the discs. Real arrays will likely be composed of turbines of approximately equal resistance to ensure symmetric operation with respect to oscillatory currents and approximately equal distributions of applied thrust and extracted power.

Draper and Nishino also compare the centred and staggered arrangements to two limiting cases in which wake interactions are avoided: those of two discs placed in the same plane (two discs effectively merged into one in the case of a centred arrangement) and two discs placed far upstream and downstream of each other. The comparisons suggest that for centred discs, both maximum average power coefficient $C_{P(max)}$ and average extraction

efficiency η increase with increasing streamwise separation while for staggered discs, $C_{P(max)}$ and η increase with decreasing streamwise separation. For discs of equal resistance, the maximum power available to a staggered arrangement is found to be greater than that available to a centred arrangement, but still less than the power available to discs placed in the same plane (Draper and Nishino, 2014a,b). This is explained as follows. In a centred (staggered) arrangement, the reduced (enhanced) inflow experienced by the second disc means that the maximum power output of the two disc configuration is less (greater) than if the discs had been placed in isolation but, importantly, optimal performance of the second disc requires suboptimal performance of the first (Draper and Nishino, 2014a,b). A better strategy is to arrange discs for maximum blockage. Placing discs in the same plane not only produces more power than centred and staggered arrangements, but ensures an equal distribution of thrust and power between the discs.

Interestingly, the single row is also the most efficient arrangement considered. The enhanced inflow experienced by the second disc in a staggered arrangement enables the discs to extract power more efficiently than two discs in isolation. Due to the finite streamwise separation between the discs, however, the staggered arrangement incurs greater mixing losses than the single row. Least efficient of all is the centred arrangement, which, by combining increased streamwise separation with reduced inflow to the second disc, ensures the discs operate less efficiently than if placed in isolation.

Despite being limited to flows of low Froude number and situations in which the effects of extraction on the flow are negligible, the centred and staggered models provide several useful insights into the performance of closely spaced turbines. For discs of equal size and resistance, the models suggest trends for increasing (decreasing) power with streamwise spacing

for centred (staggered) arrangements. Although Draper and Nishino do not prove these trends to be strictly monotonic, the existence of local maxima would require the downstream disc to perform better in wakes that are either still expanding (for staggered arrangements) or have already started mixing (for centred arrangements). Results from recent three-dimensional Reynolds-averaged Navier-Stokes simulations suggest that these trends are indeed monotonic and that a single row is therefore the best arrangement for tidal turbines (Hunter et al., 2015). The fact that the single row enables both greatest power output and highest extraction efficiency is especially convenient because it suggests that this arrangement is optimal for arrays of any size in any uniform tidal channel (Draper and Nishino, 2014a,b). If practical constraints preclude the arrangement of turbines in a single row, the centred and staggered models suggest that the next best arrangements are two closely spaced (i.e. interacting) rows of staggered turbines, followed by two isolated rows (either staggered or centred) and, finally, two closely spaced rows of centred turbines (Draper and Nishino, 2014a,b).

3.4 Conclusions

The optimal design of a tidal turbine array is complicated by the fact that turbines interact with current resources over a broad range of length scales and in ways that are difficult to predict *a priori* (Adcock et al., 2015; Vennell et al., 2015). In recent years, simple theoretical models have provided a number of invaluable insights to inform the design of tidal turbine arrays. Among the most important insights are that turbines present additional resistance to flow, which implies an upper limit on the amount of power that may be extracted (Garrett and Cummins, 2005); that the power available

to the turbines constitutes only a fraction of the total power extracted from the flow (Garrett and Cummins, 2007); and that the power available to each turbine depends on both the type of channel (i.e. its geometry and dynamic balance) and the position and tuning of all the turbines within it (Vennell, 2010). These models suggest that, to maximise available power, arrays should be assembled by first filling a single row as densely as possible and then continuously adding dense new rows downstream for as long as the economics of the diminishing returns will allow (Vennell, 2010). This strategy is favourable because placing turbines in the same plane maximises their blockage — the single most important parameter in determining turbine and array performance — thereby enabling both greater power extraction and higher extraction efficiency (Draper and Nishino, 2014a,b). It has also been suggested that lateral spacing may be optimised to further enhance the performance of turbines within a single row (Nishino and Willden, 2012, 2013). As of yet, however, the extent to which local blockage effects can enhance the performance of the large arrays required to extract a significant fraction of a channel's potential is unknown.

The potential for local blockage effects to enhance array performance forms the central focus of the second part of this thesis. Chapter 4 describes the development of a depth-averaged numerical model to explore the performance of a single row of turbines in a tidal channel. This model extends the two-scale actuator disc theory in a number of important ways; most notably to describe the effects of local blockage in flow conditions that are more representative of real tidal currents.

Chapter 4

Combined array and channel model

Simple theoretical models have shown that tidal turbines should be arranged in a single cross-stream row to maximise available power (Vennell, 2010). More recent works suggest that the power output of such a row can be further increased (albeit at the expense of a reduction in extraction efficiency) by varying the lateral spacing between turbines to exploit local blockage effects (Nishino and Willden, 2012, 2013). This chapter describes the development of a simple numerical model to explore more fully the effects of local blockage on array performance.

A combined model of a turbine array in a tidal channel is developed to investigate the ways in which turbine resistance (defined in terms of local blockage and tuning) interacts with local-, array-, and channel-scale flows to determine the maximum available power. This model is used to extend the two-scale actuator disc theory by: (i) giving a two-dimensional description of flow around a partial-width array; (ii) allowing turbine resistance not only to divert flow between individual turbines and around the entire array,

but also to reduce the channel flow rate; (iii) incorporating the effects of channel background roughness and fluid inertia, and; (iv) enable comparison of different arrangements not only in terms of power coefficient but also in terms of absolute power. Realistic channel dimensions and flow parameters are used but the model is otherwise simplified to enable comparison with theory and to ensure that its findings are broadly applicable.

4.1 Numerical scheme

The equations that describe fluid flow are derived from the conservation laws of classical physics. Fluid elements move, rotate, and deform under the action of unbalanced forces but in accordance with the laws of mass, momentum, and energy conservation (Anderson, Jr., 2008; Zikanov, 2010). A set of partial differential equations to describe the motion of such elements may be developed by analysing flow through a fixed region in space or following the path of a single element in time (Ferziger and Perić, 1996). The nonlinearity of these equations, added to the complexity of the typical fluid problem, requires that they be solved by using numerical techniques to approximate the continuous flow field at discrete points in space and time (Fletcher, 1988).

Shallow water equations

If the horizontal scales of a time-varying flow are much larger than the vertical scales, the flow may be considered horizontal and its three dimensions reduced to two by assuming that horizontal velocities are constant over the depth, that vertical accelerations are negligible, and that fluid pressure is purely hydrostatic. The shallow water equations, which are most commonly

derived by depth-averaging the continuity and Reynolds-averaged Navier-Stokes equations (e.g. Falconer, 1993) or from control volume analysis of a fluid element extending from the bed to the free surface (e.g. Abbott, 1979), may be expressed as:

$$\partial_t(\xi) + \partial_x(Hu) + \partial_y(Hv) = 0, \tag{4.1}$$

$$\begin{aligned}\partial_t(Hu) + \partial_x\left(Hu^2 + \frac{1}{2}g(H^2 - h^2)\right) + \partial_y(Huv) = -gH\partial_x(\xi) \\ -C_d u\sqrt{u^2+v^2} + \nu\big(2\partial_{xx}(Hu) + \partial_{yy}(Hu) + \partial_{xy}(Hv)\big),\end{aligned} \tag{4.2}$$

$$\begin{aligned}\partial_t\left(Hv\right) + \partial_x(Huv) + \partial_y\left(Hv^2 + \frac{1}{2}g(H^2 - h^2)\right) = -gH\partial_y(\xi) \\ -C_d v\sqrt{u^2+v^2} + \nu\big(\partial_{xx}(Hv) + 2\partial_{yy}(Hv) + \partial_{xy}(Hu)\big),\end{aligned} \tag{4.3}$$

in which ξ is the elevation of the free surface; h is the bathymetric depth; $H = \xi + h$ is the total depth; u and v are the depth-averaged streamwise and spanwise components of velocity, respectively; g is acceleration due to gravity; C_d is a dimensionless seabed drag coefficient; and ν is a horizontal eddy viscosity coefficient. Implicit in the presentation of these equations are the assumptions of a fixed seabed (i.e. no erosion or sedimentation); a quadratic seabed drag; a spatially- and temporally-constant eddy viscosity; negligible Coriolis forcing; and a flow that is driven solely by the gradient in surface elevation and loses energy, in the unexploited case, only to background roughness and turbulent mixing.

The shallow water equations have long been the model of choice for tidal hydrodynamics (Adcock et al., 2015). Modelling tides as horizontal flows simplifies computation but also reduces the accuracy with which certain features can be reproduced. Most notably, depth-averaged models are unable to represent correctly variations in fluid velocity and shear stress within the water column, which limits their ability to simulate separation

and remixing of flow around complex bathymetric features and tidal turbines (Draper, 2011; Stansby, 2006; Vogel, 2014). However, the aim of this thesis is simply to understand the interactions between turbine resistance and bulk flow through the array, a task for which depth-averaged models are well suited (Adcock et al., 2015).

DG finite element solver

A numerical model requires a domain of interest, boundary and initial conditions, and a means by which to replace the continuous flow field described by the governing partial differential equations with discrete numerical approximations (Toro, 2013; Zikanov, 2010). Following Kubatko et al. (2009, 2006), Draper (2011), and Serhadlıoğlu (2014), the shallow water equations are discretised spatially using the discontinuous Galerkin (DG) finite element method and advanced using an explicit Runge-Kutta (RK) time-stepping scheme. DGRK solvers conserve mass locally and can achieve high order spatial and temporal accuracy (Draper, 2011). Local conservation, combined with the use of discontinuous polynomial basis functions, allows the code to be modified to incorporate the actuator disc model of Houlsby et al. (2008) at sub-grid scale.

The momentum sink associated with tidal turbines, which are defined by their local blockage and tuning, is related via actuator disc theory to a head drop, which is represented in the numerical model as a discontinuous change in fluid depth. This coupling allows the turbines to interact dynamically with the flow and eliminates the need to represent the turbine structure or approximate highly three-dimensional local-scale mixing processes. The sub-grid scale actuator disc implementation was first developed by Draper et al. (2010), used to investigate the maximum power available from a num-

ber of generic coastal geometries by Draper (2011), and later incorporated into the DG version of the open-source hydrodynamic model ADCIRC (Kubatko et al., 2009, 2006; Luettich, Jr. et al., 1992) by Serhadlıoğlu (2014). The modified code of Serhadlıoğlu has been used extensively to assess tidal current resources both in idealised problems (Adcock, 2015; Draper et al., 2013a) and at real sites (e.g. Adcock et al., 2013; Serhadlıoğlu et al., 2013). This code is also the basis for the model developed herein, which, for ease of computation, uses linear basis functions and a second-order RK time-stepping scheme.

4.2 Tidal channel

As illustrated in figure 4.1, the depth-averaged domain is 4 km wide and 120 km long, with a 20 m deep channel making up the central 20 km. The northern and southern boundaries are mainland slip boundaries and the eastern and western boundaries are ocean boundaries at which the water level must be prescribed. A regular unstructured mesh is used to divide the domain into 17,436 triangular elements with sides varying in length from 100 m in the channel to more than 2 km at the flow boundaries, and a time step of 1 s is specified.

Flow is driven through the channel by raising or lowering the water level at the western boundary while the water level at the eastern boundary is held constant. Following Adcock (2015), the depth outside the central channel is increased linearly to 1 km at the ends of the domain to minimise the reflection of error waves from the open boundaries (e.g. Adcock et al., 2011; Garrett and Greenberg, 1977). The drag on the flow due to bed roughness is given by $\mathbf{F} = \rho A_b \mathbf{u}|\mathbf{u}|C_d$, in which ρ is the fluid density, A_b is

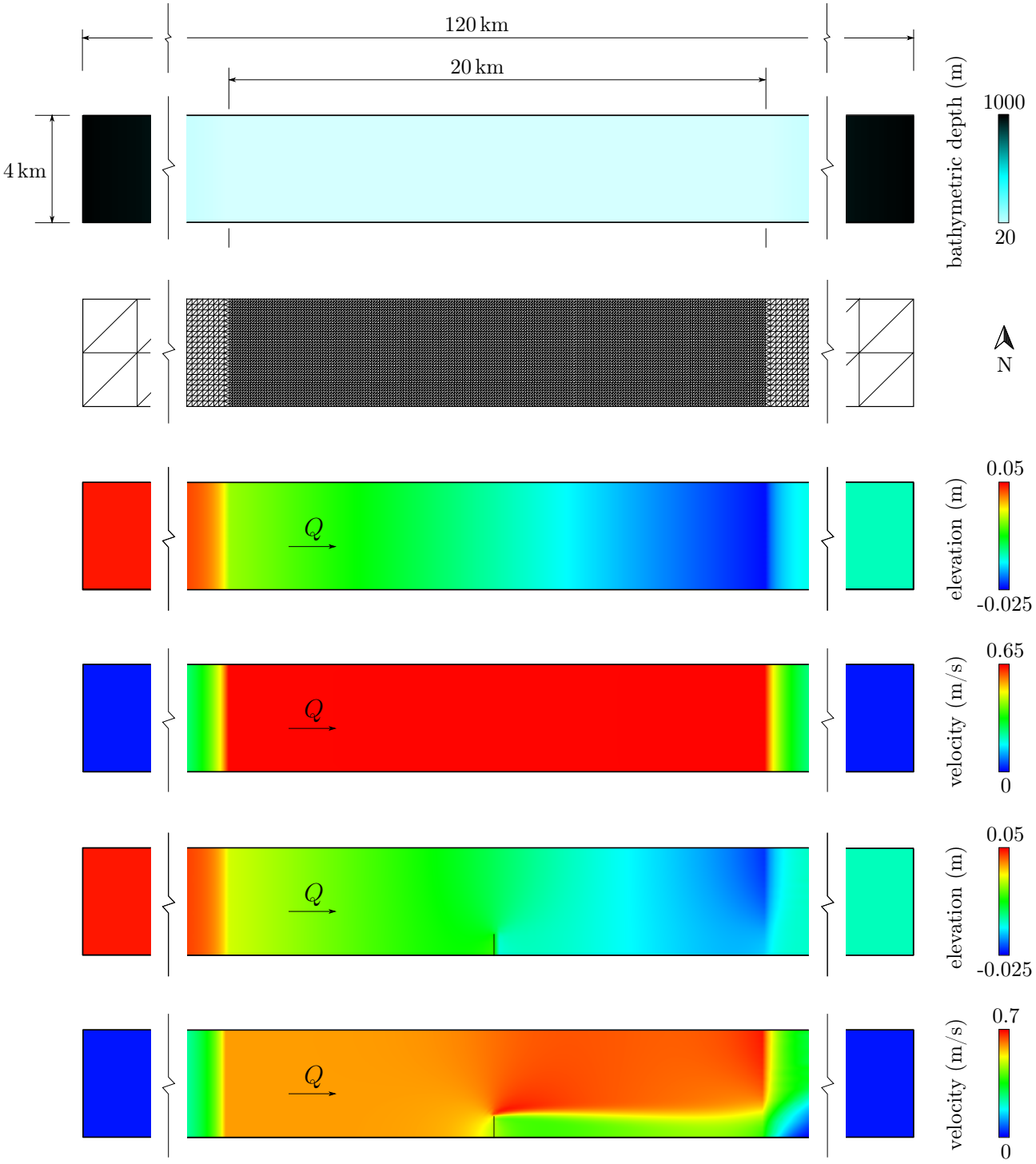

Figure 4.1: Plan views of the model domain showing the bathymetric profile, numerical mesh, and typical surface elevation and depth-averaged velocity profiles for simulations excluding and including the turbine array.

the plan area of the seabed, $\mathbf{u}$ is the depth-averaged velocity vector, and C_d is the seabed drag coefficient. Realistic values of C_d are obtained from Soulsby (1997) to represent high ($C_d = 0.003$), medium ($C_d = 0.001$), and low ($C_d = 0.0005$) roughness flows. (Using the alternative convention from mechanical engineering that includes an additional 1/2, the corresponding values would be $C_d = 0.006, 0.002$, and 0.001.) The value of the eddy viscosity coefficient is determined, following Borthwick and Barber (1992), as $\nu = 5.9H|\mathbf{u}|\sqrt{C_d} \approx 2.55\,\mathrm{m}^2/\mathrm{s}$. A sensitivity analysis is also performed, which shows the model results to be relatively insensitive to this value.

Validation

If the length of the channel is short compared to the wavelength of the tidal forcing, the flow rate should be independent of position along the channel. Calculation of Vennell's (1998) criterion confirms that the channel is non-divergently short and thus representative of Garrett and Cummins' (2005) analytical model. To compare the models, a number of simulations are performed using different drag coefficients and tidal forcings. Steady flows are driven by a constant head difference ζ across the channel (Z across the entire domain) and the resulting flow rates Q recorded. Oscillatory flows are driven by an oscillating head difference of ξ across the channel (Ξ across the entire domain) and period 44,700 s ($\sim$12.42 h), and the maximum flow rates $Q_{(max)}$ and phase differences between head and current ϕ recorded. Tables 4.1 and 4.2 compare the values predicted by the numerical model with those predicted by the analytical model of Garrett and Cummins and show good agreement in all cases*.

* The predictions from the analytical model of Garrett and Cummins (2005) presented in tables 4.1 and 4.2 were kindly provided by Lei Chen, a graduate student under the supervision of the author at the time of writing.

C_d	Z (m)	ζ (m)	Q (m^3/s)	$Q_{(\mathrm{GC05})}$ (m^3/s)
0.003	0.05	0.0479	31.611×10^3	31.644×10^3
0.001	0.05	0.0483	54.722×10^3	55.066×10^3
0.0005	0.05	0.0486	77.272×10^3	78.122×10^3

Table 4.1: Numerically (Q) and analytically ($Q_{(\mathrm{GC05})}$) predicted flow rates for selected steady flow cases.

C_d	Ξ (m)	ξ (m)	T (s)	$Q_{(max)}$ (m^3/s)	ϕ (deg.)	$Q_{(max)\,(\mathrm{GC05})}$ (m^3/s)	$\phi_{(\mathrm{GC05})}$ (deg.)
0.003	0.1	0.0727	44,700	19.875×10^3	71.52	19.751×10^3	75.14
0.003	0.4	0.3116	44,700	68.914×10^3	38.66	67.382×10^3	45.91
0.001	0.1	0.0746	44,700	20.109×10^3	82.63	20.763×10^3	84.72
0.001	0.2	0.1449	44,700	40.116×10^3	79.73	39.962×10^3	79.89
0.0005	0.1	0.0726	44,700	20.107×10^3	86.01	20.255×10^3	87.46
0.0005	0.2	0.1475	44,700	40.216×10^3	85.53	41.051×10^3	84.81

Table 4.2: Numerically ($Q_{(max)}, \phi$) and analytically ($Q_{(max)\,(\mathrm{GC05})}, \phi_{(\mathrm{GC05})}$) predicted maximum flow rates and average phase differences for selected oscillatory flow cases.

To ensure the mesh and time step independence of its solutions, the numerical model is then tested with three different meshes and time steps. New meshes are created by halving and doubling the original node spacings and each mesh is tested with time steps of 0.5 s, 1 s, and 2 s. In each case, C_d is set to 0.003, Ξ to 0.5 m, T to 44,700 s, and the model is allowed to spin up for 3 days before results from the next complete tidal cycle are analysed. Surface elevation results from nodes at the channel inlet and outlet, as well as depth-averaged velocity results from a node in the centre of the channel, are then extracted and compared. Time domain results are not shown but are found to be in excellent agreement. Tables 4.3–4.5 compare the frequency domain amplitudes of the driving signals at each node for each simulation and show excellent agreement between the different meshes and time steps.

	0.5 s time step	1 s time step	2 s time step
70,152 elements	0.45357767		
17,436 elements	0.45360726	0.45360602	
4,358 elements	0.45372119	0.45372119	0.45372119

Table 4.3: Frequency domain amplitudes of inlet node surface elevation (m)

	0.5 s time step	1 s time step	2 s time step
70,152 elements	0.42363532		
17,436 elements	0.42363267	0.42363267	
4,358 elements	0.42363027	0.42362540	0.42362542

Table 4.4: Frequency domain amplitudes of central node velocity (m/s)

	0.5 s time step	1 s time step	2 s time step
70,152 elements	0.05830394		
17,436 elements	0.05828663	0.05828663	
4,358 elements	0.05822420	0.05822419	0.05822418

Table 4.5: Frequency domain amplitudes of outlet node surface elevation (m)

4.3 Turbine array

Line sink of momentum

The DG ADCIRC code of Serhadlıoğlu (2014) is used as the basis for this numerical model because it has been modified, following Draper et al. (2010) and Draper (2011), to incorporate the actuator disc model of Houlsby et al. (2008) at sub-grid scale. Detailed descriptions are given by Draper and Serhadlıoğlu but the basic idea behind this turbine representation is quite simple. The DG finite element method approximates the flow field using piecewise polynomial functions that may be modified to incorporate discon-

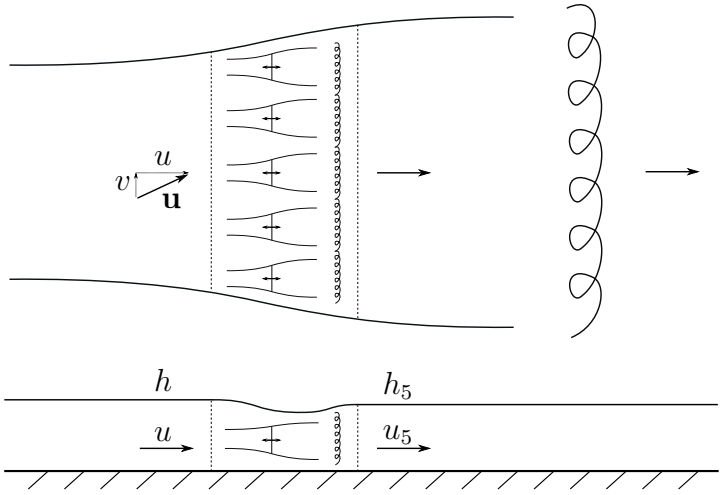

Figure 4.2: Line sink representation of a turbine array in a depth-averaged domain. Plan view (above) and side view (below), adapted from Draper (2011).

tinuities on the shared edge between adjacent elements. The code developed by Serhadlıoğlu includes the open channel actuator disc model as a subroutine, which is used to calculate the power available to turbines placed within certain specified edges and alter the momentum of the flow accordingly.

The idea is best illustrated by figure 4.2. A number of turbine edges are arranged in a single cross-stream row and assigned values of local blockage B and tuning α_4. These values are constant in time and the blockage is based on the still water depth. Within each turbine edge, the streamwise component of velocity u and depth h of the flow entering are used to calculate the upstream Froude number Fr, which is then used, along with B and α_4, to solve the actuator disc model. At each time step, this sub-grid scale model outputs both the power available to the turbine and the power dissipated in local-scale wake mixing, and imposes the corresponding changes in depth $\triangle h$ and velocity $\triangle u$ on the flow exiting the turbine edge. The spanwise component of velocity v is unaltered because it is assumed, as in the theoretical model, that the turbine does not exert a force in the tangential direction (Draper et al., 2010).

On passing through a turbine edge, the flow experiences a discontinuous change in depth and velocity as power is extracted by the turbine within it. The line sink is a convenient means by which to represent energy extraction but naturally requires a number of additional assumptions. The most obvious of these are that local-scale mixing lengths must be small compared to the size of the mesh elements and that flow through the domain must change sufficiently slowly as to be considered quasi-steady (Draper et al., 2010). The line sink approach is known to provide an imperfect model of velocity variations both across an array (Vogel et al., 2013) and beyond its ends where the applied thrust drops to zero (Draper, 2011) but has been shown to produce reasonably accurate predictions of the force exerted on, and presumably the power extracted by, strips of porous discs representing model-scale turbine arrays (Draper et al., 2013b).

Validation

With the turbines in place, the model is allowed time to spin up and for the available power results to reach a steady state before they are extracted for analysis. For steady flow, the model is allowed to spin up for 2 days — just long enough to accommodate the longer settling time required for the low roughness flows — after which the results from the following 12 hours are extracted and time-averaged to filter out minor fluctuations (figure 4.3). Problems arise for the combination of low channel background roughness and high turbine thrust, which produces an unsteady array-scale wake, perhaps due to the reflection of error waves from the downstream flow boundary. This unsteadiness means that the available power results never fully settle and that the use of this sampling period consistently overestimates the performance of high local blockage arrays in steady, low roughness flow.

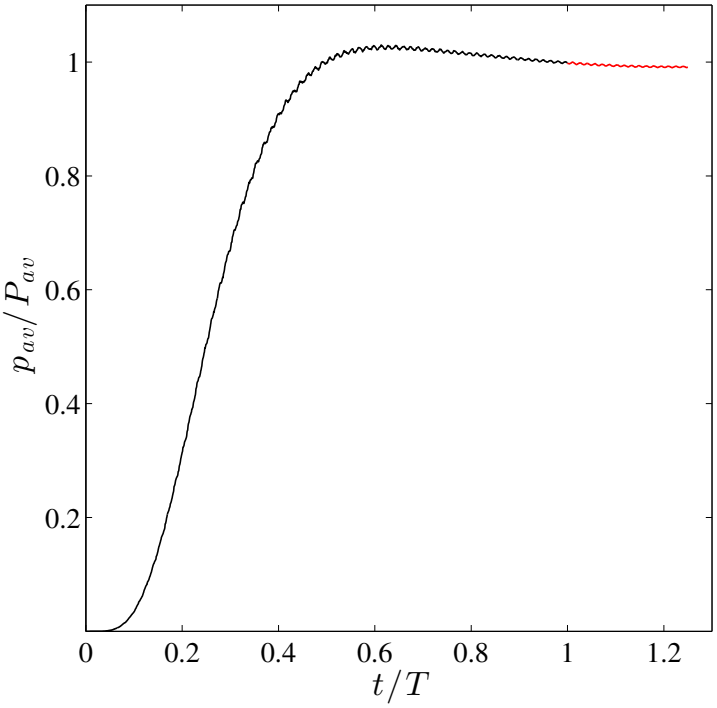

Figure 4.3: Typical model spin up for steady flow: Variation of instantaneous available power p_{av} (normalised by the time-average of the sampled power P_{av}) over time t (time to settle $T = 2$ days) with sampling period highlighted in red.

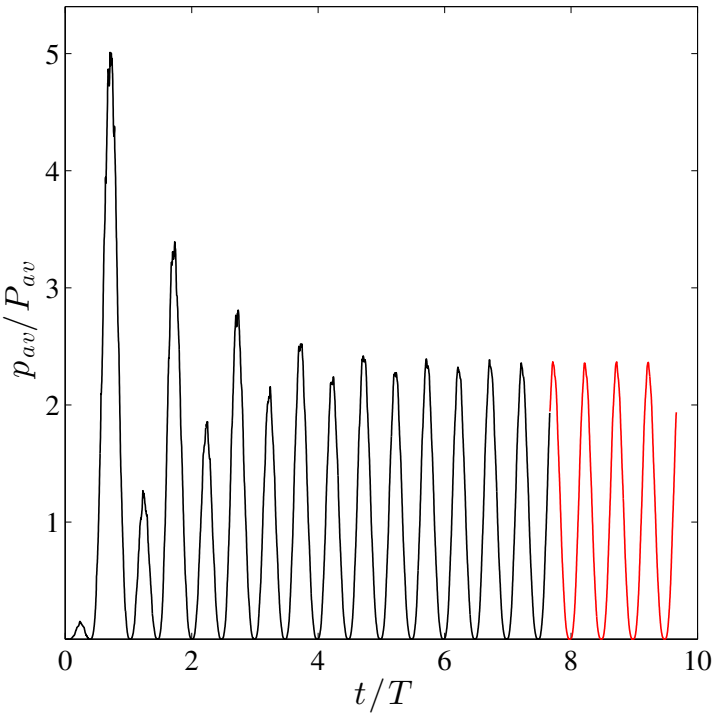

Figure 4.4: Typical model spin up for oscillatory flow: Variation of instantaneous available power p_{av} (normalised by the time-average of the sampled power P_{av}) over time t (tidal period $T = \sim$12.42 h) with sampling period highlighted in red.

Treatment of these results as approximate does not affect the conclusions drawn in the following chapters, however. For oscillatory flow, the model is allowed to spin up until the amount of power produced over the flood and ebb tides is approximately equal — allowing extra time, in this case, for the low roughness flows to settle fully — after which the results from last two complete cycles are extracted and time-averaged (figure 4.4).

Validation tests performed by Serhadlıoğlu (2014) have demonstrated that this sub-grid scale actuator disc model accurately imposes the prescribed nondimensional depth change on the flow. Herein the implementation is tested by cross-validation; by comparing the estimates of maximum extractable power calculated using both the line sink approach and the most popular alternative: a patch of enhanced bed roughness. A steady flow is driven through the channel by establishing a constant head difference ($Z = 0.05\,\mathrm{m}$) between the flow boundaries. For each of the high, medium, and low roughness flows, power is extracted using: (i) a patch of additional bed roughness, spanning the 4 km width of the channel and extending 2 km in the streamwise direction, and; (ii) a single row of turbine edges representing a full-width array of exceedingly high local blockage ($B_G = B_L = 0.8$). The DG ADCIRC code calculates the power extracted by the array $P_{ex\,(A)}$ using equation 3.44, while the power extracted by the patch is calculated as $P_{ex\,(P)} = \rho A_P u^3 (C'_d - C_d)$, in which A_P is the plan area of the patch, u is the average streamwise velocity, and C'_d and C_d are the enhanced and natural drag coefficients, respectively. Estimates of the maximum extractable power are made by interpolating between the results of a number of simulations run with different patch roughnesses and array tunings.

Table 4.6 compares the estimates of maximum extractable power with the values predicted by the analytical model of Garrett and Cummins

C_d	ζ (m)	Q (m^3/s)	$P_{ex(max)\,(P)}$ (MW)	$P_{ex(max)\,(A)}$ (MW)	$P_{ex(max)\,(\mathrm{GC})}$ (MW)
0.003	0.0479	31.611×10^3	5.8807	5.9665	5.9068
0.001	0.0483	54.722×10^3	10.1821	10.3319	10.3130
0.0005	0.0486	77.272×10^3	14.3900	14.6003	14.6379

Table 4.6: Numerically ($P_{ex(max)\,(P)}, P_{ex(max)\,(A)}$) and analytically ($P_{ex(max)\,(\mathrm{GC})}$) predicted channel potentials for selected steady flow cases.

(2005), calculated as $P_{ex(max)\,(\mathrm{GC})} = (2/(3^{3/2}))\rho g Q \zeta$, in which Q is the unexploited channel flow rate and ζ is the constant head difference between its ends. It should be noted that, because the analytical model does not account for the back effect of extraction on the driving head and because the way in which the patch is discretised by the numerical model makes the exact amount of additional roughness difficult to determine, both approaches are likely to underestimate the extractable power. Despite this, however, good agreement is shown in all cases.

Finally, the sub-grid scale model's ability to describe local blockage effects is tested. An array of low global blockage ($B_G = 0.1$) is placed into a low roughness channel ($C_d = 0.0005$) and a steady flow ($Z = 0.05\,\mathrm{m}$) established. The array is extended inward from one side of the channel to minimise 'end effects' — errors associated with the discontinuous change in thrust applied to the flow at the end of the array. The model is run with a number of different array tunings and the maximum global power coefficient is determined by interpolation. The effects of local blockage on array performance are explored by considering eight different arrangements of this global blockage within the cross-section, ranging from a full-width array of small turbines ($B_A = 1, B_L = 0.1$) to a short array of exceedingly large turbines ($B_A = 0.125, B_L = 0.8$) (figure 4.5). In each case, the array is tuned to produce $C_{PG(max)}$ and the numerically-predicted variation in array

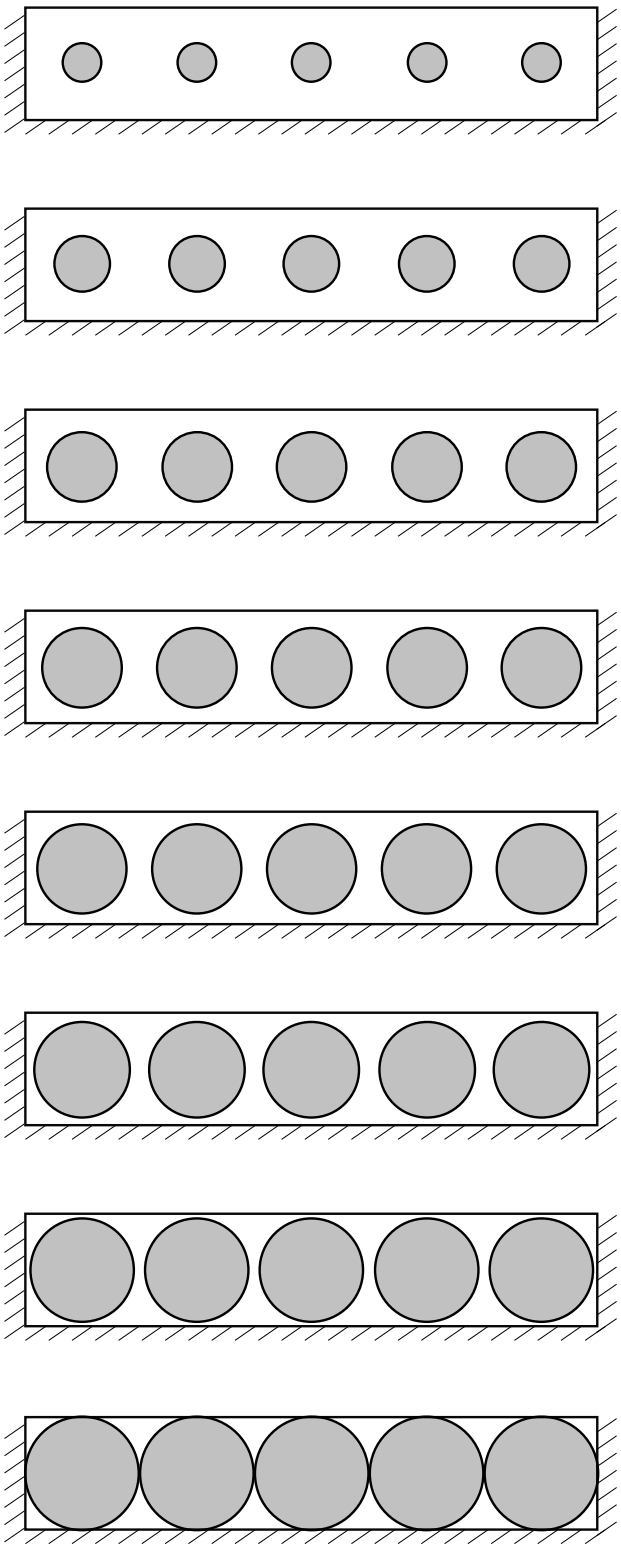

Figure 4.5: Schematic representations (cross-sectional views) of the eight local blockage ratios considered: $B_L = 0.1, 0.2, 0.3077, 0.4, 0.5, 0.5714, 0.6667$, and 0.8.

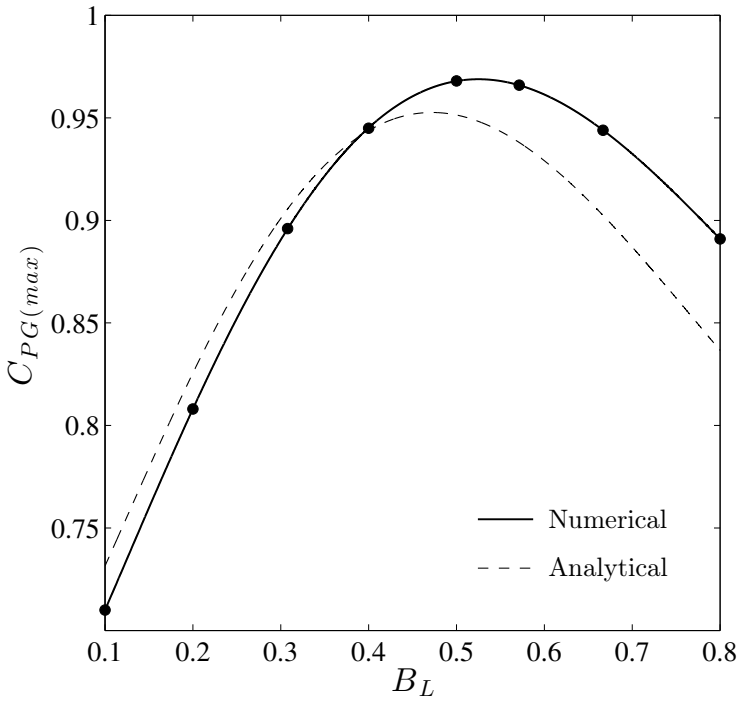

Figure 4.6: Numerically and analytically predicted variations of maximum global power coefficient $C_{PG(max)}$ with local blockage B_L. A high-order polynomial is fit to dots representing the values obtained using the eight local blockage ratios.

performance is compared with that predicted by the analytical model of Nishino and Willden (2012) (figure 4.6).

Although the numerical and analytical models incorporate many different assumptions — the numerical model describing two-dimensional, head-driven flow through a channel with background roughness that does not fully contain the array-scale mixing — figure 4.6 shows reasonable agreement between the two. Contrary to the findings of Perez-Campos and Nishino (2015), the predictions of the numerical model are lower than those of the analytical model for low B_L but higher for high B_L. For the purposes of this thesis, however, the most important finding is that an optimal local blockage is identified, which shows that the combined array and channel model can be used to analyse — qualitatively, at least — the potential for local blockage effects to enhance array performance.

4.4 Conclusions

A simple numerical model is developed to explore the performance of a turbine array in a tidal channel. Validation tests show the channel model to reproduce accurately predictions from the analytical model of Garrett and Cummins (2005) and the array model to reproduce qualitatively predictions from the analytical model of Nishino and Willden (2012). In the following chapters, the combined array and channel model is used to explore the potential for local blockage effects to enhance the performance of turbine arrays in flow conditions that are more representative of real tidal currents.

Chapter 5

Effects of local blockage in flow with background roughness*

In this chapter, the combined array and channel model is used to explore the potential for local blockage effects to enhance the performance of arrays in flow with background roughness.

An array of low global blockage ($B_G = 0.1$) is placed into a channel with drag coefficient C_d and a steady flow is produced by establishing a constant head difference ($Z = 0.05\,\mathrm{m}$) between the flow boundaries. The model is allowed to spin up for 2 days, after which results from the following 12 hours are extracted and time-averaged. The effects of local blockage are explored by comparing eight different arrangements of this global blockage within the cross-section, ranging from a full-width array of small turbines ($B_A = 1, B_L = 0.1$) to a short array of exceedingly large turbines ($B_A = 0.125, B_L = 0.8$). For each arrangement, the model is run with different array tunings to determine by interpolation both the maximum power coefficient and maximum available power. Optimal arrangements,

* An abridged version of section 5.1 has been published as a workshop abstract — see Bonar et al. (2016).

each defined by a local blockage and tuning, are identified for each metric by interpolating between these eight data points. This analysis is then repeated for low, medium, and high channel drag coefficients to explore the ways in which the optimal arrangements change with background roughness.

5.1 Maximum power coefficient

Figure 5.1 illustrates the variation of maximum global power coefficient $C_{PG(max)}$ with local blockage B_L and channel drag coefficient C_d, and figures 5.2–5.4 show the corresponding local tunings, local-scale efficiencies, and channel-scale kinetic fluxes, respectively. The solid dots used to indicate the optimal arrangement for a given C_d show that the effect of increasing background roughness is to increase both the peak $C_{PG(max)}$ and the optimal local blockage at which it occurs — a result that has been reported by both Bonar et al. (2016) and Creed et al. (2017).

To explain this, it is useful to begin with a single arrangement — $B_L = 0.5$, for instance. In low roughness flow, the maximum power coefficient for this arrangement is 0.9682, achieved when $\alpha_{4L} = 0.5265$; whereas in high roughness, the same local blockage and tuning produces a power coefficient of 1.0841. This enhancement is due to the fact that uniformly increasing the background roughness affects the core and bypass streamtubes differently. The natural drag on the flow is proportional to the square of the velocity, so the same increase in C_d slows the faster bypass flow relatively more than it does the slower core flow. This has the effect of increasing the resistance to array-scale bypass flow, which helps to funnel more flow through the array and thereby enhance its performance. This change in relative resistance also allows the turbines to be retuned to apply a larger thrust and further

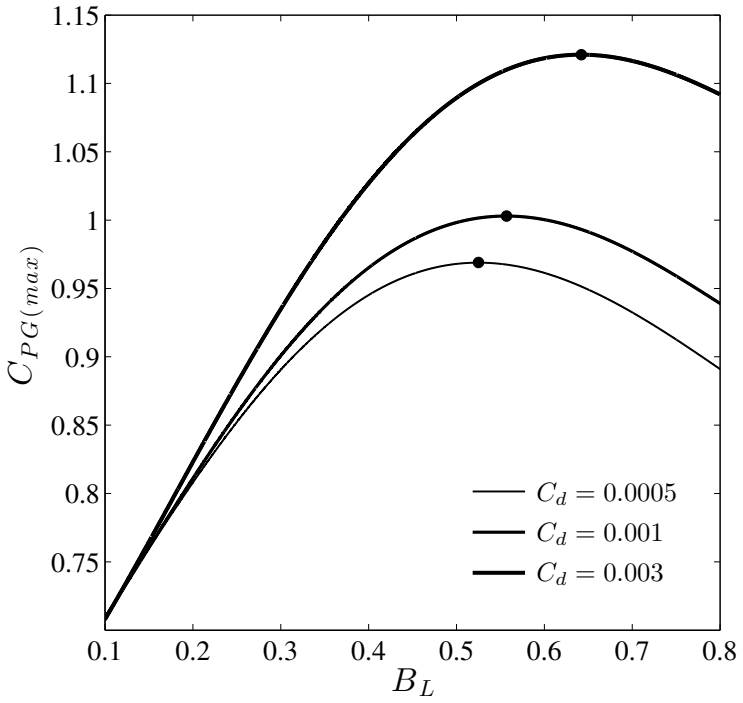

Figure 5.1: Variations of maximum global power coefficient $C_{PG(max)}$ with local blockage B_L and channel drag coefficient C_d. Dots indicate the points of peak power coefficient.

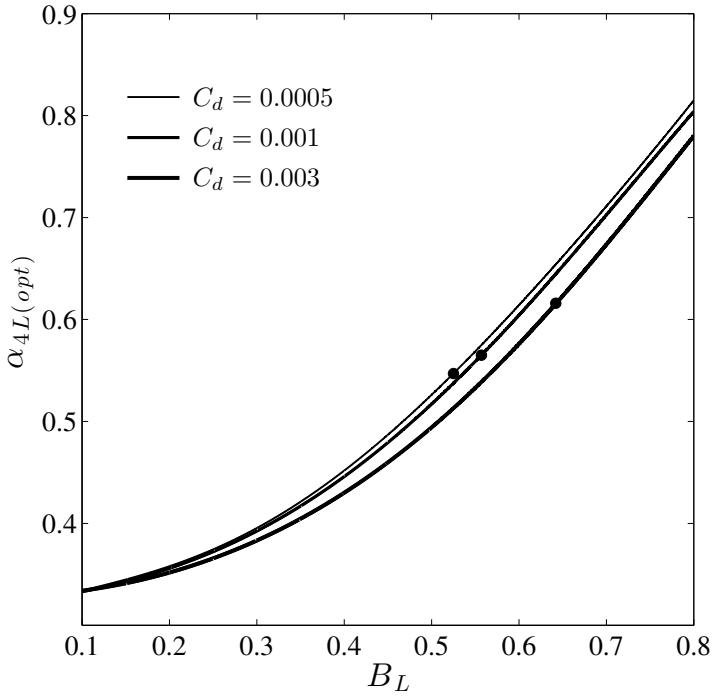

Figure 5.2: Local tunings α_{4L} corresponding to maximum global power coefficient $C_{PG(max)}$. Dots indicate the points of peak power coefficient.

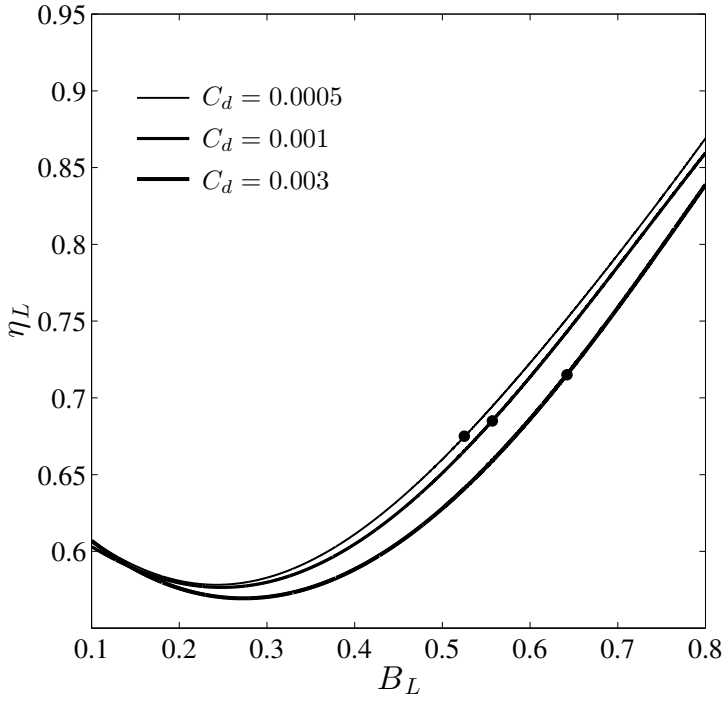

Figure 5.3: Local extraction efficiencies η_L corresponding to maximum global power coefficient $C_{PG(max)}$. Dots indicate the points of peak power coefficient.

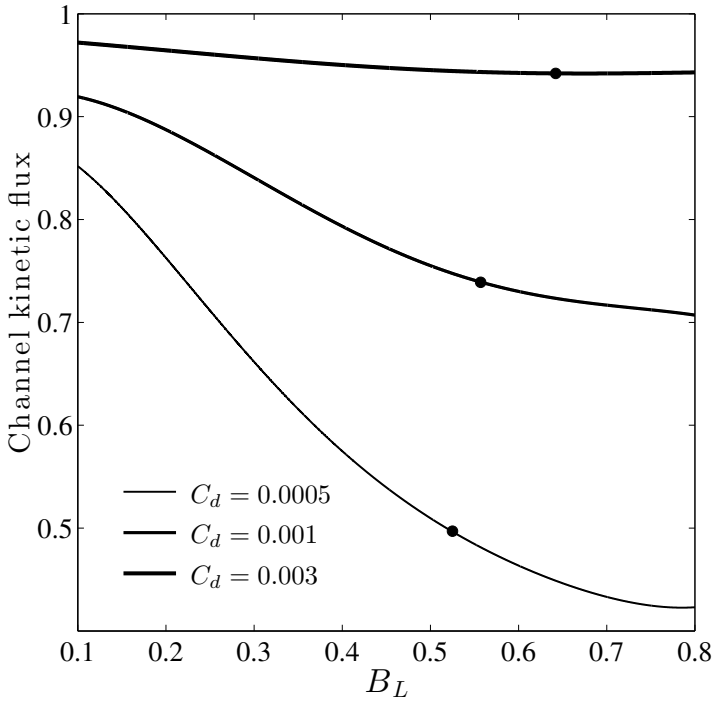

Figure 5.4: Changes in channel kinetic flux corresponding to maximum global power coefficient $C_{PG(max)}$. Dots indicate the points of peak power coefficient.

increase C_{PG}. In the foregoing example, C_{PG} can be increased to 1.0895 by retuning to $\alpha_{4L} = 0.4955$.

As discussed in chapter 3, the performance of a partial-width array is maximised by tuning turbines to slow the flow as much as possible without producing excessive diversion of flow either around the turbines within the array or around the array as a whole. It seems intuitive, however, that this optimal resistance depends not only on the turbine arrangement but also on the natural resistance to flow, represented herein by background roughness.

For a given local blockage, a uniform increase in background roughness can enhance the global power coefficient via a 'resistance boost', in which the natural resistance to the array-scale bypass flow is increased relative to that of the core flow, and a 'retuning boost', in which the turbines may then be retuned to apply a larger thrust. Although not considered in this thesis, it is clear that further increasing the bypass resistance relative to the core resistance would further enhance $C_{PG(max)}$.

In two scales, an increase in C_d is also shown to shift the peak $C_{PG(max)}$ to a higher local blockage. This is because the magnitudes of both the resistance and retuning boosts increase with local blockage. For optimally-tuned turbines, the difference between core and bypass velocities increases with B_L and therefore so do the amounts by which the increase in C_d slows the bypass flow relatively more than the core flow (figure 5.5) and thus enhances C_{PG} for a fixed tuning (figure 5.6). This means that both the amounts by which the turbines should be retuned after increasing C_d (figure 5.5), and thus C_{PG} can be enhanced by retuning (figure 5.6), also increase with B_L. The amount by which an increase in C_d can enhance C_{PG} appears to be an increasing function of B_L, which explains why its addition to the concave function representing the variation of $C_{PG(max)}$ with B_L shifts its

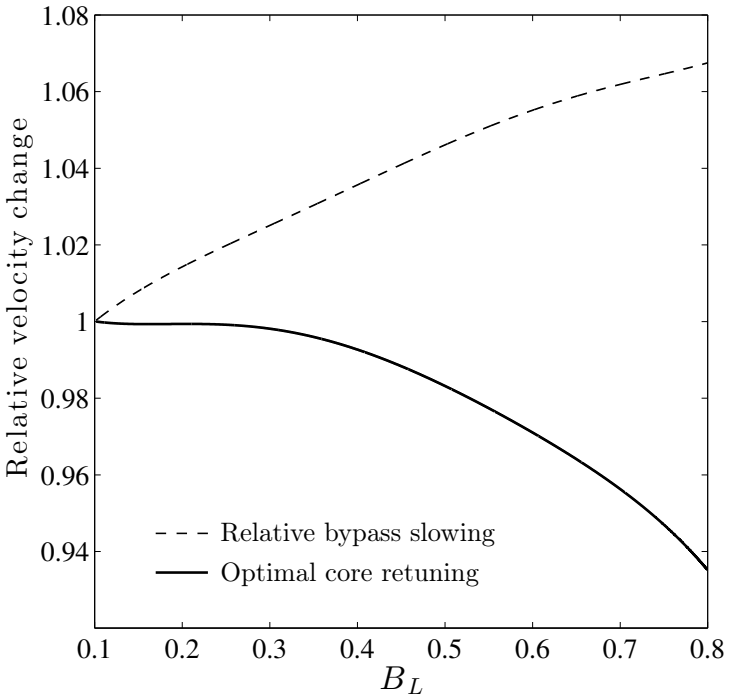

Figure 5.5: Amounts by which increasing the channel drag coefficient C_d from 0.0005 to 0.003 slows the bypass flow more than the core flow (dashed line) and the core flow should then be retuned to maximise the global power coefficient C_{PG} (solid line).

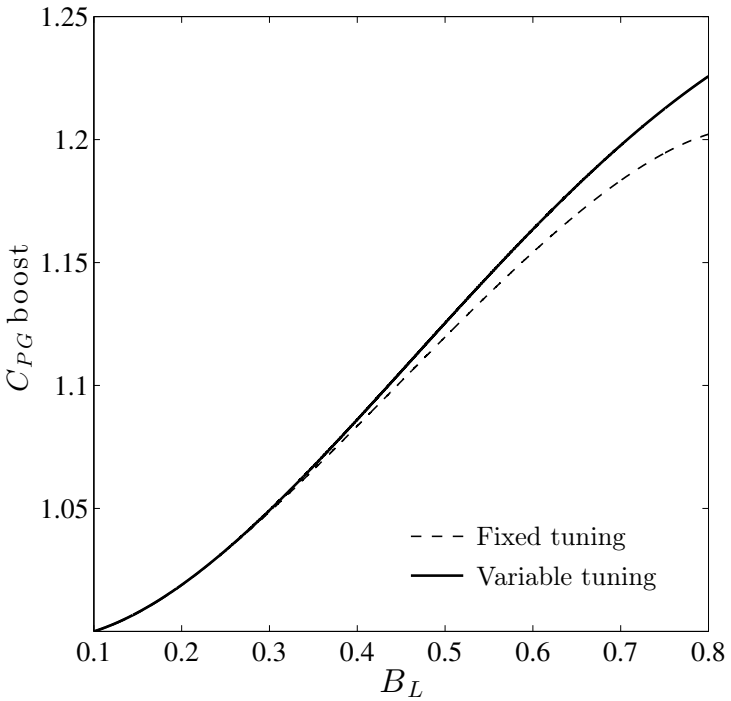

Figure 5.6: Amounts by which increasing the channel drag coefficient C_d from 0.0005 to 0.003 can enhance the global power coefficient C_{PG} for fixed (dashed line) and variable array tunings (solid line).

maximum to a point that is higher in both $C_{PG(max)}$ and B_L.

The local tunings, local-scale efficiencies, and channel-scale kinetic fluxes corresponding to $C_{PG(max)}$ vary as expected. Optimal local tunings increase smoothly with B_L, diverging from $\alpha_{4L} = 1/3$ such that, for a given B_L, the optimal tuning decreases with increasing C_d (figure 5.2). Local-scale efficiencies vary in accordance with the two-scale theory, increasing smoothly with B_L following an initial reduction (figure 5.3). For a given B_L, the local-scale efficiency corresponding to $C_{PG(max)}$ decreases with increasing C_d because the optimal tuning is lower, so relatively more power is dissipated in local-scale mixing. The effect of turbine thrust on the channel-scale kinetic flux is found to increase with increasing B_L but decrease with increasing C_d as natural dissipation becomes dominant (figure 5.4). Figure 5.4 is important because it shows that the applied thrust reduces not only the local and array-scale flows as described by the two-scale theory of Nishino and Willden (2012) but also the channel-scale flow — a fact that can be easily overlooked if performance is measured solely in terms of power coefficient.

It is also worth noting that these trends cannot be reproduced by simply coupling the models of Garrett and Cummins (2005) and Nishino and Willden (2012) because the zero-dimensional models do not account properly for the physics of array-scale diversion captured herein*.

5.2 Maximum available power

Figure 5.7 illustrates the variation of maximum available power $P_{av(max)}$, normalised by the channel potential, with local blockage B_L and channel drag coefficient C_d, and figures 5.8–5.10 show the corresponding local tun-

* This result was kindly provided by Lei Chen, a graduate student under the supervision of the author at the time of writing.

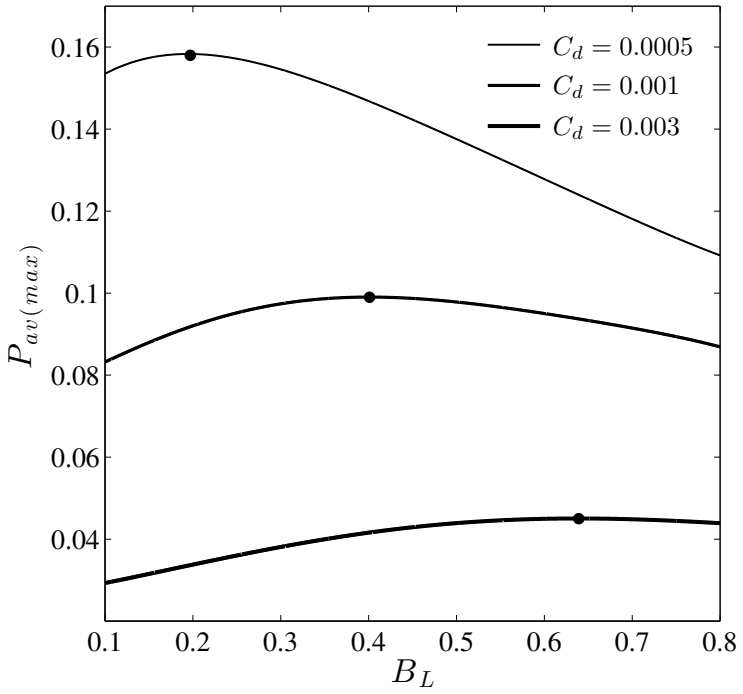

Figure 5.7: Variations of normalised maximum available power $P_{av(max)}$ with local blockage B_L and channel drag coefficient C_d. Dots indicate the points of peak available power.

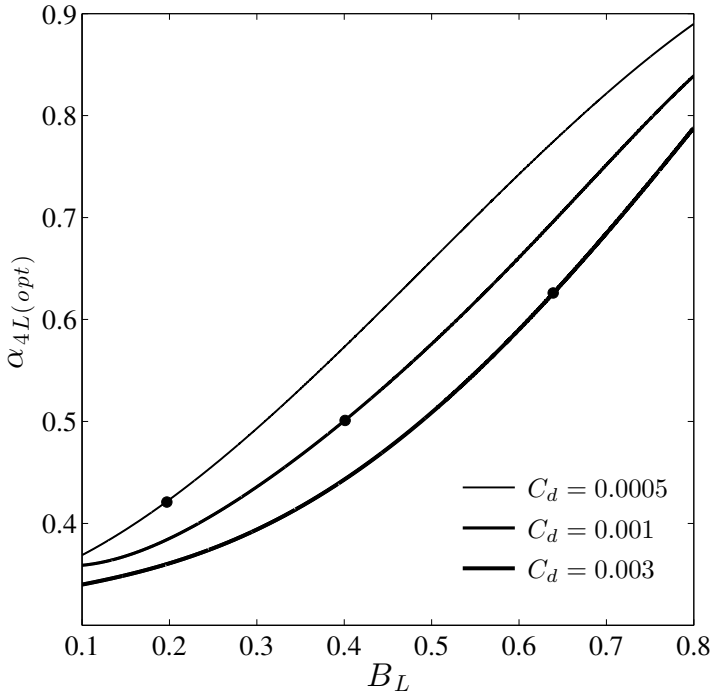

Figure 5.8: Local tunings α_{4L} corresponding to maximum available power $P_{av(max)}$. Dots indicate the points of peak available power.

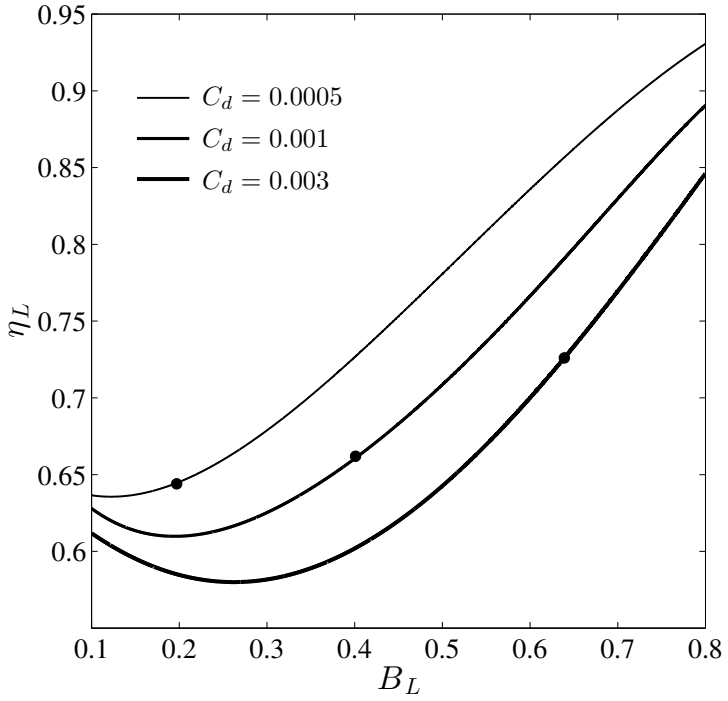

Figure 5.9: Local extraction efficiencies η_L corresponding to maximum available power $P_{av(max)}$. Dots indicate the points of peak available power.

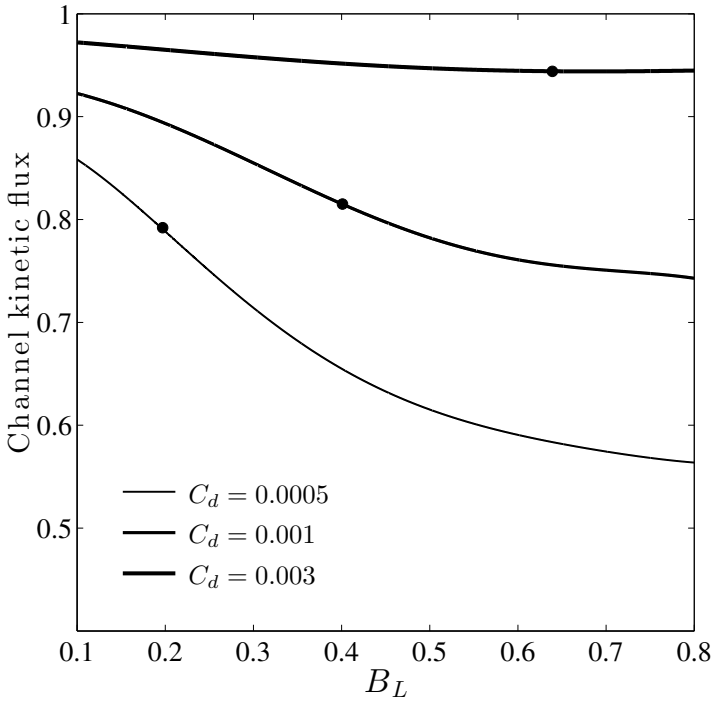

Figure 5.10: Changes in channel kinetic flux corresponding to maximum available power $P_{av(max)}$. Dots indicate the points of peak available power.

ings, local-scale efficiencies, and channel-scale kinetic fluxes, respectively. Trends for available power are essentially the same as those discussed for power coefficient but with one important difference: while the maximum global power coefficient increases with increasing background roughness, the maximum available power decreases.

For each C_d, there is also an optimal local blockage to maximise available power. Unsurprisingly, however, the local blockages that maximise available power and power coefficient — the ratio of available power to upstream kinetic flux — are not the same. In low roughness flow, for instance, the maximum available power begins to reduce after its peak at $B_L = 0.197$ while the maximum power coefficient continues to increase because the upstream kinetic flux is reducing faster than the available power.

Just as with power coefficient, the local blockage to maximise available power increases with increasing C_d due to the increasing resistance to flow around the turbines. Unlike for power coefficient, however, the maximum available power decreases with increasing C_d. In fact, figure 5.7 shows that the maximum available power is not only lower in high roughness flow, but a smaller fraction of the maximum extractable power. This is due to the fact that as the amount of power dissipated over the bed increases for a given head difference, the maximum amount that turbines can extract (i.e. the channel potential) decreases. Moreover, as C_d increases so too does the natural resistance to flow, so for a given global blockage with limited capacity to exert thrust on the incoming flow, a smaller fraction of the potential is available for extraction. These findings are consistent with the works of Garrett and Cummins (2005) and Vennell (2010).

The effects of local blockage are isolated by normalising the variations of $C_{PG(max)}$ and $P_{av(max)}$ with local blockage by the values obtained for

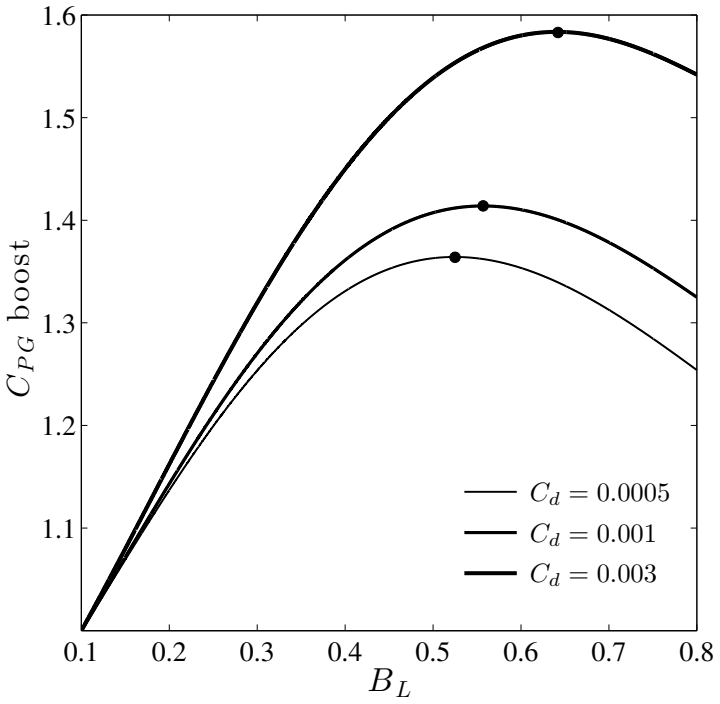

Figure 5.11: Variations of the potential for global power coefficient C_{PG} enhancement with local blockage B_L and channel drag coefficient C_d. Dots indicate the points of peak power coefficient.

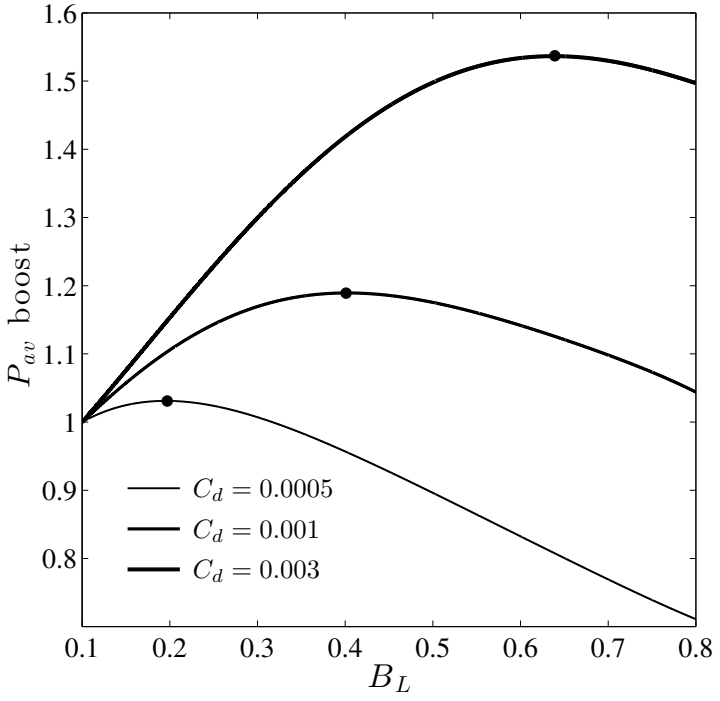

Figure 5.12: Variations of the potential for available power P_{av} enhancement with local blockage B_L and channel drag coefficient C_d. Dots indicate the points of peak available power.

the respective full-width arrays ($B_L = B_G = 0.1$). Figures 5.11 and 5.12 demonstrate that for both metrics, array performance can be enhanced significantly by exploiting local blockage effects and that the potential for enhancement increases with increasing natural resistance to flow, represented herein by channel background roughness.

5.3 Conclusions

Results from the combined array and channel model show that there is an optimal turbine arrangement to maximise available power and it is not the same as the arrangement that maximises the global power coefficient. These optimal arrangements are also shown to depend on the channel background roughness. Increasing background roughness increases the resistance to flow around the turbines, which allows them to be placed closer together, apply a greater thrust, and produce a higher power coefficient. However, increasing background roughness also increases the amount of energy dissipated over the seabed, which means that even though the power coefficient is higher, the turbines produce less power. As background roughness increases, the peak power coefficient increases but the maximum available power decreases. For both metrics, however, the potential for local blockage effects to enhance array performance is found to increase with increasing background roughness as the natural dissipation becomes more significant and the thrust from the turbines becomes less significant.

Chapter 6

Nonuniform arrays in uniform flow

The previous chapter sought optimal turbine arrangements based on the assumption that the optimal layout for an initially uniform flow would also be uniform (i.e. that each turbine edge within the row would have the same local blockage and tuning). In this chapter, the combined array and channel model is used to explore the potential for nonuniform arrays to produce a higher power coefficient or generate more power.

An array of low global blockage ($B_G = 0.1$) is placed into a low drag ($C_d = 0.0005$) channel and a steady flow is produced by establishing a constant head difference ($Z = 0.05\,\mathrm{m}$) between the flow boundaries. The model is allowed to spin up for 2 days, after which results from the following 12 hours are extracted and time-averaged. Then, starting from near-optimal uniform arrangements, the effects of nonuniformity on array performance are explored by varying the local blockage B_L and local tuning α_{4L} linearly across the width of the array. The nonuniform profiles considered herein are bilaterally symmetric due to their reflective symmetry about the southern

mainland boundary (figure 6.1) and include arrays with uniform B_L but nonuniform α_{4L}, uniform α_{4L} but nonuniform B_L, and selected examples in which both B_L and α_{4L} are nonuniform.

6.1 Maximum power coefficient

In the previous chapter, it was shown that, for $B_G = 0.1$, a maximum power coefficient of 0.969 could be produced by setting a uniform B_L of 0.525 and a uniform α_{4L} of 0.547. However, given that it is not possible to produce this configuration with the current mesh (because this arrangement, which was identified via interpolation, cannot be achieved using a whole number of turbine edges), a near-optimal arrangement with $B_L = 0.5714$, $\alpha_{4L} = 0.583$, and $C_{PG} = 0.966$ is instead chosen as the starting point for the analysis. In this configuration the array blockage is 0.175, so turbines occupy 7 of the 40 cross-stream element edges. In all cases B_L and α_{4L} are varied linearly across these edges, with variations denoted by their extreme values at the edges nearest to (the central edge) and furthest from (the end edge) the southern mainland boundary.

The analysis begins by exploring the performance of arrays with uniform local blockage but nonuniform local tuning. For a uniform B_L of 0.5714, figures 6.2–6.4 illustrate the variations of global power coefficient C_{PG}, local-

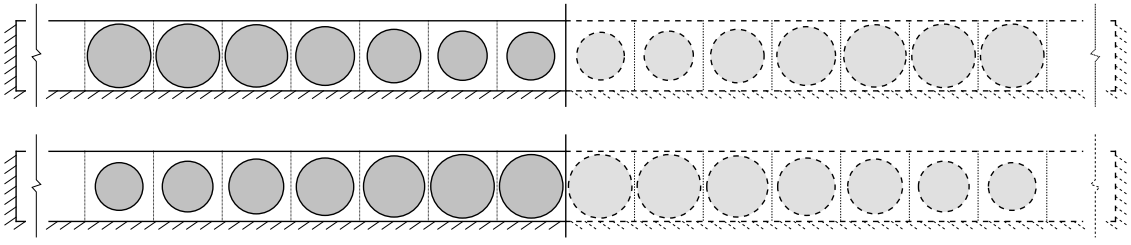

Figure 6.1: Schematic representations (cross-sectional views) of arrays with nonuniform local blockage profiles and their implied reflective symmetries.

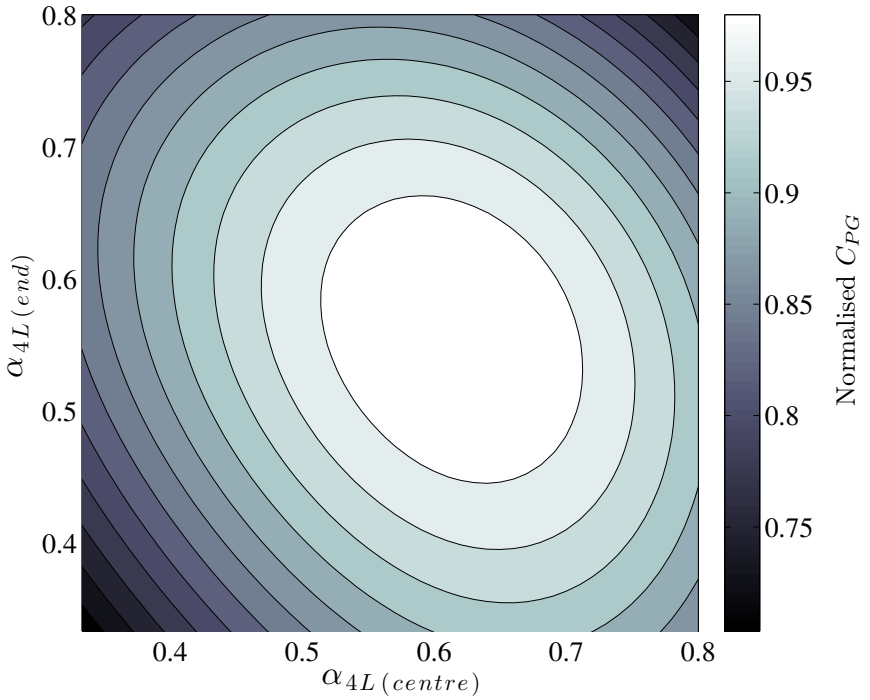

Figure 6.2: Variation of normalised global power coefficient C_{PG} with central and end local tuning α_{4L} for an array with uniform local blockage $B_L = 0.5714$.

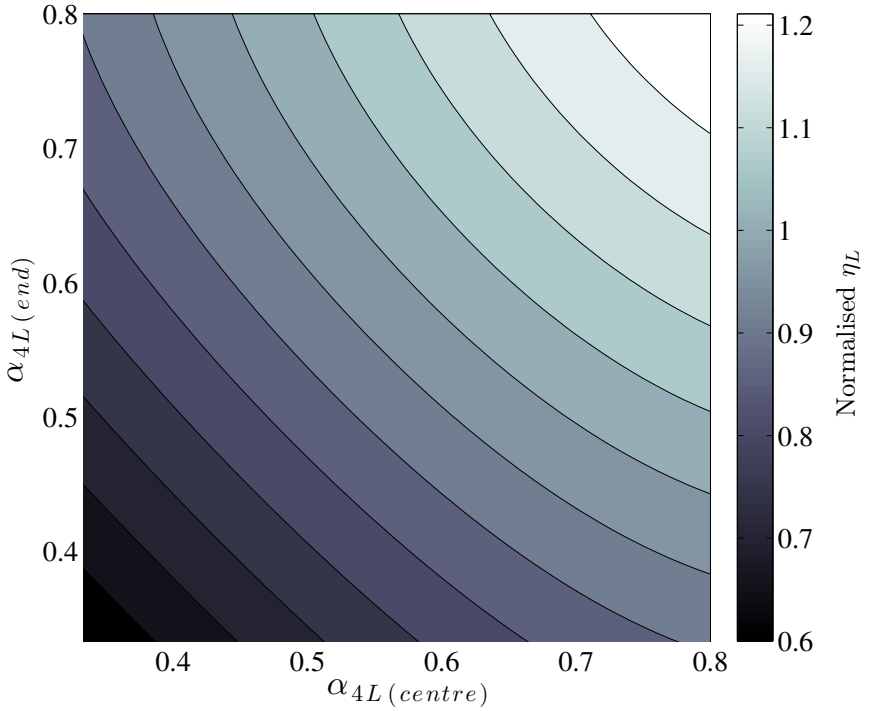

Figure 6.3: Variation of normalised local extraction efficiency η_L with central and end local tuning α_{4L} for an array with uniform local blockage $B_L = 0.5714$.

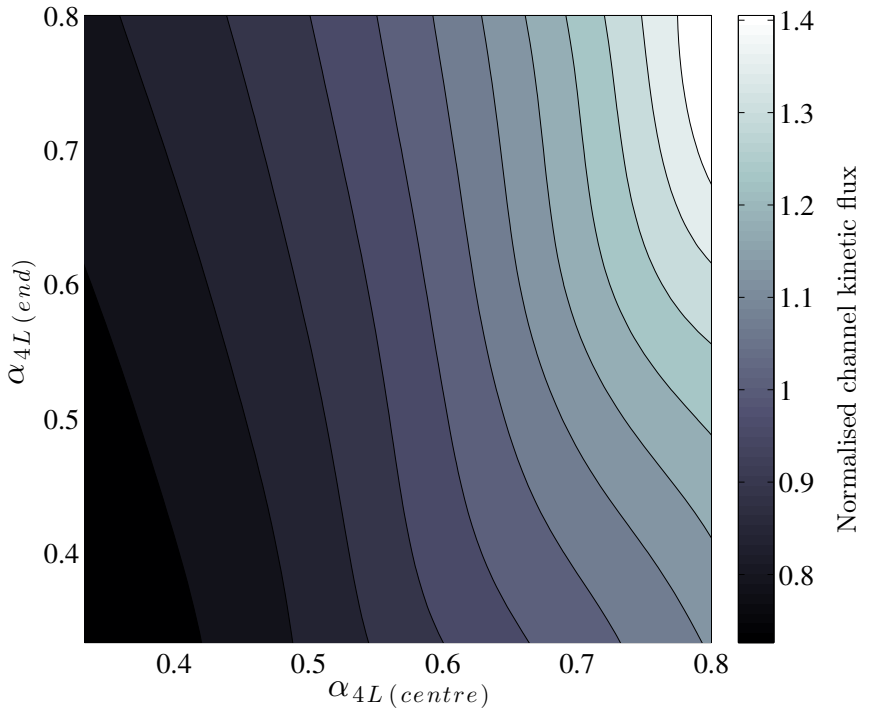

Figure 6.4: Variation of normalised channel kinetic flux with central and end local tuning α_{4L} for an array with uniform local blockage $B_L = 0.5714$.

scale extraction efficiency η_L, and channel-scale kinetic flux with central and end local tuning α_{4L}, normalised by the corresponding values obtained for the initial uniform arrangement. Figure 6.2 shows that the power coefficients produced by the nonuniform tunings are not as high as produced by the uniform tuning but that there is a range of nonuniform tunings that produce power coefficients within 2% of this value. This agrees with the findings of Adcock (2015), who used a similar model to show that although linear variations can produce up to 5% more power in horizontally sheared flow, the performance of the array is relatively insensitive to the tuning profile.

Arrays with uniform local tuning but nonuniform local blockage are considered next. For a uniform α_{4L} of 0.583, tables 6.1–6.3 illustrate the variations of C_{PG}, η_L, and channel kinetic flux with central and end B_L, normalised by the corresponding values obtained for the uniform arrangement.

Table 6.1: Variation of normalised global power coefficient C_{PG} with central (x-axis) and end (y-axis) local blockage B_L for an array with uniform local tuning $\alpha_{4L} = 0.583$.

0.8	0.8032	0.8779	0.9670			
0.7	0.9020	0.9493	1.0006			
0.6			0.9993			
0.5				0.9719	0.9053	0.7757
0.4					0.8435	0.7178
0.3					0.8270	0.6779
	0.3	0.4	0.5	0.6	0.7	0.8

Table 6.2: Variation of normalised local extraction efficiency η_L with central (x-axis) and end (y-axis) local blockage B_L for an array with uniform local tuning $\alpha_{4L} = 0.583$.

0.8	0.9785	0.9857	0.9923			
0.7	0.9814	0.9900	0.9948			
0.6			0.9973			
0.5				0.9973	0.9956	0.9971
0.4					0.9881	0.9906
0.3					0.9809	0.9808
	0.3	0.4	0.5	0.6	0.7	0.8

Table 6.3: Variation of normalised channel kinetic flux with central (x-axis) and end (y-axis) local blockage B_L for an array with uniform local tuning $\alpha_{4L} = 0.583$.

0.8	1.0794	1.0856	1.0853			
0.7	1.0915	1.1040	1.0947			
0.6			1.0978			
0.5				0.9447	0.8092	0.7635
0.4					0.7954	0.7425
0.3					0.7884	0.7252
	0.3	0.4	0.5	0.6	0.7	0.8

Fewer nonuniform profiles are examined in this case because the variation of local blockage is subject to the additional constraint that the global blockage must always equal 0.1. Table 6.1 shows greater variation in C_{PG} than was seen for nonuniform tuning and that there are two nonuniform local blockage profiles that produce values similar to that of the uniform profile — one of which is slightly higher. It also appears from table 6.2 that the local efficiency is relatively insensitive to the local blockage profile but it should be noted that these figures are the averages of the individual edge values, which display greater variation.

Lastly, two examples of arrays with both nonuniform local blockage and nonuniform local tuning are considered. Figures 6.5, 6.7, and 6.9 illustrate the variations of C_{PG}, η_L, and channel kinetic flux with central and end edge tunings α_{4L} for an array with greater local blockage at its ends (B_L = 0.7) than at its centre (B_L = 0.4) whilst figures 6.6, 6.8, and 6.10 show the corresponding variations for an array with greater local blockage at its centre (B_L = 0.7) than at its ends (B_L = 0.4). Once again, these are normalised by the respective values obtained for the uniform arrangement. Figures 6.5 and 6.6 show that neither of these nonuniform arrays can match the performance of the uniform array but that, of the two, the array with greater local blockage at its ends performs better than the one with greater local blockage at its centre. The peak global power coefficient for this array is not only greater than that of the array with greater local blockage at its centre (0.9935 cf. 0.9618) but is achieved with less variation in local tuning across its width (0.48–0.71 cf. 0.76–0.44), a higher channel kinetic flux (1.135 cf. 1.008), and only slightly lower local efficiency (1.024 cf. 1.035). In both cases, the peak global power coefficient is achieved by tuning the smaller turbines to a lower value of α_{4L} than the larger turbines.

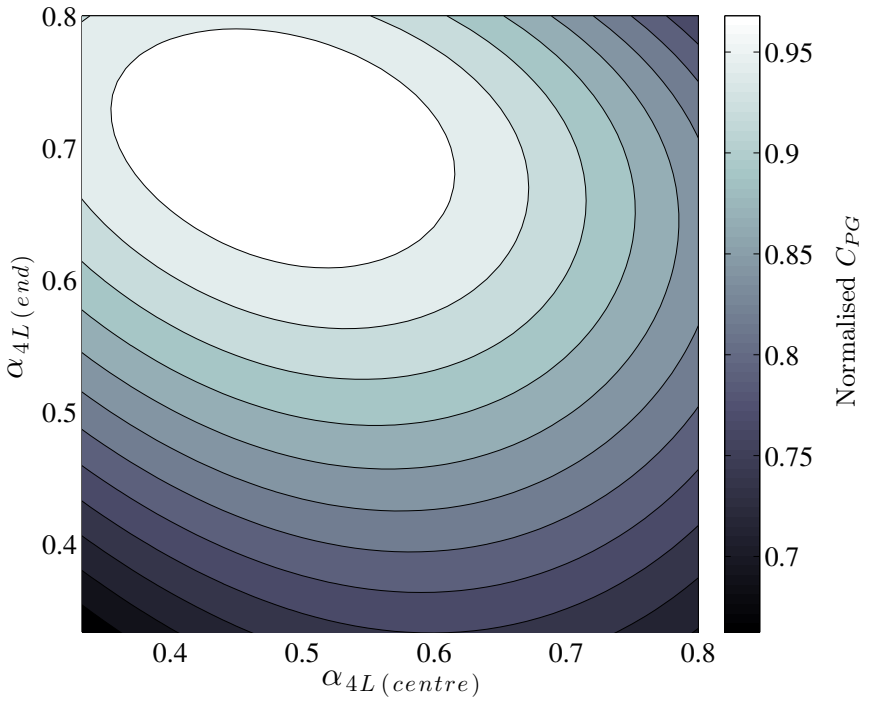

Figure 6.5: Variation of normalised global power coefficient C_{PG} with central and end local tuning α_{4L} for an array with greater local blockage at its ends ($B_L = 0.7$) than at its centre ($B_L = 0.4$).

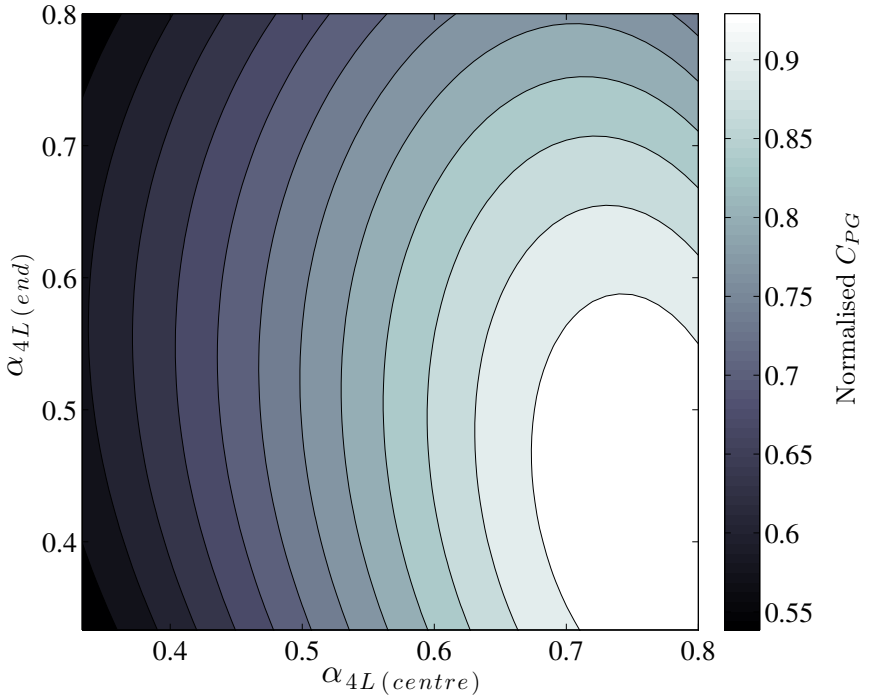

Figure 6.6: Variation of normalised global power coefficient C_{PG} with central and end local tuning α_{4L} for an array with greater local blockage at its centre ($B_L = 0.7$) than at its ends ($B_L = 0.4$).

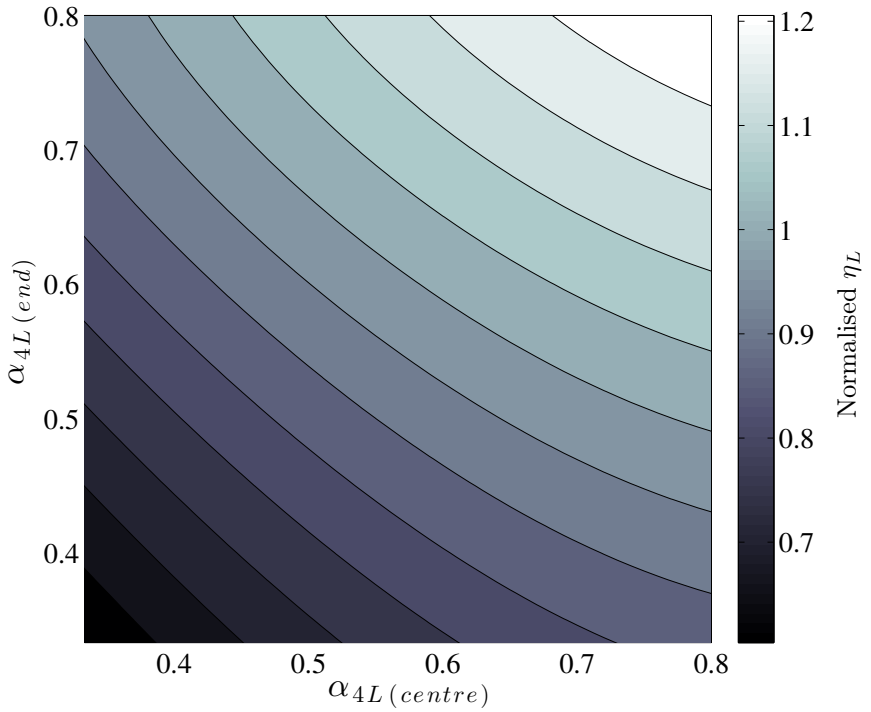

Figure 6.7: Variation of normalised local extraction efficiency η_L with central and end local tuning α_{4L} for an array with greater local blockage at its ends ($B_L = 0.7$) than at its centre ($B_L = 0.4$).

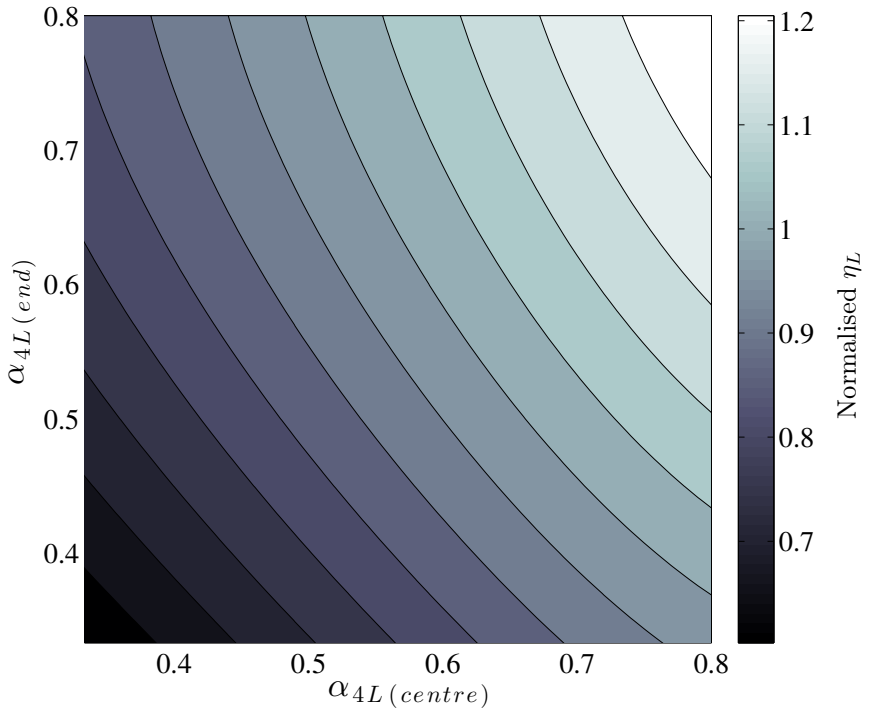

Figure 6.8: Variation of normalised local extraction efficiency η_L with central and end local tuning α_{4L} for an array with greater local blockage at its centre ($B_L = 0.7$) than at its ends ($B_L = 0.4$).

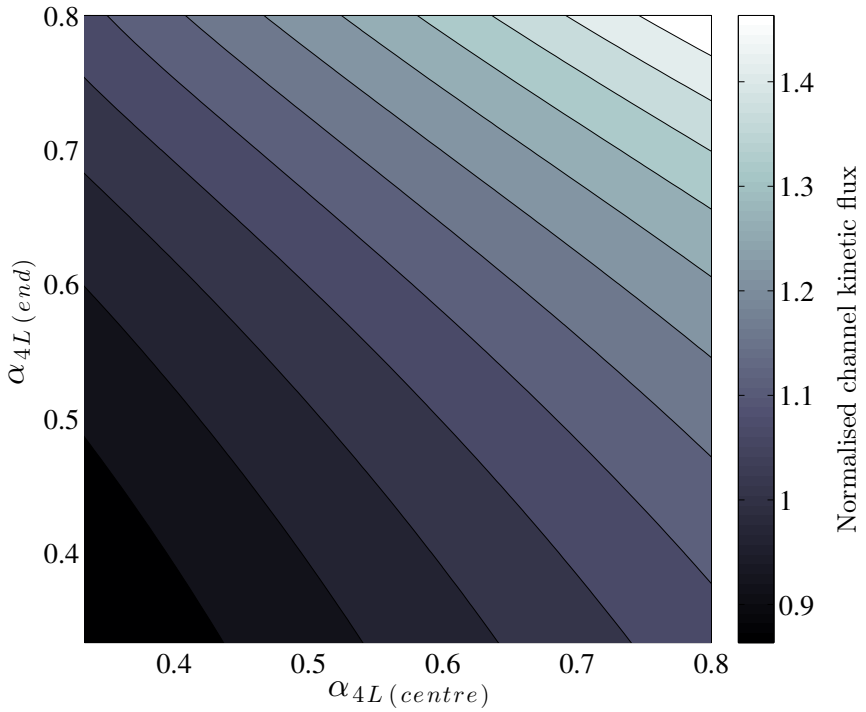

Figure 6.9: Variation of normalised channel kinetic flux with central and end local tuning α_{4L} for an array with greater local blockage at its ends ($B_L = 0.7$) than at its centre ($B_L = 0.4$).

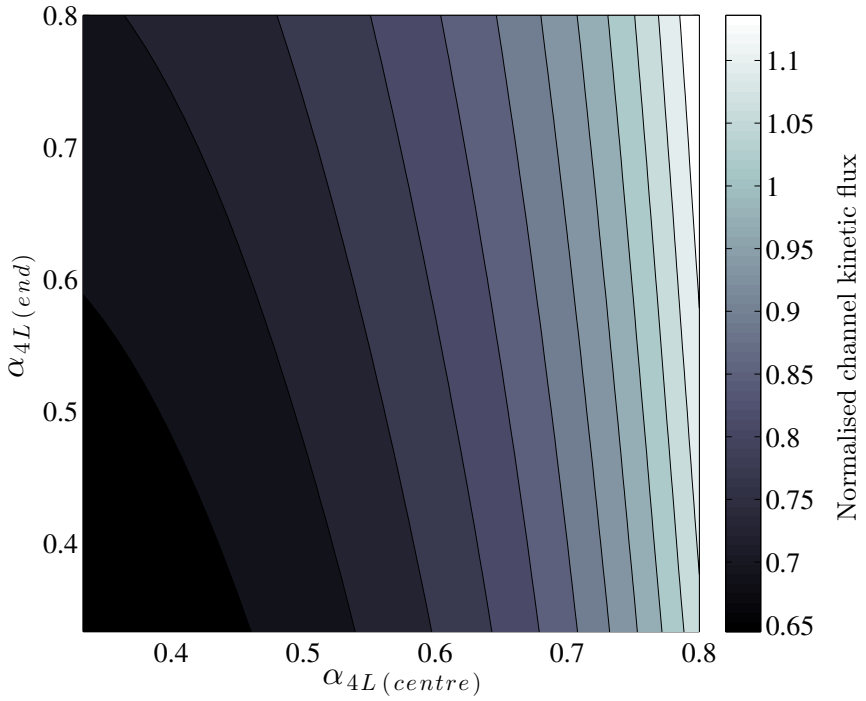

Figure 6.10: Variation of normalised channel kinetic flux with central and end local tuning α_{4L} for an array with greater local blockage at its centre ($B_L = 0.7$) than at its ends ($B_L = 0.4$).

6.2 Maximum available power

The analysis is now repeated to explore the potential for a nonuniform array to generate more power than a uniform array. In this case, the starting point is the near-optimal arrangement with uniform $B_L = 0.2$ and uniform $\alpha_{4L} = 0.424$, in which 2.311 MW (or 15.83% of the channel potential) is available to the turbines that occupy 20 of the 40 cross-stream element edges.

Figures 6.11–6.13 and tables 6.4–6.6 show that, just as with the power coefficient, the power available to arrays with uniform local blockage and nonuniform local tuning, or uniform local tuning and nonuniform local blockage, is less than that available to the uniform array. Similarly, figures 6.14–6.19 show that neither of the arrays in which both local blockage (which is varied from $B_L = 0.1$ to $B_L = 0.4$ in this case) and local tuning vary nonuniformly across the width can match the performance of the uniform array. Once again the array with greater local blockage at its ends performs better than the one with greater local blockage at its centre.

It is important to note that the combination of high thrust and low background roughness means that for the majority of the results shown herein, the array power output has not achieved steady state within the chosen sampling period. As such, the results presented in this chapter should be treated as approximate. However, given that the power output reduces over time within these samples, this error consistently overestimates the performance of the nonuniform arrays and does not therefore affect the overall conclusion that they do not perform as well as the uniform arrays.

Given that turbine performance is a function of both blockage and tuning, it is unsurprising that array performance cannot be improved significantly — for initially uniform flow, at least — by varying either local block-

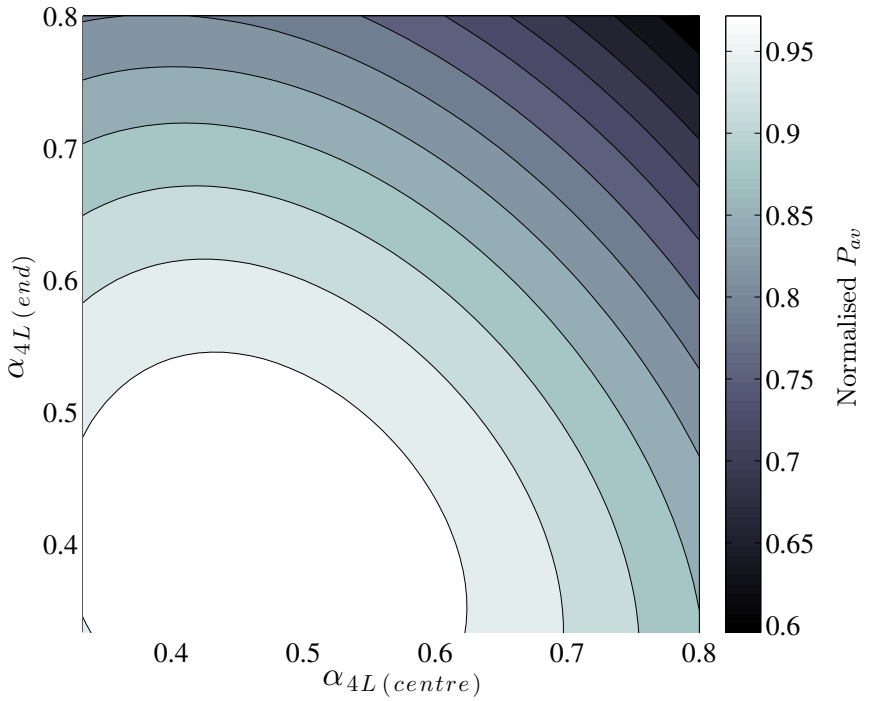

Figure 6.11: Variation of normalised available power P_{av} with central and end local tuning α_{4L} for an array with uniform local blockage $B_L = 0.2$.

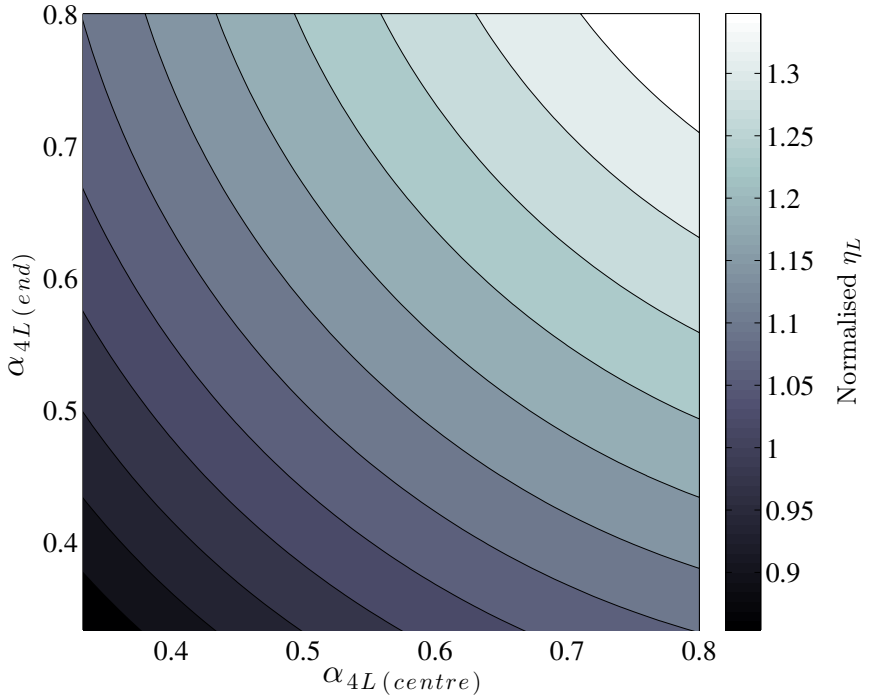

Figure 6.12: Variation of normalised local extraction efficiency η_L with central and end local tuning α_{4L} for an array with uniform local blockage $B_L = 0.2$.

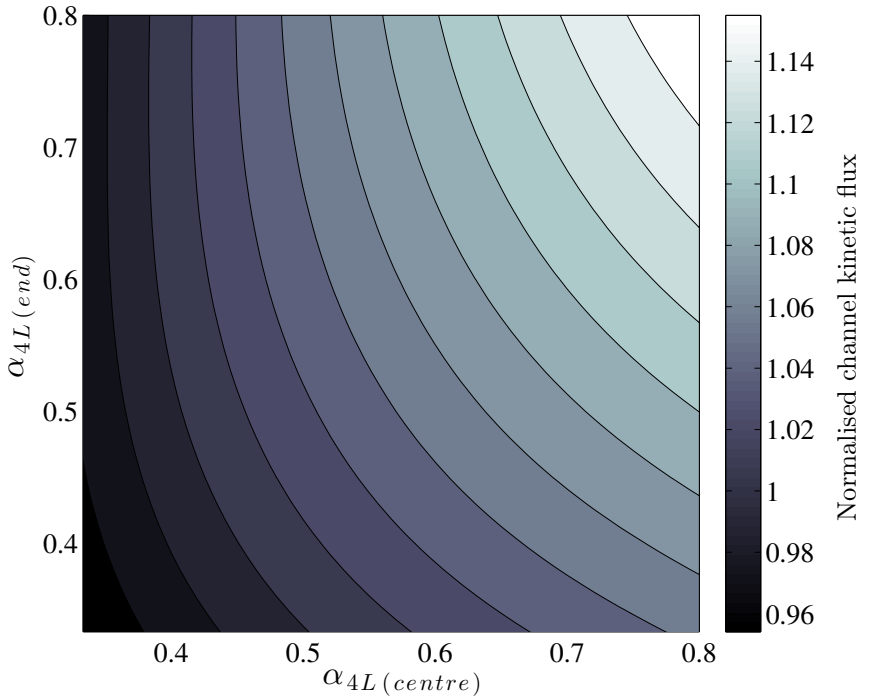

Figure 6.13: Variation of normalised channel kinetic flux with central and end local tuning α_{4L} for an array with uniform local blockage $B_L = 0.2$.

Table 6.4: Variation of normalised available power P_{av} with central (x-axis) and end (y-axis) local blockage B_L for an array with uniform local tuning $\alpha_{4L} = 0.424$.

0.5	0.8148	0.9238							
0.45	0.8617	0.9410							
0.4	0.9091	0.9567							
0.35	0.9268	0.9590							
0.3	0.9401	0.9746							
0.25	0.9800	0.9938							
0.2			1.0000						
0.15				0.9430	0.8769	0.8198	0.7590	0.6905	0.6211
0.1				0.9582	0.9033	0.8361	0.7709	0.6987	0.6228
	0.1	0.15	0.2	0.25	0.3	0.35	0.4	0.45	0.5

Table 6.5: Variation of normalised local extraction efficiency η_L with central (x-axis) and end (y-axis) local blockage B_L for an array with uniform local tuning $\alpha_{4L} = 0.424$.

0.5	0.9327	0.9643							
0.45	0.9480	0.9699							
0.4	0.9626	0.9763							
0.35	0.9693	0.9794							
0.3	0.9750	0.9871							
0.25	0.9888	0.9946							
0.2			1.0000						
0.15				0.9946	0.9870	0.9794	0.9766	0.9707	0.9662
0.1				0.9888	0.9748	0.9692	0.9627	0.9482	0.9331
	0.1	0.15	0.2	0.25	0.3	0.35	0.4	0.45	0.5

Table 6.6: Variation of normalised channel kinetic flux with central (x-axis) and end (y-axis) local blockage B_L for an array with uniform local tuning $\alpha_{4L} = 0.424$.

0.5	0.7780	0.9037							
0.45	0.8209	0.9168							
0.4	0.8686	0.9318							
0.35	0.8876	0.9360							
0.3	0.9043	0.9574							
0.25	0.9614	0.9856							
0.2			1.0000						
0.15				0.9348	0.8616	0.8017	0.7442	0.6815	0.6217
0.1				0.9391	0.8677	0.8011	0.7393	0.6712	0.6043
	0.1	0.15	0.2	0.25	0.3	0.35	0.4	0.45	0.5

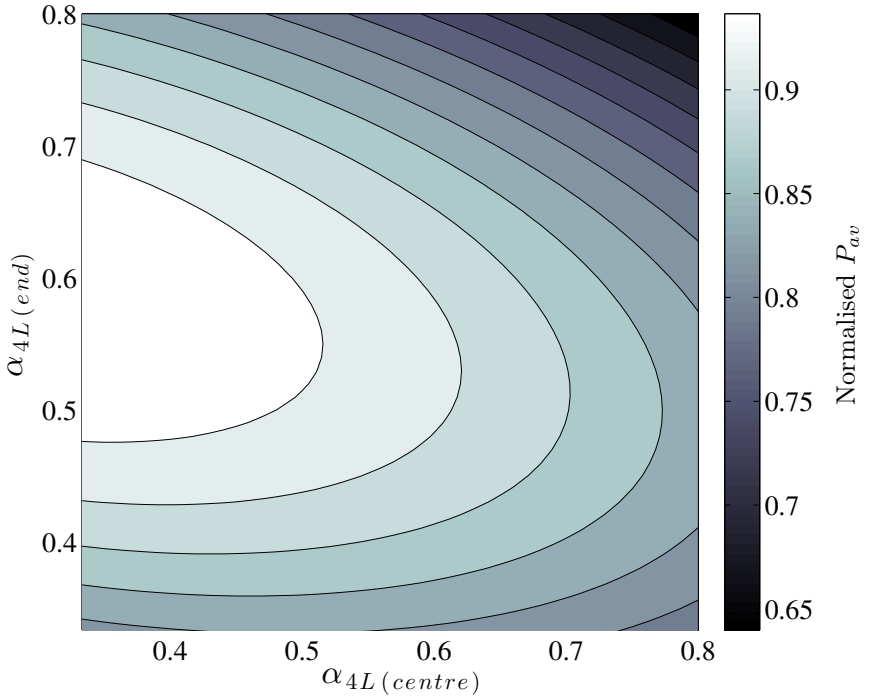

Figure 6.14: Variation of normalised available power P_{av} with central and end local tuning α_{4L} for an array with greater local blockage at its ends ($B_L = 0.4$) than at its centre ($B_L = 0.1$).

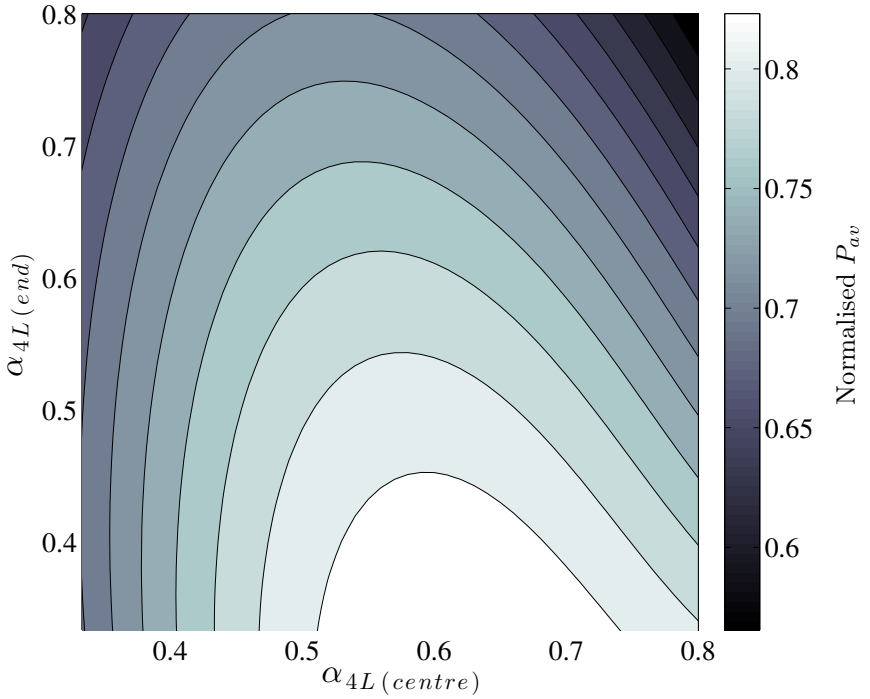

Figure 6.15: Variation of normalised available power P_{av} with central and end local tuning α_{4L} for an array with greater local blockage at its centre ($B_L = 0.4$) than at its ends ($B_L = 0.1$).

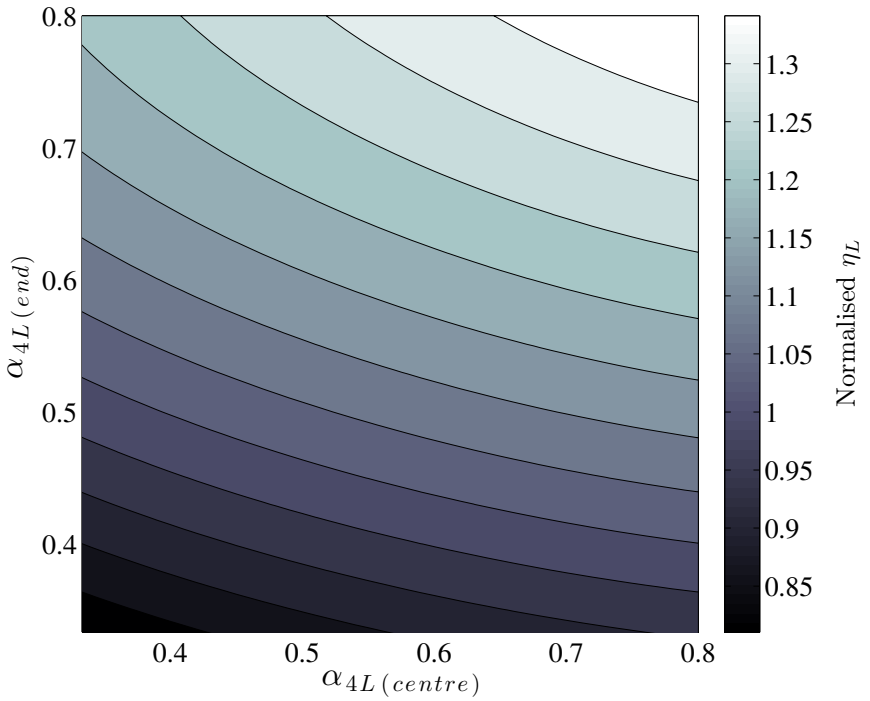

Figure 6.16: Variation of normalised local extraction efficiency η_L with central and end local tuning α_{4L} for an array with greater local blockage at its ends ($B_L = 0.4$) than at its centre ($B_L = 0.1$).

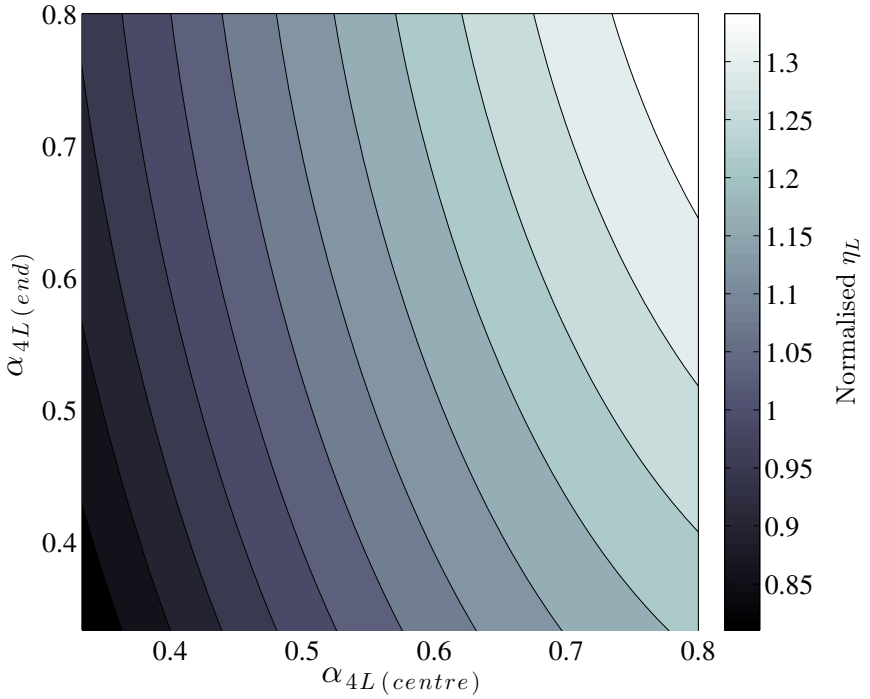

Figure 6.17: Variation of normalised local extraction efficiency η_L with central and end local tuning α_{4L} for an array with greater local blockage at its centre ($B_L = 0.4$) than at its ends ($B_L = 0.1$).

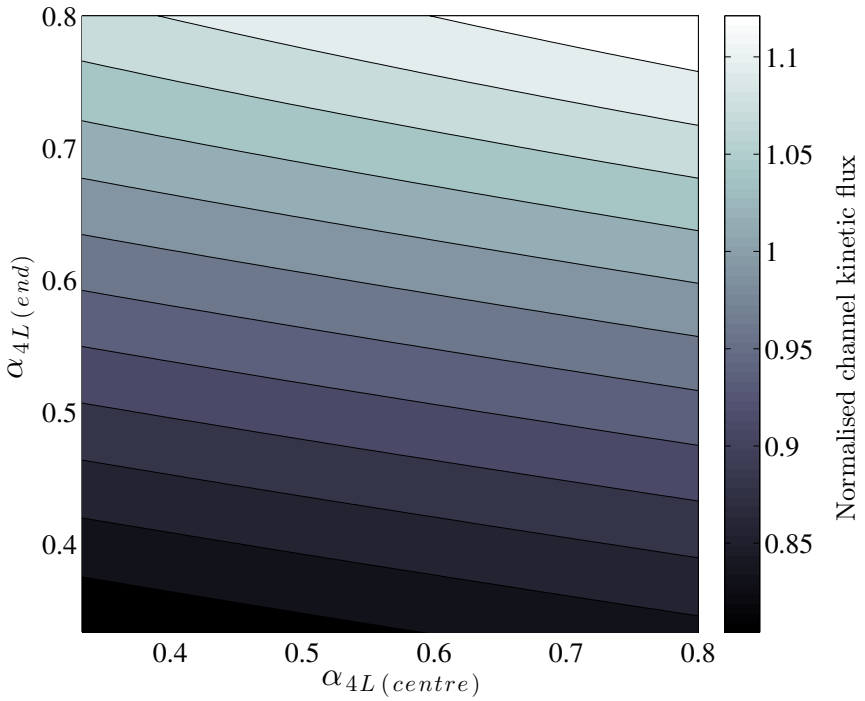

Figure 6.18: Variation of normalised channel kinetic flux with central and end local tuning α_{4L} for an array with greater local blockage at its ends ($B_L = 0.4$) than at its centre ($B_L = 0.1$).

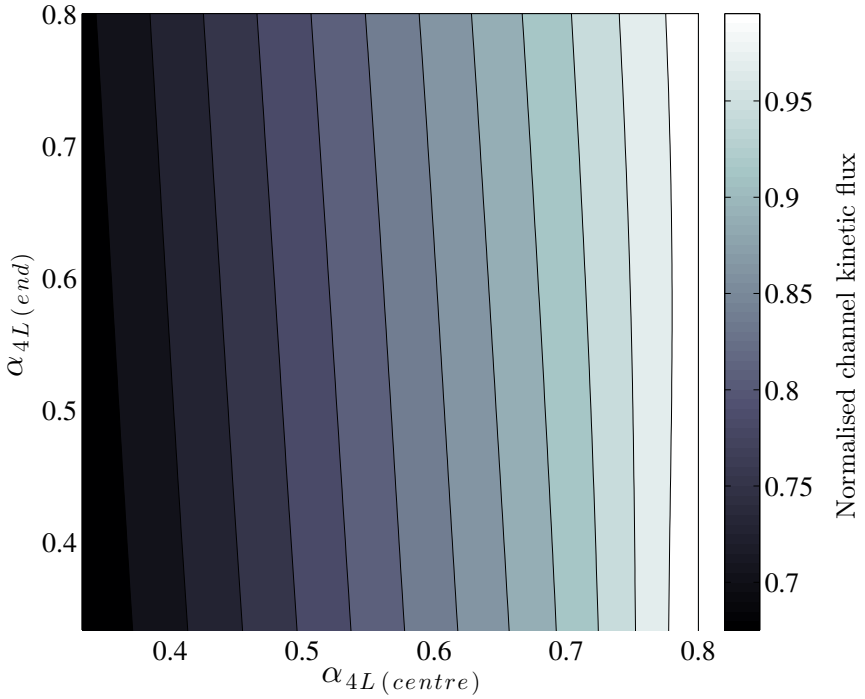

Figure 6.19: Variation of normalised channel kinetic flux with central and end local tuning α_{4L} for an array with greater local blockage at its centre ($B_L = 0.4$) than at its ends ($B_L = 0.1$).

age or local tuning across the width. For a given blockage, there exists a unique tuning to maximise a chosen performance metric. It seems intuitive then, that varying local blockage and local tuning independently of each other will result in suboptimal performance for the vast majority of the turbines within the row. This result agrees with the findings of Hunter et al. (2015), who used three-dimensional Reynolds-averaged Navier-Stokes simulations of porous discs to show that the global power coefficient for a single row of uniform local blockage is maximised by a uniform local tuning, but not with the findings of Cooke et al. (2016), who showed that a three-scale actuator disc model, with uniform local tuning but nonuniform local blockage, can produce a higher global power coefficient than the two-scale model, for which both local tuning and local blockage are uniform. It should be noted, however, that the third scale of wake mixing introduced by Cooke et al. divides the single row into multiple sub-rows within the same plane, thereby creating nonuniform local blockage profiles that are much more complicated than the simple linear variations considered herein.

Interestingly, it appears that array performance cannot be improved significantly by varying both local blockage and local tuning across the width either. To explore the performance of these nonuniform arrays further, surface elevation and velocity data are extracted and used to approximate the local power coefficient, local thrust coefficient, available power, and applied thrust for each turbine edge using the actuator disc model of Houlsby et al. (2008). The spanwise variations of these properties shown in figures 6.20–6.23 demonstrate that although some nonuniform arrays can produce power coefficients or generate amounts of power that are similar to the corresponding uniform arrays, their operation is fundamentally different at local scale, requiring large variations in both power and thrust across the array width.

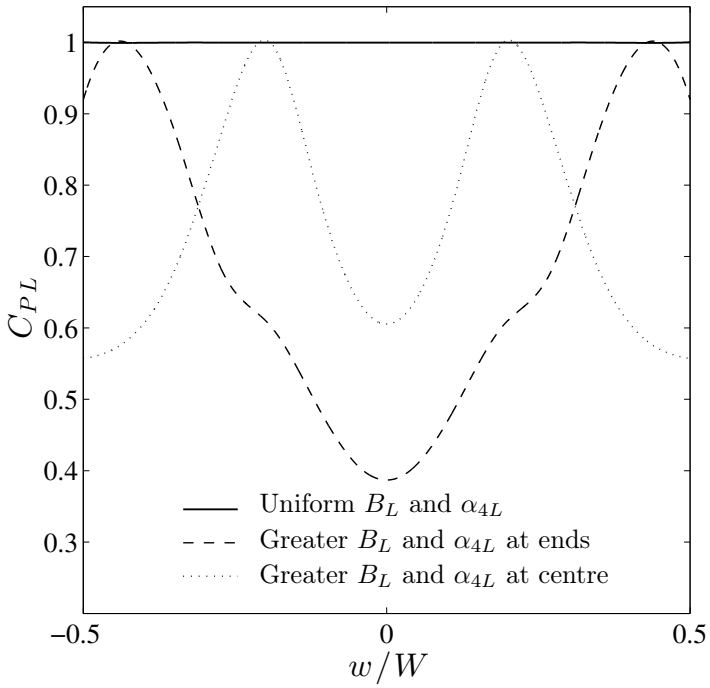

Figure 6.20: Variations of normalised local power coefficient C_{PL} across the array width W (14 edges) for near-optimally tuned uniform and nonuniform arrays.

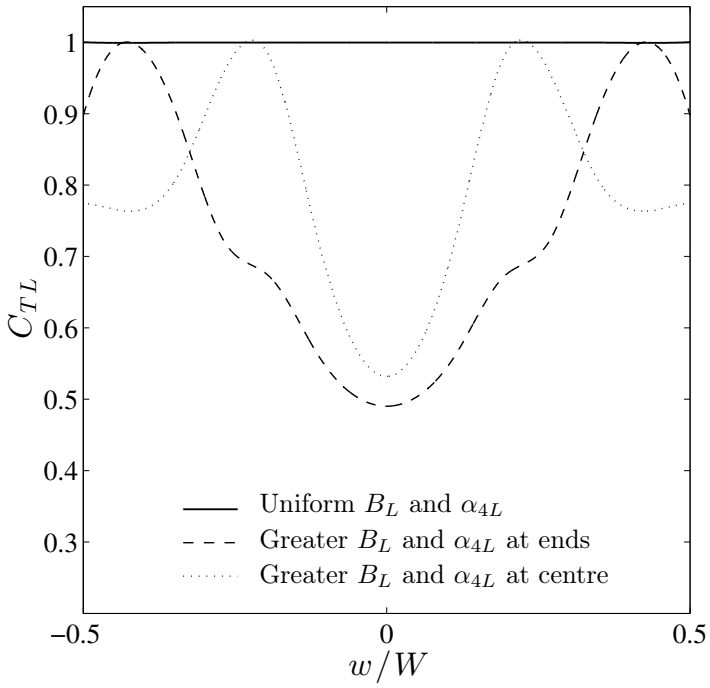

Figure 6.21: Variations of normalised local thrust coefficient C_{TL} across the array width W (14 edges) for near-optimally tuned uniform and nonuniform arrays.

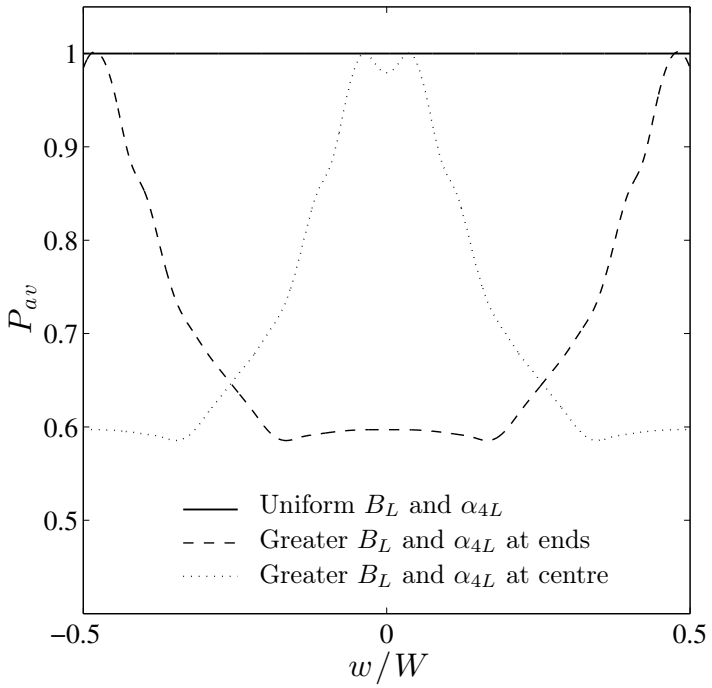

Figure 6.22: Variations of normalised available power P_{av} across the array width W (40 edges) for near-optimally tuned uniform and nonuniform arrays.

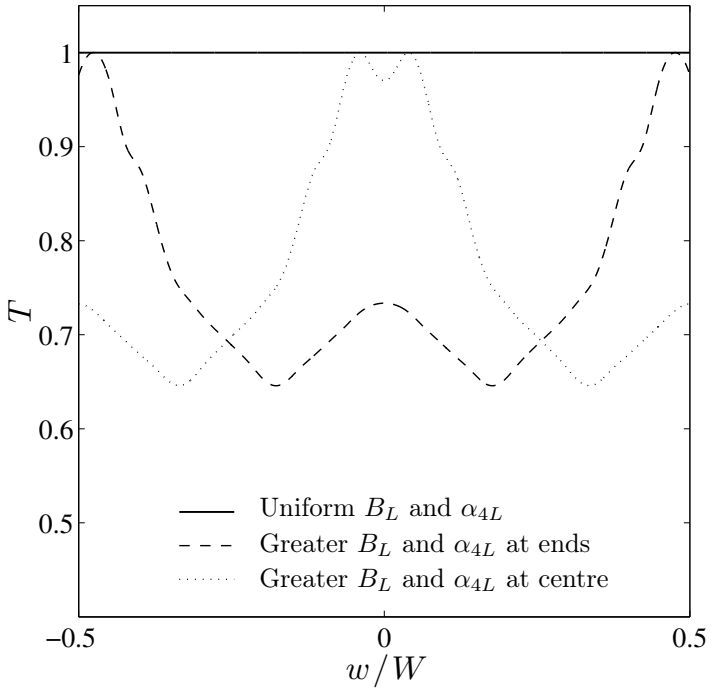

Figure 6.23: Variations of normalised thrust T across the array width W (40 edges) for near-optimally tuned uniform and nonuniform arrays.

The optimal strategy for the nonuniform arrays appears to be to tune the smaller turbines to be more resistant than the larger turbines. This does not appear to be a means by which to compensate for the variation in local blockage across the array width because it is not the most uniform variations of thrust and power that produce peak array performance. Rather, it suggests that there is some advantage in tuning the smaller turbines, which produce the least power, suboptimally in order to divert more flow into the path of the larger turbines that produce the most. This would also explain why it appears to be better to place the smaller, more resistant turbines in the centre of the array rather than at its ends — to ensure that there are larger turbines on either side to take full advantage of the flow that they divert both left and right.

6.3 Conclusions

Results from the combined array and channel model suggest that to optimise the performance of a single row of turbines in an initially uniform flow, each turbine should have the same local blockage and tuning. This finding is encouraging because it is more economical and much simpler to design an array for an equal distribution of thrust and power among the turbines. The result is also somewhat intuitive and, together with the findings of Adcock (2015) and Draper et al. (2016), who explored the performance of turbines and arrays in horizontally and vertically sheared flows, suggests a more general conclusion that arrays perform best when their blockage and tuning profiles have been designed to account specifically for the flow conditions that they will experience.

Chapter 7

Effects of local blockage in oscillatory flow

The amount by which local blockage effects can enhance array performance has previously been shown to depend on the channel background roughness, which determines the natural resistance to flow around the turbines. In this chapter, the effects of fluid inertia are considered as the combined array and channel model is used to explore the potential for local blockage effects to enhance the performance of arrays in oscillatory flow.

An array of low global blockage ($B_G = 0.1$) is placed into a channel with drag coefficient C_d and an oscillatory flow is produced by raising and lowering the water level at the western flow boundary with amplitude Ξ and period 44,700 s (∼12.42 hours) while the water level at the eastern boundary is held constant. The model is allowed to reach steady state, after which results from the last two complete tidal cycles are extracted and time-averaged. The effects of local blockage are explored by comparing eight different arrangements of this global blockage within the cross-section, ranging from a full-width array of small turbines ($B_A = 1, B_L = 0.1$) to a

short array of exceedingly large turbines ($B_A = 0.125, B_L = 0.8$). For each arrangement, the model is run with different array tunings to determine by interpolation the maximum available power, averaged over the tidal cycle. An optimal arrangement, defined by a local blockage and tuning, is identified by interpolating between these eight data points. This analysis is then repeated for a number of different tidal forcings and channel drag coefficients to explore the ways in which the optimal arrangements change with the channel's natural dynamic balance.

7.1 Maximum available power

The natural dynamic balance λ_0 is a function of both channel background roughness and tidal forcing amplitude (e.g. Garrett and Cummins, 2005). Having previously established the effects of background roughness on the potential for local blockage effects to enhance array performance — as well as on the channel potential and maximum available power — the effects of fluid inertia are first explored by comparing the effects of forcing amplitude, for a given background roughness, on the potential local blockage boost. Figures 7.1, 7.3, and 7.5 illustrate the variations of the potential for available power P_{av} enhancement with local blockage B_L, channel drag coefficient C_d, and forcing amplitude Ξ. Varying C_d and Ξ also varies both the channel potential and maximum available power so, as in chapter 5, the effects of local blockage are isolated by normalising the variations of $P_{av(max)}$ by the values obtained for the respective full-width arrays ($B_L = B_G = 0.1$). Results from the steady flow analysis performed in chapter 5 are also included for comparison, and the corresponding local tunings are shown in figures 7.2, 7.4, and 7.6.

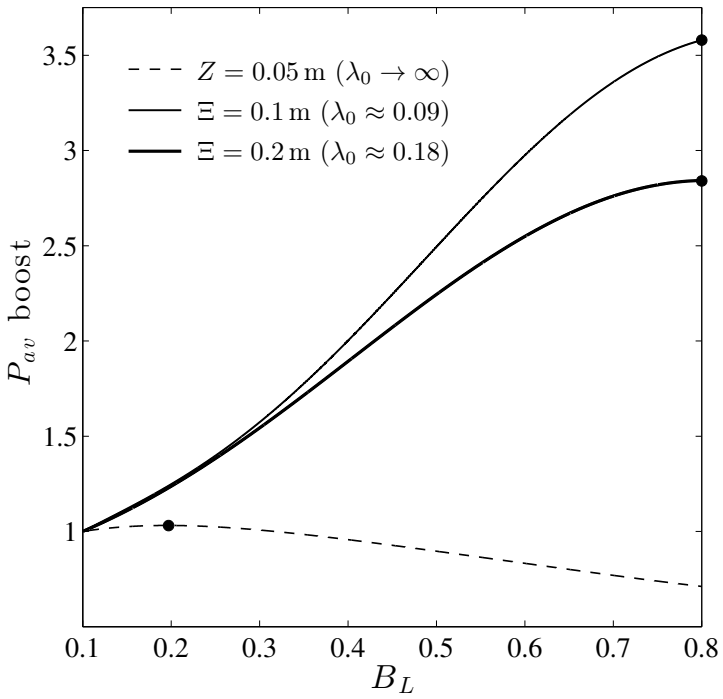

Figure 7.1: Variations of the potential for available power P_{av} enhancement with local blockage B_L for channel drag coefficient $C_d = 0.0005$ and constant and oscillatory forcing amplitudes Z and Ξ (natural dynamic balances λ_0). Dots indicate the points of peak available power.

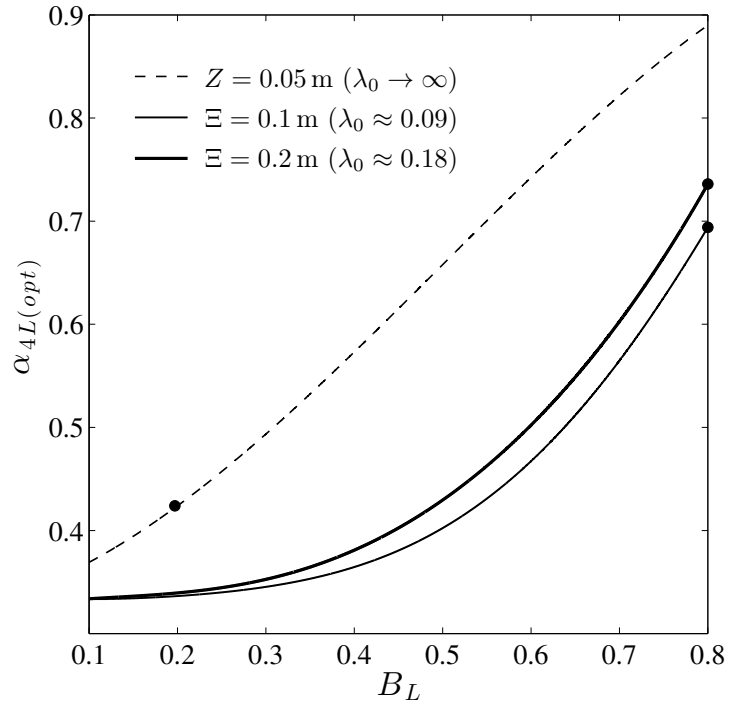

Figure 7.2: Local tunings α_{4L} corresponding to maximum available power $P_{av(max)}$. Dots indicate the points of peak available power.

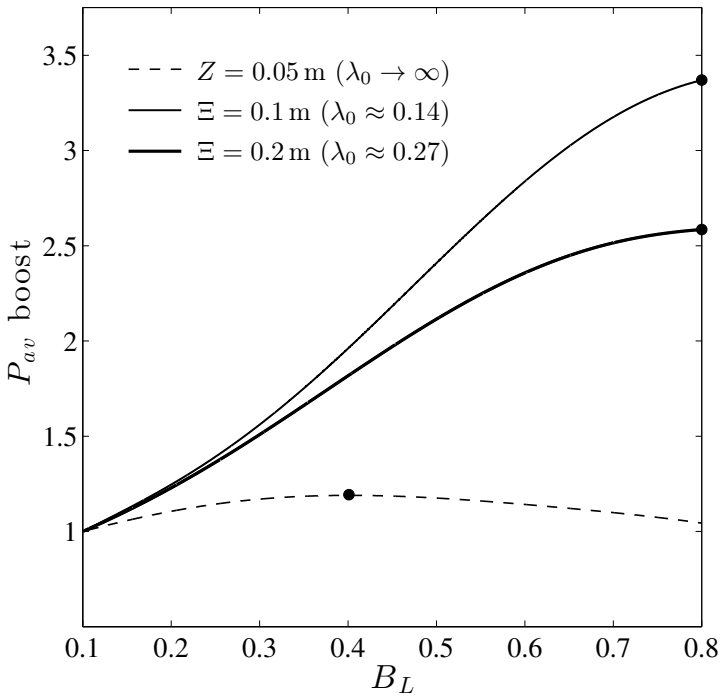

Figure 7.3: Variations of the potential for available power P_{av} enhancement with local blockage B_L for channel drag coefficient $C_d = 0.001$ and constant and oscillatory forcing amplitudes Z and Ξ (natural dynamic balances λ_0). Dots indicate the points of peak available power.

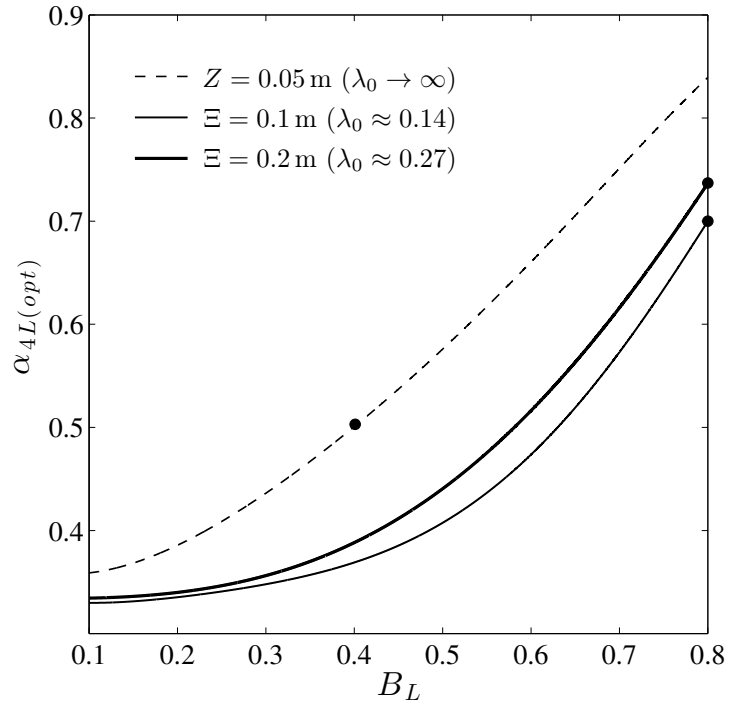

Figure 7.4: Local tunings α_{4L} corresponding to maximum available power $P_{av(max)}$. Dots indicate the points of peak available power.

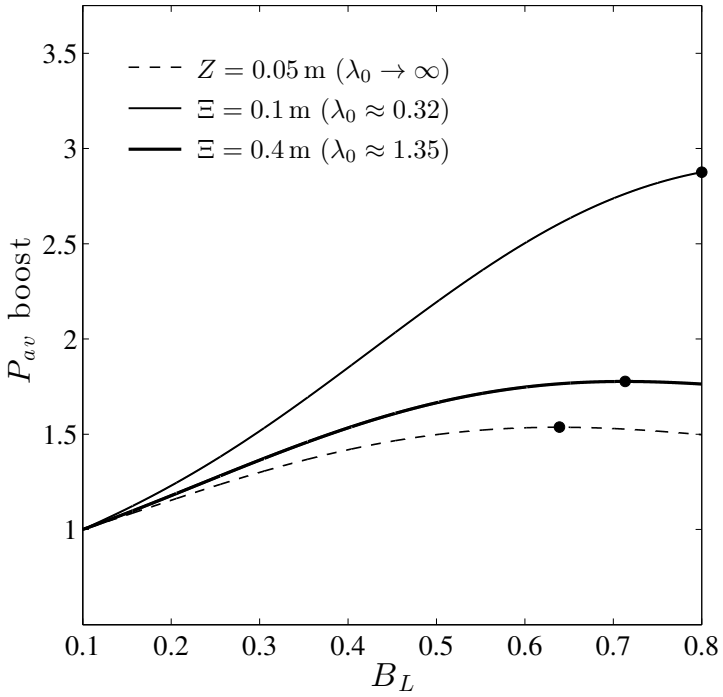

Figure 7.5: Variations of the potential for available power P_{av} enhancement with local blockage B_L for channel drag coefficient $C_d = 0.003$ and constant and oscillatory forcing amplitudes Z and Ξ (natural dynamic balances λ_0). Dots indicate the points of peak available power.

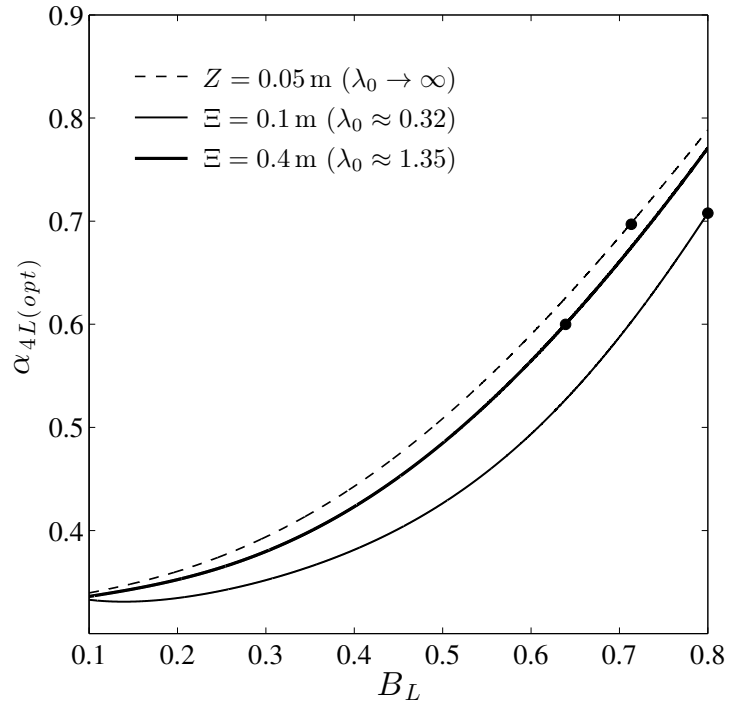

Figure 7.6: Local tunings α_{4L} corresponding to maximum available power $P_{av(max)}$. Dots indicate the points of peak available power.

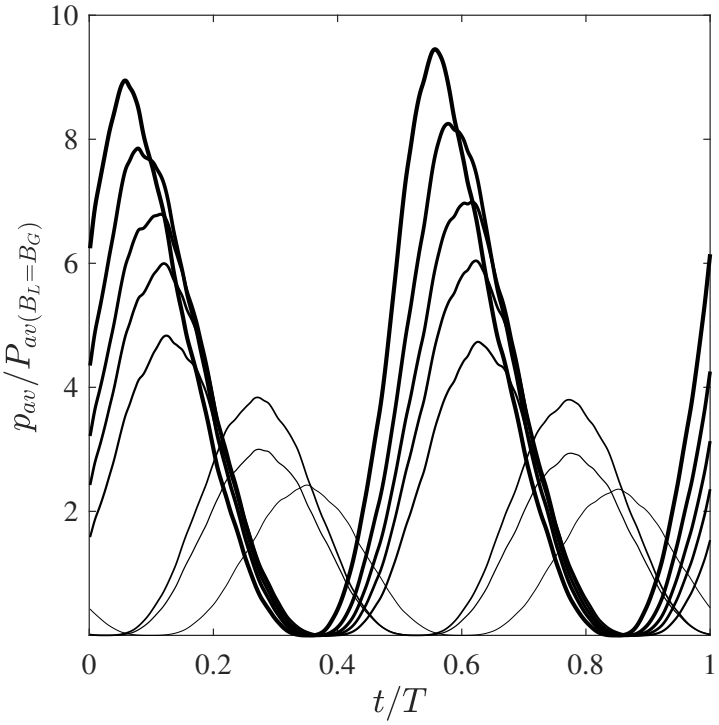

Figure 7.7: Variations of instantaneous available power p_{av} (normalised by the time-average of the power available to the full-width array) over time t (tidal period T) for eight different turbine arrangements with near-optimal tuning in a channel with natural dynamic balance $\lambda_0 \approx 0.09$. Lines increase in thickness from $B_L = 0.1$ (thinnest) to $B_L = 0.8$ (thickest).

The results are striking. The solid dots used to indicate the optimal arrangement for a given forcing and drag coefficient show that the power available to high local blockage arrays increases dramatically in oscillatory flow. Consider, for instance, the performance of arrays in the low drag channel. In a steady flow ($Z = 0.05\,\mathrm{m}$), the maximum power available to the short array of exceedingly large turbines is $\sim$29% less than that available to the full-width array of small turbines, whereas in an oscillatory flow ($\Xi = 0.1\,\mathrm{m}$, for instance), the high local blockage array can produce $\sim$258% more power than the low local blockage array (figure 7.7).

To explain this, it is useful to consider first how the physics of the problem changes in moving from steady to oscillatory flow. In steady flow, the depth and velocity at a given point are constant in time whereas in

oscillatory flow, depth and velocity vary over time and with a phase shift between them. Garrett and Cummins (2005) explain that the amount by which the flow lags the tidal forcing is determined by the channel's natural dynamic balance λ_0, which represents the ratio of inertial to drag forces, and show that the phase lag decreases with increasing resistance to flow. In their analysis, however, Garrett and Cummins only considered arrays that block the cross-section completely. Nishino and Willden (2012) later showed that when an array blocks only part of the cross-section, the flow separates into array-scale core and bypass flows. However, Nishino and Willden only considered the performance of partial-width arrays in steady flow. To the author's knowledge, the present analysis is the first to describe both the dynamics of flow through a partial-width array within a channel and the effects of local blockage in oscillatory flow. Using realistic length and timescales, the combined array and channel model shows that in oscillatory flow, the array-scale core and bypass flows oscillate side by side but with a phase shift between them. It is this newly-identified phase shift that underlies the dramatic increase in power available to high local blockage arrays in oscillatory flow.

The means by which this phase shift enhances array performance is described as follows. In oscillatory flow, both core and bypass flows experience drag due to background roughness but the core flow also experiences the additional drag due to turbine thrust. The difference in resistance between the two regions means that the core flow with modified dynamic balance λ' follows the forcing more closely than does the bypass flow with natural dynamic balance λ_0. Now consider, as illustrated in figure 7.8, an instant in the tidal cycle at which flow is moving from left to right. As the tide turns, the core and bypass flows slow, stop, and then begin to move from

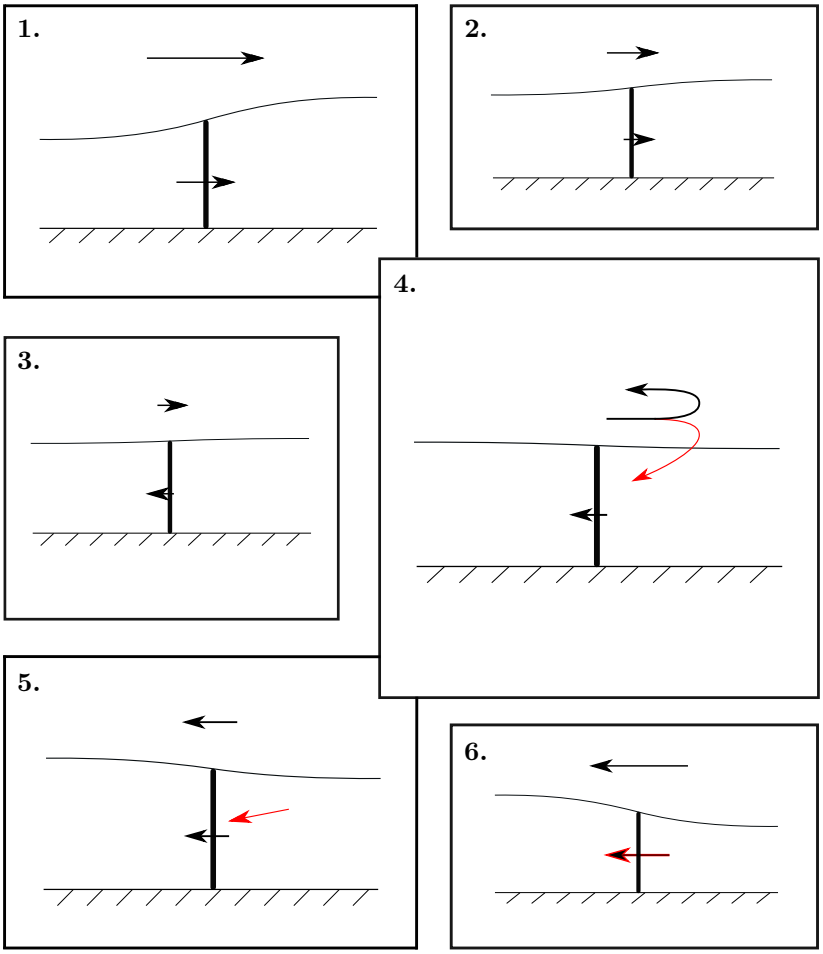

Figure 7.8: Schematic representation (plan views) of the 'reversal boost' observed in oscillatory flow.

right to left. Being both easier to turn and phase-shifted ahead, however, the core flow begins to move from right to left while the bypass flow is still moving from left to right. This means that when the bypass flow turns, part of the flow, rather than retracing its path, diverts into the core region and through the array, thereby enhancing its performance. The inertia of the lagging bypass flow temporarily makes the leading core flow the path of least resistance, resulting in a 'reversal boost' for the turbines each time the flow changes direction. This kick-start at the turn of the tide produces a stronger core flow that generates more power over the tidal cycle. A similar dynamic has formed the basis of a recently proposed optimal tuning strategy

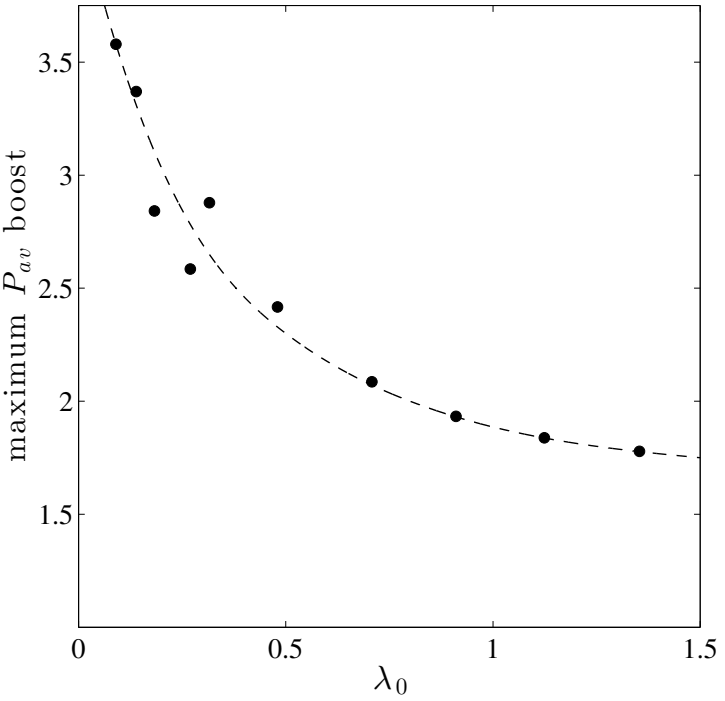

Figure 7.9: Variation of the potential for available power P_{av} enhancement with the channel's natural dynamic balance λ_0. A low-order polynomial is fit to dots representing values obtained using the low, medium, and high friction channels.

for tidal turbines (Vennell, 2016; Vennell and Adcock, 2014). Vennell (2016) suggests that tuning turbines to apply a lower resistance around slack water allows for the development of stronger currents later in the cycle, and that the additional amount of power that may be produced later in the cycle more than makes up for the amount forgone earlier.

In steady flow, array performance is maximised by tuning turbines to slow the flow as much as possible without producing either excessive diversion of flow around the turbines within the array or excessive reduction of flow through the array. In oscillatory flow, however, the optimal strategy is different because tuning the turbines to apply a greater thrust increases the difference in both velocity amplitude and velocity phase between the core and bypass flows, allowing for a greater funnelling of bypass flow through the array when the tide turns. The performance enhancement due to the

reversal boost in oscillatory flow is shown to be considerably greater than the enhancement due to local blockage effects in steady flow, and is found to increase with both increasing local blockage — though not monotonically (figures 7.1–7.6) — and decreasing natural dynamic balance (figure 7.9).

7.2 Conclusions

Results from the combined array and channel model show that, for realistic length and timescales, the potential for performance enhancement through optimising local blockage is much greater in oscillatory flow than in steady flow. A phase shift between the core and bypass flows causes part of the bypass flow to funnel through the array when the tide turns, resulting in a 'reversal boost' for the turbines each time the flow changes direction.

The magnitude of the reversal boost observed in oscillatory flow is found to be considerably greater than the boost due to local blockage effects in steady flow. The greatest enhancements are shown to require local blockage ratios that may be difficult to achieve in practice but the results show that, in oscillatory flow, more power can be produced by tightly packing turbines into a small part of the cross-section than by placing them evenly across it, as suggested by Adcock et al. (2013), or in an arrangement optimised for the equivalent steady flow, following Nishino and Willden (2012). Perhaps most importantly, the results show that the assumption of steady flow in simple models of tidal turbines neglects important flow phenomena.

Chapter 8

Conclusions and recommendations

The optimal design of a tidal turbine array is a great challenge involving many competing economic, technical, and environmental constraints. By providing a deeper understanding of the ways in which turbines interact with both tidal current resources and marine ecosystems, this thesis takes two important steps toward establishing best practice in array design.

In the first part of the thesis, the social and ecological impacts of marine energy development are reviewed. In the second part, theoretical models of tidal turbines are examined and a simple numerical model is used to extend existing theories on optimal turbine arrangement. In this chapter, the main conclusions of the thesis are summarised and topics for further research are suggested.

8.1 Social and ecological impacts

Social impacts

Social acceptance of renewable energy development is found to be closely linked to both the public perception of renewable energy and the level of stakeholder involvement in project planning. The nature of public opinion is found to be complex because even those individuals who support a given project in principle may object to any aspect of its development — from the location and proposed timeline to the choice of developer and their methods — but the threat of opposition should not deter developers from engaging with stakeholders. Rather, developers should seek to improve existing engagement practices with a focus on nurturing consent. Naturally, there is no simple formula to enhance public support but Devine-Wright et al. (2013) emphasise the importance of local benefit provision, timely and meaningful engagement, trust, and fair and inclusive planning procedures. Further research may wish to explore the lessons learned from ongoing and completed projects, whether and how public opinions have changed post-development, and the potential for direct ownership of such projects to benefit local communities.

Ecological impacts

Perhaps the greatest barrier to the deployment of marine energy is the uncertainty surrounding the environmental impacts, which is exacerbated by considerable variation in device design, a lack of baseline environmental data, and the complexity of assessing the ecological impacts on a range of species (Copping et al., 2013; Shields et al., 2009; Witt et al., 2012). The

threat of adverse impact should not discourage development, however. The ecological impacts of marine energy can be minimised by assessing proposals on a case-by-case basis and by considering the marine ecosystem at each phase of development; by selecting sites appropriately, conducting baseline environmental studies and risk assessments, identifying and mitigating adverse effects as early as possible, and continuously monitoring for long-term and cumulative impacts (Bell and Side, 2011; Gill, 2005; Shields et al., 2009; Witt et al., 2012). A more strategic and collaborative research effort between developers, academia, and the public sector will lead to improvements in environmental monitoring standards and in best practices for device and array design (Boehlert and Gill, 2010; Freeman et al., 2013; Kirby et al., 2013; Leeney et al., 2014). Further research may wish to explore the potential for marine energy devices to modify natural patterns of sediment and nutrient transport and the effects of increasing noise and collision risk on the health and behaviour of marine species.

8.2 Array design

Combined array and channel model

A simple numerical model is developed to explore the potential for local blockage effects to enhance the performance of turbine arrays in flow conditions that are more representative of real tidal currents. The shallow water equations are used to simulate flow through an idealised channel and a sub-grid scale actuator disc model is used to represent a single row of tidal turbines as a line sink of momentum, following the methodology established by Draper et al. (2010) and Draper (2011) and using the numerical solver

developed by Serhadlıoğlu (2014). Validation tests show the channel model to reproduce accurately predictions from the analytical model of Garrett and Cummins (2005) and the array model to reproduce qualitatively predictions from the analytical model of Nishino and Willden (2012). The combined array and channel model may be thought of as either extending the model of Nishino and Willden (2012) to include channel-scale dynamics or the model of Vennell (2010) to include array-scale dynamics.

Effects of local blockage in flow with background roughness

In steady flow, increasing background roughness is shown to increase the resistance to flow around the turbines, which allows them to be placed closer together, apply a greater thrust, and produce a higher power coefficient. Increasing background roughness is also shown to increase the amount of energy dissipated over the seabed, however, which means that even though the power coefficient is higher, the turbines produce less power. As background roughness increases, the peak power coefficient increases and the maximum available power decreases but, for both metrics, the potential for local blockage effects to enhance array performance increases with increasing background roughness as the natural dissipation becomes more significant and the thrust from the turbines becomes less significant.

Nonuniform arrays in uniform flow

In a uniform flow, it is shown that array performance cannot be improved significantly by varying either the local blockage or local tuning across the

array width. Some nonuniform arrays may produce power coefficients or generate amounts of power that are similar to the corresponding uniform arrays but their operation is fundamentally different at local scale, requiring large variations in both power and thrust across the array width. Results suggest that to optimise the performance of an array in an initially uniform flow, each turbine should have the same local blockage and tuning. This finding is encouraging because it is more economical and much simpler to design an array for an equal distribution of thrust and power among the turbines. The result is also somewhat intuitive and, together with the findings of Adcock (2015) and Draper et al. (2016), who explored the performance of turbines and arrays in horizontally and vertically sheared flows, suggests a more general conclusion that arrays perform best when their blockage and tuning profiles have been designed to account specifically for the flow conditions that they will experience.

Effects of local blockage in oscillatory flow

Finally, it is shown that the potential for performance enhancement through optimising local blockage is much greater in oscillatory flow than in steady flow. A newly-identified phase shift between the core and bypass flows causes part of the bypass flow to funnel through the array when the tide turns, resulting in a 'reversal boost' for the turbines each time the flow changes direction. The magnitude of the reversal boost observed in oscillatory flow is found to be considerably greater than the boost due to local blockage effects in steady flow. The greatest enhancements are shown to require local blockage ratios that may be difficult to achieve in practice but the results show that, in oscillatory flow, more power can be produced

by tightly packing turbines into a small part of the cross-section than by placing them evenly across it, as suggested by Adcock et al. (2013), or in an arrangement optimised for the equivalent steady flow, following Nishino and Willden (2012). Perhaps most importantly, the results show that the assumption of steady flow in simple models of tidal turbines neglects important flow phenomena.

Further research

The simple numerical model developed herein could be easily extended to consider the optimal arrangement of turbines in different idealised domains and the performance of arrays placed in series and in parallel. The DG ADCIRC code could be modified to incorporate time-variable turbine tunings, power capping, and to output the power and thrust of individual turbine edges to enable more realistic array representations and analysis of spanwise performance variations. Further exploration of the local blockage effects identified herein using more sophisticated modelling techniques and/or physical experiments would make a promising topic for future research.

Our understanding of tidal current resources and their response to energy extraction has advanced considerably in recent years but is by no means complete. The foregoing analyses have considered highly idealised flow conditions but real tidal currents are considerably more complicated, incorporating vertically and laterally sheared flow profiles, wave-current interactions, and three-dimensional turbulence. It is recommended that future research be directed toward more sophisticated resource modelling techniques, making use of, for instance, three-dimensional Reynolds-averaged Navier-Stokes or large eddy simulations. More sophisticated models could

be adapted to include more realistic representations of tidal turbines, used for in-depth analysis of adjoint-optimised arrangements, and coupled with environmental models to consider, for instance, the collision risk posed to marine life or the resulting effects on sediment and nutrient transport. These models will also require comprehensive sets of field measurements for calibration, which may be supplemented using advanced prediction techniques such as those based on machine learning (e.g. Sarkar et al., 2016).

Epilogue

The optimal design of a tidal turbine array is a great and multifaceted challenge, but one worth pursuing. This thesis focuses primarily on the problem of arranging tidal turbines for maximum power output; a task that is complicated by the interactions between the turbines and the flow.

In designing large arrays, the challenge is to maintain a high flow rate through the turbines without using additional barriers to constrain the flow. The most obvious way to do this is to arrange the turbines to block as much of the flow as possible. Naturally, however, there will still be gaps for flow to pass around the turbines. In this scenario, the two-scale actuator disc theory predicts that the optimal strategy is not to distribute the turbines evenly across the flow cross-section but to place them closer together to exploit local blockage effects. The optimal local blockage is, put simply, the arrangement that makes it most difficult for flow to pass around the turbines. This configuration allows the turbines to extract more power but also greatly increases the thrust exerted on the turbines by the flow and vice versa. The trade-off between power, thrust, and extraction efficiency will be an important consideration in array design.

This thesis extends the two-scale theory to show that local blockage effects can increase considerably the power available to turbines in flow conditions that are more representative of real tidal currents, but also that both the maximum available power and optimal turbine arrangement will depend on site-specific natural conditions. Results also suggest a trend of increasing power with local blockage, particularly in oscillatory flow where a newly-identified 'reversal boost' is found to improve dramatically the performance of short, highly-blocked arrays. While this reversal boost is consistent with existing theoretical works, its magnitude suggests that there is still much to learn about optimal array design.

References

Abbott, M. B. (1979). Computational hydraulics: Elements of the theory of free surface flows. Pitman Publishing Ltd, London.

Adcock, T. A. A. (2015). On tidal stream turbines placed off headlands. *Journal of Renewable and Sustainable Energy*, 7(6):061706.

Adcock, T. A. A., Borthwick, A. G. L., and Houlsby, G. T. (2011). The open boundary problem in tidal basin modelling with energy extraction. *Proceedings of the 9th European Wave and Tidal Energy Conference (EWTEC), Southampton, UK.*

Adcock, T. A. A., Draper, S., Houlsby, G. T., Borthwick, A. G. L., and Serhadlıoğlu, S. (2013). The available power from tidal stream turbines in the Pentland Firth. *Proceedings of the Royal Society of London A: Mathematical, Physical, and Engineering Sciences*, 469(2157):20130072.

Adcock, T. A. A., Draper, S., and Nishino, T. (2015). Tidal power generation – A review of hydrodynamic modelling. *Proceedings of the Institution of Mechanical Engineers, Part A: Journal of Power and Energy*, 229(7):755–771.

Ahmadian, R., Falconer, R., and Bockelmann-Evans, B. (2012). Far-field modelling of the hydro-environmental impact of tidal stream turbines. *Renewable Energy*, 38:107–116.

Ahmadian, R. and Falconer, R. A. (2012). Assessment of array shape of tidal stream turbines on hydro-environmental impacts and power output. *Renewable Energy*, 44:318–327.

Alexander, K. A., Wilding, T. A., and Heymans, J. J. (2013). Attitudes of Scottish fishers towards marine renewable energy. *Marine Policy*, 37:239–244.

Anderson, Jr., J. D. (2008). Basic philosophy of CFD. In Wendt, J. F., Computational fluid dynamics: An introduction, Springer Science & Business Media.

Atwater, J. F. and Lawrence, G. A. (2010). Power potential of a split tidal

channel. *Renewable Energy*, 35(2):329–332.

Bailey, I., West, J., and Whitehead, I. (2011). Out of sight but not out of mind? Public perceptions of wave energy. *Journal of Environmental Policy & Planning*, 13(2):139–157.

Bell, D., Gray, T., and Haggett, C. (2005). The 'social gap' in wind farm siting decisions: Explanations and policy responses. *Environmental Politics*, 14(4):460–477.

Bell, D., Gray, T., Haggett, C., and Swaffield, J. (2013). Re-visiting the 'social gap': Public opinion and relations of power in the local politics of wind energy. *Environmental Politics*, 22:115–135.

Bell, M. and Side, J. (2011). Tidal technologies: Key issues across planning and development for environmental regulators. Background Report on Task 2 of Sniffer ER20: Environmental impacts of tidal and wave power developments and key issues for consideration by environment agencies.

Benjamins, S., Harnois, V., Smith, H. C. M., Johanning, L., Greenhill, L., Carter, C., and Wilson, B. (2014). Understanding the potential for marine megafauna entanglement risk from marine renewable energy developments. Scottish Natural Heritage Commissioned Report No. 791.

Betz, A. (1920). Das Maximum der Theoretisch Möglichen Ausnützung des Windes durch Windmotoren. *Zeitschrift für das Gesamte Turbinenwesen*, 26(307–309):8.

Black and Veatch (2005). The UK tidal stream resource and tidal stream technology. Report prepared for the Carbon Trust Marine Energy Challenge.

Blanchfield, J., Garrett, C., Wild, P., and Rowe, A. (2008). The extractable power from a channel linking a bay to the open ocean. *Proceedings of the Institution of Mechanical Engineers, Part A: Journal of Power and Energy*, 222(3):289–297.

Bochert, R. and Zettler, M. L. (2004). Long-term exposure of several marine benthic animals to static magnetic fields. *Bioelectromagnetics*, 25(7):498–502.

Boehlert, G. W. and Gill, A. B. (2010). Environmental and ecological effects of ocean renewable energy development: A current synthesis. *Oceanography*, 23:68–81.

Bonar, P. A. J., Bryden, I. G., and Borthwick, A. G. L. (2015). Social and ecological impacts of marine energy development. *Renewable and Sustainable Energy Reviews*, 47:486–495.

Bonar, P. A. J., Venugopal, V., Borthwick, A. G. L., and Adcock, T. A. A. (2016). Numerical modelling of two-scale flow dynamics. *Proceedings of the 5th Oxford Tidal Energy Workshop, Oxford, UK*.

Borthwick, A. G. L. and Barber, R. W. (1992). River and reservoir flow modelling using the transformed shallow water equations. *International Journal for Numerical Methods in Fluids*, 14:1193–1217.

Bronfman, N. C., Jiménez, R. B., Arévalo, P. C., and Cifuentes, L. A. (2012). Understanding social acceptance of electricity generation sources. *Energy Policy*, 46:246–252.

Bryden, I. G. and Couch, S. J. (2006). ME1 – Marine energy extraction: Tidal resource analysis. *Renewable Energy*, 31(2):133–139.

Burningham, K., Barnett, J., and Thrush, D. (2006). The limitations of the NIMBY concept for understanding public engagement with renewable energy technologies: A literature review. School of Environment and Development, University of Manchester.

Cada, G., Ahlgrimm, J., Bahleda, M., Bigford, T., Stavrakas, S. D., Hall, D., Moursund, R., and Sale, M. (2007). Potential impacts of hydrokinetic and wave energy conversion technologies on aquatic environments. *Fisheries*, 32(4):174–181.

Caltrans (2001). Fisheries impact assessment – Oakland Bay bridge east span seismic safety project. PIPD EA 012081. Caltrans, San Francisco.

Carstensen, J., Henriksen, O. D., and Teilmann, J. (2006). Impacts of offshore wind farm construction on harbour porpoises: Acoustic monitoring of echolocation activity using porpoise detectors (T-PODs). *Marine Ecology Progress Series*, 321:295–308.

Cartwright, D. E. (1999). Tides: A scientific history. Cambridge University Press.

Cass, N., Walker, G., and Devine-Wright, P. (2010). Good neighbours, public relations, and bribes: The politics and perceptions of community benefit provision in renewable energy development in the UK. *Journal of Environmental Policy & Planning*, 12(3):255–275.

Consoli, P., Romeo, T., Ferraro, M., Sarà, G., and Andaloro, F. (2012). Factors affecting fish assemblages associated with gas platforms in the Mediterranean Sea. *Journal of Sea Research*, 77:45–52.

Conway, F., Stevenson, J., Hunter, D., Stefanovich, M., Campbell, H., Covell, Z., and Yin, Y. (2010). Ocean space, ocean place: The human dimensions of wave energy in Oregon. *Oceanography*, 23:82–91.

Cooke, S. C., Willden, R. H. J., and Byrne, B. W. (2016). The potential of cross-stream aligned sub-arrays to increase tidal turbine efficiency. *Renewable Energy*, 97:284–292.

Copping, A., Hanna, L., Whiting, J., Geerlofs, S., Grear, M., Blake, K., Coffey, A., Massaua, M., Brown-Saracino, J., and Battey, H. (2013). Environmental effects of marine energy development around the world for the OES Annex IV. Annex IV Final Report. IEA Ocean Energy Systems Initiative, Annex IV, Richland, WA, USA; Pacific Northwest National Laboratory, Richland, WA, USA.

Corten, G. P. (2000). Heat generation by a wind turbine. *14th IEA symposium on the aerodynamics of wind turbines, Golden, CO, USA*.

Couch, S. J. and Bryden, I. G. (2004). The impact of energy extraction on tidal flow development. *Proceedings of the Third IMarEST International Conference on Marine Renewable Energy, Blyth, UK*.

Creed, M. J., Draper, S., Nishino, T., and Borthwick, A. G. L. (2017). Flow through a very porous obstacle in a shallow channel. *Proc. R. Soc. A*, 473:20160672.

Cummins, P. F. (2013). The extractable power from a split tidal channel: An equivalent circuit analysis. *Renewable Energy*, 50:395–401.

Dacre, S. L. (2007). The environmental impacts and developmental constraints of tidal current energy generation. PhD Thesis, The Robert Gordon University, UK.

Davis, L. W. (2011). The effect of power plants on local housing values and rents. *Review of Economics and Statistics*, 93(4):1391–1402.

Davis, N., VanBlaricom, G. R., and Dayton, P. K. (1982). Man-made structures on marine sediments: Effects on adjacent benthic communities. *Marine Biology*, 70(3):295–303.

Department of Energy & Climate Change (2014). DECC public attitudes tracking survey – Wave 9: Summary of headline findings. Available at: https://www.gov.uk/government/publications/public-attitudes-tracking-survey-wave-9.

Devine-Wright, P. (2011a). Enhancing local distinctiveness fosters public acceptance of tidal energy: A UK case study. *Energy Policy*, 39:83–93.

Devine-Wright, P. (2011b). Public engagement with large-scale renewable energy technologies: Breaking the cycle of NIMBYism. *Wiley Interdisciplinary Reviews: Climate Change*, 2:19–26.

Devine-Wright, P., Burningham, K., Barnett, J., Devine-Wright, H., Walker, G., Infield, D., Evans, B., Howes, Y., Evans, F. S., Cass, N., Theobald, K., Parks, J., Barton, J., Thrush, D., and Speller, G. (2013). Beyond NIMBYism: Project summary report. School of Environment and Development, University of Manchester.

Devine-Wright, P. and Howes, Y. (2010). Disruption to place attachment and the protection of restorative environments: A wind energy case study. *Journal of Environmental Psychology*, 30(3):271–280.

Divett, T. (2014). Optimising design of large tidal energy arrays in channels: Layout and turbine tuning for maximum power capture using large eddy simulations with adaptive mesh. PhD Thesis, University of Otago, New Zealand.

Divett, T., Vennell, R., and Stevens, C. (2013). Optimization of multiple turbine arrays in a channel with tidally reversing flow by numerical modelling with adaptive mesh. *Philosophical Transactions of the Royal Society A: Mathematical, Physical, and Engineering Sciences*, 371(1985):20120251.

Divett, T., Vennell, R., and Stevens, C. (2014). Channel scale optimisation of large tidal turbine arrays in packed rows using large eddy simulations with adaptive mesh. *Proceedings of the 2nd Asian Wave and Tidal Energy Conference (AWTEC), Tokyo, Japan.*

Dolman, S. and Simmonds, M. (2010). Towards best environmental practice for cetacean conservation in developing Scotland's marine renewable energy. *Marine Policy*, 34(5):1021–1027.

Draper, S. (2011). Tidal stream energy extraction in coastal basins. DPhil Thesis, University of Oxford, UK.

Draper, S. (2015). Personal Communication.

Draper, S., Adcock, T. A. A., Borthwick, A. G. L., and Houlsby, G. T. (2014a). A note on the power potential of tidal currents in channels. *International Journal of Marine Energy*, 6:1–17.

Draper, S., Adcock, T. A. A., Borthwick, A. G. L., and Houlsby, G. T. (2014b). An electrical analogy for the Pentland Firth tidal stream power resource. *Proceedings of the Royal Society of London A: Mathematical, Physical, and Engineering Sciences*, 470(2161):20130207.

Draper, S., Adcock, T. A. A., Borthwick, A. G. L., and Houlsby, G. T. (2014c). Estimate of the tidal stream power resource of the Pentland Firth. *Renewable Energy*, 63:650–657.

Draper, S., Borthwick, A. G. L., and Houlsby, G. T. (2013a). Energy potential of a tidal fence deployed near a coastal headland. *Philosophical Transactions of the Royal Society of London A: Mathematical, Physical, and Engineering Sciences*, 371(1985):20120176.

Draper, S., Houlsby, G. T., Oldfield, M. L. G., and Borthwick, A. G. L. (2010). Modelling tidal energy extraction in a depth-averaged coastal domain. *IET Renewable Power Generation*, 4(6):545–554.

Draper, S. and Nishino, T. (2014a). Centred and staggered arrangements of tidal turbines. *Journal of Fluid Mechanics*, 739:72–93.

Draper, S. and Nishino, T. (2014b). Centred and staggered arrangements of tidal turbines – ERRATUM. *Journal of Fluid Mechanics*, 743:636.

Draper, S., Nishino, T., Adcock, T. A. A., and Taylor, P. H. (2016). Performance of an ideal turbine in an inviscid shear flow. *Journal of Fluid Mechanics*, 796:86–112.

Draper, S., Stallard, T., Stansby, P., Way, S., and Adcock, T. A. A. (2013b). Laboratory scale experiments and preliminary modelling to investigate basin scale tidal stream energy extraction. *Proceedings of the 10th European Wave and Tidal Energy Conference (EWTEC), Aalborg, Denmark*.

Dröes, M. and Koster, H. (2014). Renewable energy and negative externalities: The effect of wind turbines on house prices. Tinbergen Institute Discussion Paper 14-124/VIII.

Echeverria, J. D. (2000). No success like failure: The Platte River collaborative watershed planning process. *William & Mary Environmental Law and Policy Review*, 25:559–604.

El-Geziry, T. M., Bryden, I. G., and Couch, S. J. (2009). Environmental impact assessment for tidal energy schemes: An exemplar case study of the Strait of Messina. *Journal of Marine Engineering and Technology*, 2009(13):39–48.

Evans, P. G. H. (2007). Concluding remarks on offshore wind farms and marine mammals: Impacts & methodologies for assessing impacts. *Proceedings of the Agreement on the Conservation of Small Cetaceans of the Baltic and North Seas (ASCOBANS)/European Cetacean Society (ECS) Workshop, San Sebastian, Spain*.

Falconer, R. A. (1993). An introduction to nearly-horizontal flows. Coastal, Estuarial, and Harbour Engineer's Handbook, E. & F. N. Spon Ltd, London.

Ferziger, J. H. and Perić, M. (1996). Computational methods for fluid

dynamics. Springer-Verlag Berlin Heidelberg.

Firestone, J. and Kempton, W. (2007). Public opinion about large offshore wind power: Underlying factors. *Energy Policy*, 35(3):1584–1598.

Fletcher, C. A. J. (1988). Computational techniques for fluid dynamics, vol. 1: Fundamental and general techniques. Berlin and New York, Springer-Verlag.

Freeman, S. M., Hawkins, K. R., Kirby, A. D., McCall, R. A., Blyth-Skyrme, R., and Edhouse, E. S. (2013). Impacts on fish and shellfish ecology. Natural Environment Research Council (NERC) Wave and Tidal Consenting Position Paper Series.

Frid, C., Andonegi, E., Depestele, J., Judd, A., Rihan, D., Rogers, S. I., and Kenchington, E. (2012). The environmental interactions of tidal and wave energy generation devices. Environmental Impact Assessment Review.

Froude, R. E. (1889). On the part played in propulsion by differences of fluid pressure. *Transactions of the Institute of Naval Architects*, 30:390–405.

Funke, S. W., Farrell, P. E., and Piggott, M. D. (2014). Tidal turbine array optimisation using the adjoint approach. *Renewable Energy*, 63:658–673.

Funke, S. W., Kramer, S. C., and Piggott, M. D. (2016). Design optimisation and resource assessment for tidal-stream renewable energy farms using a new continuous turbine approach. *Renewable Energy*, 99:1046–1061.

Garrett, C. and Cummins, P. (2005). The power potential of tidal currents in channels. *Proceedings of the Royal Society of London A: Mathematical, Physical, and Engineering Sciences*, 461(2060):2563–2572.

Garrett, C. and Cummins, P. (2007). The efficiency of a turbine in a tidal channel. *Journal of Fluid Mechanics*, 588:243–251.

Garrett, C. and Cummins, P. (2008). Limits to tidal current power. *Renewable Energy*, 33(11):2485–2490.

Garrett, C. and Greenberg, D. (1977). Predicting changes in tidal regime: The open boundary problem. *Journal of Physical Oceanography*, 7(2):171–181.

Gibbons, S. (2014). Gone with the wind: Valuing the visual impacts of wind turbines through house prices. London School of Economics and Political Sciences & Spatial Economics Research Centre.

Gill, A., Huang, Y., Gloyne-Philips, I., Metcalfe, J., Quayle, V., Spencer, J., and Wearmouth, V. (2009). COWRIE 2.0 electromagnetic fields (EMF)

phase 2: EMF-sensitive fish response to EM emissions from sub-sea electricity cables of the type used by the offshore renewable energy industry. Commissioned by COWRIE Ltd (project reference COWRIE-EMF-1-06).

Gill, A. B. (2005). Offshore renewable energy: Ecological implications of generating electricity in the coastal zone. *Journal of Applied Ecology*, 42:605–615.

Gill, A. B. and Bartlett, M. (2010). Literature review on the potential effects of electromagnetic fields and subsea noise from marine renewable energy developments on Atlantic salmon, sea trout, and European eel. Scottish Natural Heritage Commissioned Report No. 401.

Gill, A. B., Bartlett, M., and Thomsen, F. (2012). Potential interactions between diadromous fishes of UK conservation importance and the electromagnetic fields and subsea noise from marine renewable energy developments. *Journal of Fish Biology*, 81(2):664–695.

Gipe, P. (1995). Wind energy comes of age. John Wiley and Sons.

Glauert, H. (1928a). A theoretical estimate of the pressure gradient in a wind tunnel. Aeronautical Research Committee Reports and Memoranda, No. 1159.

Glauert, H. (1928b). The effect of a static pressure gradient on the drag of a body tested in a wind tunnel. Aeronautical Research Committee Reports and Memoranda, No. 1158.

Glauert, H. (1933). Wind tunnel interference on wings, bodies, and airscrews. Aeronautical Research Committee Reports and Memoranda, No. 1566.

Glauert, H. (1947). The elements of aerofoil and airscrew theory. Cambridge University Press.

Grecian, W. J., Inger, R., Attrill, M. J., Bearhop, S., Godley, B. J., Witt, M. J., and Votier, S. C. (2010). Potential impacts of wave-powered marine renewable energy installations on marine birds. *International Journal of Avian Science*, 152(4):683–697.

Gross, C. (2007). Community perspectives of wind energy in Australia: The application of a justice and community fairness framework to increase social acceptance. *Energy Policy*, 35(5):2727–2736.

Haggett, C. (2008). Over the sea and far away? A consideration of the planning, politics and public perception of offshore wind farms. *Journal of Environmental Policy & Planning*, 10(3):289–306.

Haggett, C. (2011). Understanding public responses to offshore wind power. *Energy Policy*, 39(2):503–510.

Halvorsen, M. B., Carlson, T. J., and Copping, A. (2011). Effects of tidal turbine noise on fish hearing and tissues – Draft final report. PNNL Report-20787 for US Department of Energy by Pacific Northwest National Laboratory, Sequim, WA, USA.

Hammar, L., Andersson, S., Eggertsen, L., Haglund, J., Gullström, M., Ehnberg, J., and Molander, S. (2013). Hydrokinetic turbine effects on fish swimming behaviour. *PloS one*, 8(12):e84141.

Helvey, M. (2002). Are southern California oil and gas platforms essential fish habitat? *ICES Journal of Marine Science: Journal du Conseil*, 59:S266–S271.

Houlsby, G. T., Draper, S., and Oldfield, M. L. G. (2008). Application of linear momentum actuator disc theory to open channel flow. Report No. OUEL 2296/08, University of Oxford, UK.

Houlsby, G. T. and Vogel, C. R. (2016). The power available to tidal turbines in an open channel flow. *Proceedings of the Institution of Civil Engineers – Energy*:1–10.

Hunter, W., Nishino, T., and Willden, R. H. J. (2015). Investigation of tidal turbine array tuning using 3D Reynolds-averaged Navier–Stokes simulations. *International Journal of Marine Energy*, 10:39–51.

Inger, R., Attrill, M. J., Bearhop, S., Broderick, A. C., Grecian, W. J., Hodgson, D. J., Mills, C., Sheehan, E., Votier, S. C., Witt, M. J., and Godley, B. J. (2009). Marine renewable energy: Potential benefits to biodiversity? An urgent call for research. *Journal of Applied Ecology*, 46(6):1145–1153.

Irvin, R. A. and Stansbury, J. (2004). Citizen participation in decision making: Is it worth the effort? *Public Administration Review*, 64:55–65.

Jack Faucett Associates, Inc. (1981). Study of domestic social and economic impacts of ocean thermal energy conversion (OTEC) commercial development, vol. 1: Economic impacts. Submitted to the US Department of Energy, Office of Conservation and Renewable Energy.

Jeffrey, H., Jay, B., and Winskel, M. (2013). Accelerating the development of marine energy: Exploring the prospects, benefits and challenges. *Technological Forecasting and Social Change*, 80(7):1306–1316.

Jenkins, L. D. and Garrison, K. (2013). Fishing gear substitution to reduce bycatch and habitat impacts: An example of social-ecological research to

inform policy. *Marine Policy*, 38:293–303.

Johnson, K., Kerr, S., and Side, J. (2012). Accommodating wave and tidal energy – Control and decision in Scotland. *Ocean & Coastal Management*, 65:26–33.

Johnson, K., Kerr, S., and Side, J. (2013). Marine renewables and coastal communities – Experiences from the offshore oil industry in the 1970s and their relevance to marine renewables in the 2010s. *Marine Policy*, 38:491–499.

Jones, C. R. and Eiser, J. R. (2010). Understanding 'local' opposition to wind development in the UK: How big is a backyard? *Energy Policy*, 38(6):3106–3117.

Joukowsky, N. E. (1920). Windmill of the NEJ type. *Transactions of the Central Institute for Aero-hydrodynamics of Moscow*, 1:57.

Kadiri, M., Ahmadian, R., Bockelmann-Evans, B., Rauen, W., and Falconer, R. (2012). A review of the potential water quality impacts of tidal renewable energy systems. *Renewable and Sustainable Energy Reviews*, 16:329–341.

Kellermann, A., Eskildsen, K., and Frank, B. (2006). The MINOS project: Ecological assessments of possible impacts of offshore wind energy projects. In Progress in Marine Conservation in Europe, pp. 239–248.

Kirby, A. D., Hawkins, K. R., Freeman, S. M., McCall, R. A., Furness, R. W., and Edhouse, E. S. (2013). Ornithological impacts. Natural Environment Research Council (NERC) Wave and Tidal Consenting Position Paper Series.

Krivtsov, V. and Linfoot, B. (2012). Disruption to benthic habitats by moorings of wave energy installations: A modelling case study and implications for overall ecosystem functioning. *Ecological Modelling*, 245:121–124.

Krohn, S. and Damborg, S. (1999). On public attitudes towards wind power. *Renewable Energy*, 16(1–4):954–960.

Krueger, A. D., Parsons, G. R., and Firestone, J. (2011). Valuing the visual disamenity of offshore wind power projects at varying distances from the shore: An application on the Delaware shoreline. *Land Economics*, 87(2):268–283.

Kubatko, E. J., Bunya, S., Dawson, C., Westerink, J. J., and Mirabito, C. (2009). A performance comparison of continuous and discontinuous finite element shallow water models. *Journal of Scientific Computing*, 40 (1):315–339.

Kubatko, E. J., Westerink, J. J., and Dawson, C. (2006). *hp* discontinuous Galerkin methods for advection dominated problems in shallow water flow. *Computer Methods in Applied Mechanics and Engineering*, 196 (1):437–451.

Ladenburg, J. (2010). Attitudes towards offshore wind farms – The role of beach visits on attitude and demographic and attitude relations. *Energy Policy*, 38(3):1297–1304.

Ladenburg, J. and Dubgaard, A. (2007). Willingness to pay for reduced visual disamenities from offshore wind farms in Denmark. *Energy Policy*, 35(8):4059–4071.

Lanchester, F. W. (1915). A contribution to the theory of propulsion and the screw propeller. *Naval Engineers Journal*, 27(2):509–510.

Langhamer, O. (2010). Effects of wave energy converters on the surrounding soft-bottom macrofauna (west coast of Sweden). *Marine Environmental Research*, 69(5):374–381.

Langhamer, O., Haikonen, K., and Sundberg, J. (2010). Wave power – Sustainable energy or environmentally costly? A review with special emphasis on linear wave energy converters. *Renewable and Sustainable Energy Reviews*, 14(4):1329–1335.

Langhamer, O. and Wilhelmsson, D. (2009). Colonisation of fish and crabs of wave energy foundations and the effects of manufactured holes – A field experiment. *Marine Environmental Research*, 68(4):151–157.

Langhamer, O., Wilhelmsson, D., and Engström, J. (2009). Artificial reef effect and fouling impacts on offshore wave power foundations and buoys – A pilot study. *Estuarine, Coastal and Shelf Science*, 82(3):426–432.

Langlois, T. J., Anderson, M. J., and Babcock, R. C. (2005). Reef-associated predators influence adjacent soft-sediment communities. *Ecology*, 86(6):1508–1519.

Langton, R., Davies, I. M., and Scott, B. E. (2011). Seabird conservation and tidal stream and wave power generation: Information needs for predicting and managing potential impacts. *Marine Policy*, 35(5):623–630.

Lawrence, R. L. and Deagen, D. A. (2001). Choosing public participation methods for natural resources: A context-specific guide. *Society & Natural Resources*, 14(10):857–872.

Leeney, R. H., Greaves, D., Conley, D., and O'Hagan, A. M. (2014). Environmental impact assessments for wave energy developments: Learning from existing activities and informing future research priorities. *Ocean &*

Coastal Management, 99:14–22.

Lighthill, J. (1978). Waves in fluids. Cambridge University Press.

Lin, L. and Yu, H. (2012). Offshore wave energy generation devices: Impacts on ocean bio-environment. *Acta Ecologica Sinica*, 32(3):117–122.

Luettich, Jr., R. A., Westerink, J. J., and Scheffner, N. W. (1992). ADCIRC: An advanced three-dimensional circulation model for shelves, coasts and estuaries, report 1: Theory and methodology of ADCIRC-2DDI and ADCIRC-3DL. Dredging Research Program Technical Report DRP-92-6, US Army Engineers Waterways Experiment Station, Vicksburg, MS, USA.

MacKay, D. J. C. (2008a). Sustainable energy – without the hot air. UIT Cambridge, ISBN 978-0-9544529-3-3. Available free online from: http://www.withouthotair.com.

MacKay, D. J. C. (2008b). Under-estimation of the UK tidal resource. Available free online from: http://www.inference.phy.cam.ac.uk/sustainable/book/tex/TideEstimate.pdf.

Madsen, P. T., Wahlberg, M., Tougaard, J., Lucke, K., and Tyack, P. (2006). Wind turbine underwater noise and marine mammals: Implications of current knowledge and data needs. *Marine Ecology Progress Series*, 309:279–295.

McAdam, R. A., Houlsby, G. T., and Oldfield, M. L. G. (2013). Experimental measurements of the hydrodynamic performance and structural loading of the Transverse Horizontal Axis Water Turbine: Part 1. *Renewable Energy*, 59:105–114.

McLachlan, C. (2009). "You don't do a chemistry experiment in your best china": Symbolic interpretations of place and technology in a wave energy case. *Energy Policy*, 37(12):5342–5350.

MeyGen Ltd (2017). About Phase 1A. Available at: http://www.meygen.com.

Michaud, K., Carlisle, J. E., and Smith, E. R. A. N. (2008). NIMBYism vs. environmentalism in attitudes toward energy development. *Environmental Politics*, 17:20–39.

Miles, J. W. (1971). Resonant response of harbours: An equivalent-circuit analysis. *Journal of Fluid Mechanics*, 46:241–265.

Millar, D. L., Smith, H. C. M., and Reeve, D. E. (2007). Modelling analysis of the sensitivity of shoreline change to a wave farm. *Ocean Engineering*,

34(5):884–901.

Nedwell, J., Langworthy, J., and Howell, D. (2003). Assessment of sub-sea acoustic noise and vibration from offshore wind turbines and its impact on marine wildlife: Initial measurements of underwater noise during construction of offshore windfarms and comparison with background noise. Subacoustech Report ref: 544R0423, published by COWRIE Ltd.

Neill, S. P., Jordan, J. R., and Couch, S. J. (2012). Impact of tidal energy converter (TEC) arrays on the dynamics of headland sand banks. *Renewable Energy*, 37:387–397.

Neill, S. P., Litt, E. J., Couch, S. J., and Davies, A. G. (2009). The impact of tidal stream turbines on large-scale sediment dynamics. *Renewable Energy*, 34(12):2803–2812.

Nishino, T. (2016). Two-scale momentum theory for very large wind farms. *Journal of Physics: Conference Series*, 753(3):032054.

Nishino, T. and Draper, S. (2015). Local blockage effect for wind turbines. *Journal of Physics: Conference Series*, 625(1):012010.

Nishino, T. and Willden, R. H. J. (2012). The efficiency of an array of tidal turbines partially blocking a wide channel. *Journal of Fluid Mechanics*, 708:596–606.

Nishino, T. and Willden, R. H. J. (2013). Two-scale dynamics of flow past a partial cross-stream array of tidal turbines. *Journal of Fluid Mechanics*, 730:220–244.

Normandeau Associates, Inc. (2009). An estimation of survival and injury of fish passed through the Hydro Green Energy hydrokinetic system and a characterization of fish entrainment potential at the Mississippi lock and dam no. 2 hydroelectric projects. Normandeau Associates, Inc., Westmoreland, NH, USA.

Öhman, M. C., Sigray, P., and Westerberg, H. (2007). Offshore windmills and the effects of electromagnetic fields on fish. *AMBIO: A journal of the Human Environment*, 36(8):630–633.

Okulov, V. L. and van Kuik, G. A. M. (2012). The Betz–Joukowsky limit: On the contribution to rotor aerodynamics by the British, German, and Russian scientific schools. *Wind Energy*, 15(2):335–344.

Osalusi, E., Side, J., and Harris, R. (2009a). Reynolds stress and turbulence estimates in bottom boundary layer of Fall of Warness. *International Communications in Heat and Mass Transfer*, 36(5):412–421.

Osalusi, E., Side, J., and Harris, R. (2009b). Structure of turbulent flow in EMEC's tidal energy test site. *International Communications in Heat and Mass Transfer*, 36(5):422–431.

OSPAR Commission (2009). Assessment of the environmental impacts of cables. Oslo and Paris (OSPAR) Convention for the Protection of the Marine Environment of the North-East Atlantic Commission.

Page, H. M., Dugan, J. E., Culver, C. S., and Hoesterey, J. C. (2006). Exotic invertebrate species on offshore oil platforms. *Marine Ecology Progress Series*, 325:101–107.

Page, H. M., Dugan, J. E., Dugan, D. S., Richards, J. B., and Hubbard, D. M. (1999). Effects of an offshore oil platform on the distribution and abundance of commercially important crab species. *Marine Ecology Progress Series*, 185:47–57.

Palha, A., Mendes, L., Fortes, C. J., Brito-Melo, A., and Sarmento, A. (2010). The impact of wave energy farms in the shoreline wave climate: Portuguese pilot zone case study using Pelamis energy wave devices. *Renewable Energy*, 35:62–77.

Patrício, S., Moura, A., and Simas, T. (2009). Wave energy and underwater noise: State of art and uncertainties. *Oceans 2009 – Europe*.

Perez-Campos, E. and Nishino, T. (2015). Numerical validation of the two-scale actuator disc theory for marine turbine arrays. *Proceedings of the 11th European Wave and Tidal Energy Conference (EWTEC), Nantes, France*.

Polagye, B. L. and Malte, P. C. (2011). Far-field dynamics of tidal energy extraction in channel networks. *Renewable Energy*, 36:222–234.

Popper, A. N. and Hastings, M. C. (2009). The effects of anthropogenic sources of sound on fishes. *Journal of Fish Biology*, 75(3):455–489.

Portman, M. (2008). Involving the public in the impact assessment of offshore renewable energy facilities. *Marine Policy*, 33(2):332–338.

Pugh, D. T. (1996). Tides, surges, and mean sea-level. John Wiley and Sons.

Rainey, R. C. T. (2009). The optimum position for a tidal power barrage in the Severn estuary. *Journal of Fluid Mechanics*, 636:497–507.

Rainey, R. C. T. (2010). The optimum position for a tidal power barrage in the Severn estuary – ERRATUM. *Journal of Fluid Mechanics*, 644:537–538.

Rankine, W. J. M. (1865). On the mechanical principles of the action of propellers. *Transactions of the Institution of Naval Architects*, 6:13–39.

RenewableUK (2013). Wind energy in the UK: State of the industry report 2013.

RenewableUK (2017). Export nation: A year in UK wind, wave, and tidal exports.

Richardson, W. J., Greene, C. R., Malme, C. I., and Thompson, D. H. (1995). Marine mammals and noise. Academic Press, San Diego.

Robinson, S. P. and Lepper, P. A. (2013). Scoping study: Review of current knowledge of underwater noise emissions from wave and tidal stream energy devices. A report commissioned by The Crown Estate.

Rourke, F. E. (1984). Bureaucracy, politics, and public policy. Boston: Little, Brown.

Salter, S. H. (2005). Possible under-estimation of the UK tidal resource.

Salter, S. H. (2012). Are nearly all tidal stream turbine designs wrong? *4th International Conference on Ocean Energy*, Dublin, Ireland.

Salter, S. H. (2015). Personal Communication.

Sarkar, D., Osborne, M., and Adcock, T. A. A. (2016). A machine learning approach to the prediction of tidal currents. *Proceedings of the 26th International Ocean and Polar Engineering Conference (ISOPE), Rhodes, Greece*.

Scheffer, M., Bascompte, J., Brock, W. A., Brovkin, V., Carpenter, S. R., Dakos, V., Held, H., van Nes, E. H., Rietkerk, M., and Sugihara, G. (2009). Early-warning signals for critical transitions. *Nature*, 461(7260):53.

Scheffer, M., Carpenter, S., Foley, J. A., Folke, C., and Walker, B. (2001). Catastrophic shifts in ecosystems. *Nature*, 413(6856):591.

Scheffer, M., Carpenter, S. R., Lenton, T. M., Bascompte, J., Brock, W., Dakos, V., van de Koppel, J., van de Leemput, I. A., Levin, S. A., van Nes, E. H., Pascual, M., and Vandermeer, J. (2012). Anticipating critical transitions. *Science*, 338(6105):344–348.

Schroeder, D. M. and Love, M. S. (2004). Ecological and political issues surrounding decommissioning of offshore oil facilities in the southern California bight. *Ocean & Coastal Management*, 47:21–48.

Scott, B. E. (2007). A renewable engineer's essential guide to marine ecol-

ogy. *Oceans 2007 – Europe*.

Scott, B. E., Sharples, J., Ross, O. N., Wang, J., Pierce, G. J., and Camphuysen, C. J. (2010). Sub-surface hotspots in shallow seas: Fine-scale limited locations of top predator foraging habitat indicated by tidal mixing and sub-surface chlorophyll. *Marine Ecology Progress Series*, 408:207–226.

Serhadlıoğlu, S. (2014). Tidal stream resource assessment of the Anglesey Skerries and the Bristol Channel. DPhil Thesis, University of Oxford, UK.

Serhadlıoğlu, S., Adcock, T. A. A., Houlsby, G. T., Draper, S., and Borthwick, A. G. L. (2013). Tidal stream energy resource assessment of the Anglesey Skerries. *International Journal of Marine Energy*, 3:e98–e111.

Shields, M. A., Dillon, L. J., Woolf, D. K., and Ford, A. T. (2009). Strategic priorities for assessing ecological impacts of marine renewable energy devices in the Pentland Firth (Scotland, UK). *Marine Policy*, 33(4):635–642.

Shields, M. A., Woolf, D. K., Grist, E. P. M., Kerr, S. A., Jackson, A. C., Harris, R. E., Bell, M. C., Beharie, R., Want, A., Osalusi, E., Gibb, S. W., and Side, J. (2011). Marine renewable energy: The ecological implications of altering the hydrodynamics of the marine environment. *Ocean & Coastal Management*, 54:2–9.

Simas, T., Moura, A., Batty, R., Thompson, D., and Norris, J. (2009). Uncertainties regarding environmental impacts: A draft. Deliverable D6.1.3 from Equitable Testing and Evaluation of Marine Energy Extraction Devices in terms of Performance, Cost and Environmental Impact (EquiMar), European Commission.

Simmonds, M. P. and Brown, V. C. (2010). Is there a conflict between cetacean conservation and marine renewable-energy developments? *Wildlife Research*, 37(8):688–694.

Sims, S. and Dent, P. (2005). High-voltage overhead power lines and property values: A residential study in the UK. *Urban Studies*, 42(4):665–694.

Skeate, E. R., Perrow, M. R., and Gilroy, J. J. (2012). Likely effects of construction of Scroby Sands offshore wind farm on a mixed population of harbour *Phoca vitulina* and grey *Halichoerus grypus* seals. *Marine Pollution Bulletin*, 64(4):872–881.

Snyder, B. and Kaiser, M. J. (2009). Ecological and economic cost-benefit analysis of offshore wind energy. *Renewable Energy*, 34(6):1567–1578.

Soulsby, R. L. (1997). Dynamics of marine sands: A manual for practical applications. Telford, London.

Sparling, C. E., Coram, A. J., McConnell, B., Thompson, D., Hawkins, K. R., and Northridge, S. P. (2013). Marine mammal impacts. Natural Environment Research Council (NERC) Wave and Tidal Consenting Position Paper Series.

Stansby, P. K. (2006). Limitations of depth-averaged modelling for shallow wakes. *Journal of Hydraulic Engineering*, 132(7):737–740.

Street, R. O. (1917). The dissipation of energy in the tides in connection with the acceleration of the Moon's mean motion. *Philosophical Transactions of the Royal Society of London. Series A, Containing Papers of a Mathematical or Physical Character*, 93:348–359.

Sundberg, J. and Langhamer, O. (2005). Environmental questions related to point-absorbing linear wave-generators: Impact, effects, and fouling. *Proceedings of the 6th European Wave and Tidal Energy Conference (EWTEC), Glasgow, UK*.

Sutherland, G., Foreman, M., and Garrett, C. (2007). Tidal current energy assessment for Johnstone Strait, Vancouver Island. *Proceedings of the Institution of Mechanical Engineers, Part A: Journal of Power and Energy*, 221(2):147–157.

Taylor, G. I. (1920). Tidal friction in the Irish Sea. *Philosophical Transactions of the Royal Society of London. Series A, Containing Papers of a Mathematical or Physical Character*, 220:1–33.

Taylor, G. I. (1928). The forces on a body placed in a curved or converging stream of fluid. *Proceedings of the Royal Society of London A: Mathematical, Physical, and Engineering Sciences*, 120(785):260–283.

The Robert Gordon University (2002). A scoping study for an environmental impact field programme in tidal current energy. The Department of Trade and Industry (DTI) Publication URN 02/882.

Thompsen, F., Lüdemann, K., Kafemann, R., and Piper, W. (2006). Effects of offshore wind farm noise on marine mammals and fish. Hamburg, Germany on behalf of COWRIE Ltd.

Todd, P. (2012). Marine renewable energy and public rights. *Marine Policy*, 36(3):667–672.

Toro, E. F. (2013). Riemann solvers and numerical methods for fluid dynamics: A practical introduction. Springer Science & Business Media.

Tougaard, J., Carstensen, J., Henriksen, O. D., Skov, H., and Teilmann, J. (2003). Short-term effects of the construction of wind turbines on harbour porpoises at Horns Reef. Technical Report Commissioned by Techwise A/S.

Vennell, R. (1998). Oscillating barotropic currents along short channels. *Journal of Physical Oceanography*, 28(8):1561–1569.

Vennell, R. (2010). Tuning turbines in a tidal channel. *Journal of Fluid Mechanics*, 663:253–267.

Vennell, R. (2011). Tuning tidal turbines in-concert to maximise farm efficiency. *Journal of Fluid Mechanics*, 671:587–604.

Vennell, R. (2016). An optimal tuning strategy for tidal turbines. *Proceedings of the Royal Society of London A: Mathematical, Physical, and Engineering Sciences*, 472(2195):20160047.

Vennell, R. and Adcock, T. A. A. (2014). Energy storage inherent in large tidal turbine farms. *Proceedings of the Royal Society of London A: Mathematical, Physical, and Engineering Sciences*, 470(2166):20130580.

Vennell, R., Funke, S. W., Draper, S., Stevens, C., and Divett, T. (2015). Designing large arrays of tidal turbines: A synthesis and review. *Renewable and Sustainable Energy Reviews*, 41:454–472.

Vogel, C. R. (2014). Theoretical limits to tidal stream energy extraction. DPhil Thesis, University of Oxford, UK.

Vogel, C. R., Houlsby, G. T., and Willden, R. H. J. (2016). Effect of free surface deformation on the extractable power of a finite width turbine array. *Renewable Energy*, 88:317–324.

Vogel, C. R., Willden, R. H. J., and Houlsby, G. T. (2013). A correction for depth-averaged simulations of tidal turbine arrays. *Proceedings of the 10th European Wave and Tidal Energy Conference (EWTEC), Aalborg, Denmark*.

Wahlberg, M. and Westerberg, H. (2005). Hearing in fish and their reactions to sounds from offshore wind farms. *Marine Ecology Progress Series*, 288:295–309.

Waldo, Å. (2012). Offshore wind power in Sweden – A qualitative analysis of attitudes with particular focus on opponents. *Energy Policy*, 41:692–702.

Walker, G. (1995). Renewable energy and the public. *Land Use Policy*, 12:49–59.

Walker, G. (2008). What are the barriers and incentives for community-owned means of energy production and use? *Energy Policy*, 36(12):4401–4405.

Walker, G., Cass, N., Burningham, K., and Barnett, J. (2010a). Renewable energy and sociotechnical change: Imagined subjectivities of 'the public' and their implications. *Environment and planning A*, 42(4):931–947.

Walker, G., Devine-Wright, P., Hunter, S., High, H., and Evans, B. (2010b). Trust and community: Exploring the meanings, contexts, and dynamics of community renewable energy. *Energy Policy*, 38(6):2655–2663.

Warren, C. R., Lumsden, C., O'Dowd, S., and Birnie, R. V. (2005). 'Green on green': Public perceptions of wind power in Scotland and Ireland. *Journal of Environmental Planning and Management*, 48(6):853–875.

Wave Hub Ltd (2017). Our offshore energy experts — the Wave Hub team. Available at: https://www.wavehub.co.uk/about-us/the-team.

WaveNet (2003). Technical summary report: Overview of the work of the European thematic network on wave energy.

Weilgart, L. S. (2007). A brief review of known effects of noise on marine mammals. *International Journal of Comparative Psychology*, 20(2):159–168.

West, J., Bailey, I., and Whitehead, I. (2009). Stakeholder perceptions of the Wave Hub development in Cornwall, UK. *Proceedings of the 8th European Wave and Tidal Energy Conference (EWTEC), Uppsala, Sweden.*

West, J., Bailey, I., and Winter, M. (2010). Renewable energy policy and public perceptions of renewable energy: A cultural theory approach. *Energy Policy*, 38(10):5739–5748.

Westerberg, H. and Lagenfelt, I. (2008). Sub-sea power cables and the migration behaviour of the European eel. *Fisheries Management and Ecology*, 15(5–6):369–375.

Whelan, J. I., Graham, J. M. R., and Peiro, J. (2009). A free-surface and blockage correction for tidal turbines. *Journal of Fluid Mechanics*, 624:281–291.

White, F. M. (2009). Fluid Mechanics. McGraw-Hill.

Whitehouse, R. J. S., Harris, J. M., Sutherland, J., and Rees, J. (2011). The nature of scour development and scour protection at offshore windfarm foundations. *Marine Pollution Bulletin*, 62:73–88.

Wilhelmsson, D. and Malm, T. (2008). Fouling assemblages on offshore wind power plants and adjacent substrata. *Estuarine, Coastal and Shelf Science*, 79(3):459–466.

Willden, R. H. J., Nishino, T., and Schluntz, J. (2014). Tidal stream energy: Designing for blockage. *Proceedings of the 3rd Oxford Tidal Energy Workshop, Oxford, UK*.

Wilson, B., Batty, R. S., Daunt, F., and Carter, C. (2007). Collision risks between marine renewable energy devices and mammals, fish, and diving birds. Technical Report to the Scottish Executive. Scottish Association for Marine Science, Oban, Scotland, PA37 1QA.

Wilson, J. C. and Elliott, M. (2009). The habitat-creation potential of offshore wind farms. *Wind Energy*, 12(2):203–212.

Wilson, R. E. and Lissaman, P. B. S. (1974). Applied aerodynamics of wind power machines. Technical Report, Oregon State University, USA.

Witt, M. J., Sheehan, E. V., Bearhop, S., Broderick, A. C., Conley, D. C., Cotterell, S. P., Crow, E., Grecian, W. J., Halsband, C., Hodgson, D. J., Hosegood, P., Inger, R., Miller, P. I., Sims, D. W., Thompson, R. C., Vanstaen, K., Votier, S. C., Attrill, M. J., and Godley, B. J. (2012). Assessing wave energy effects on biodiversity: The Wave Hub experience. *Philosophical Transactions of the Royal Society A: Mathematical, Physical, and Engineering Sciences*, 370(1959):502–529.

Wolf, J., Walkington, I. A., Holt, J., and Burrows, R. (2009). Environmental impacts of tidal power schemes. *Proceedings of the ICE-Maritime Engineering*, 162(4):165–177.

Wolsink, M. (1996). Dutch wind power policy: Stagnating implementation of renewables. *Energy Policy*, 24(12):1079–1088.

Wolsink, M. (2000). Wind power and the NIMBY-myth: Institutional capacity and the limited significance of public support. *Renewable Energy*, 21:49–64.

Wolsink, M. (2006). Invalid theory impedes our understanding: A critique on the persistence of the language of NIMBY. *Transactions of the Institute of British Geographers*, 31:85–91.

Wolsink, M. (2007). Wind power implementation: The nature of public attitudes: Equity and fairness instead of 'backyard motives'. *Renewable and Sustainable Energy Reviews*, 11(6):1188–1207.

Wolsink, M. and Sprengers, M. (1993). Wind turbine noise: A new environmental threat? *International Commission on the Biological Effects of*

Noise, Nice, France.

Wright, A. J., Soto, N. A., Baldwin, A. L., Bateson, M., Beale, C. M., Clark, C., Deak, T., Edwards, E. F., Fernández, A., Godinho, A., Hatch, L. T., Kakuschke, A., Lusseau, D., Martineau, D., Romero, L. M., Weilgart, L. S., Wintle, B. A., Notarbartolo-di-Sciara, G., and Martin, V. (2007). Do marine mammals experience stress related to anthropogenic noise? *International Journal of Comparative Psychology*, 20(2):274–316.

Würsig, B., Greene, Jr., C. R., and Jefferson, T. A. (2000). Development of an air bubble curtain to reduce underwater noise of percussive piling. *Marine Environmental Research*, 49:79–93.

Wüstenhagen, R., Wolsink, M., and Bürer, M. J. (2007). Social acceptance of renewable energy innovation: An introduction to the concept. *Energy Policy*, 35(5):2683–2691.

Yearley, S., Cinderby, S., Forrester, J., Bailey, P., and Rosen, P. (2003). Participatory modelling and the local governance of the politics of UK air pollution: A three-city case study. *Environmental Values*, 12(2):247–262.

Zapata, A., Nishino, T., and Delafin, P.-L. (2017). Theoretically optimal turbine resistance in very large wind farms. *Journal of Physics: Conference Series*, 854:012051.

Zikanov, O. (2010). Essential computational fluid dynamics. John Wiley & Sons.

Zucco, C., Wende, W., Merck, T., Köchling, I., and Köppel, J. (2006a). Ecological research on offshore wind farms: International exchange of experiences, pt. A: Assessment of ecological impacts, BfN-Skripten.

Zucco, C., Wende, W., Merck, T., Köchling, I., and Köppel, J. (2006b). Ecological research on offshore wind farms: International exchange of experiences, pt. B: Literature review of ecological impacts, BfN-Skripten.